DISSERTATION

DEVELOPMENT AND IMPLEMENTATION OF NOVEL DRUG DELIVERY SYSTEM FOR TRANSDERMAL MATERIALS

Submitted by

Yu Sun

School of Materials Science and Engineering

In partial fulfillment of the requirements

For the Degree of Doctor of Philosophy

Colorado State University

Fort Collins, Colorado

Fall 2024

Doctoral Committee:

Advisor: Yan Vivian Li
Co-advisor: Jiangguo Liu

Travis Bailey
Claudia Gentry-Weeks

ABSTRACT

DEVELOPMENT AND IMPLEMENTATION OF NOVEL DRUG DELIVERY SYSTEM FOR TRANSDERMAL MATERIALS

There is a constant need for developing transdermal dressing materials with advanced properties such as infection monitoring and wound closure facilitation for effective chronic wound treatments. On the other than, the advancement in drug delivery systems has created innovation of precise targeting of treatment, nontoxicity, cell access, controlled release profiles, treatment variations, and antibiotics activity conservation, which offers a great opportunity in developing novel wound dressing materials. Recently, the application of nanomaterials, especially nanoparticles, in drug delivery systems has shown great potential in effective wound treatment. In this proposal, three projects are focused on developing nanostructured scaffolds loaded with antibiotic agents for novel wound dressing applications. First, the antibiotic encapsulated poly (lactic-co-glycolic acid) (PLGA) nanoparticles will be integrated into monolithic nanofiber scaffolds that can be tested in transdermal materials for antibacterial properties. Second, the antibiotics loaded PLGA nanoparticles incorporated monolithic nanofiber scaffolds will be developed into core-shell fibrous scaffolds to provide a drug delivery system with controlled release of antibiotics. Integration of the nanoparticles into nanofibers includes monolithic and core-shell structures to provide controlled release of antibiotic agents. The mechanisms of controlled release are investigated via experimental and computational methods. Finite difference methods and machine learning are used for developing mathematical models

capable of numerically quantifying antibiotic release rates, which provides a theoretical understanding of the release process in the nanostructure scaffolds. The work provides implication of utilizing PLGA nanoparticles in scaffolds to develop effective transdermal materials. Additionally, the computational models would provide tools to understand the mechanism of controlled release process, which may assist in the design of the nanoparticles as well as the nanostructured scaffolds.

ACKNOWLEDGEMENTS

Before delving into the technical aspects of this work, I would like to take a moment to express my deepest gratitude to those who have played pivotal roles in making this endeavor possible. Their unwavering support, guidance, and encouragement have been instrumental in shaping both the trajectory of my research and my personal growth throughout this journey.

I would like to express my deepest gratitude to my advisor, Yan Vivian Li, for her unwavering support, invaluable guidance, and mentorship throughout my whole academic study. Her expertise, patience, and encouragement have not only shaped my research endeavors but also contributed significantly to my personal development. I am profoundly fortunate to have benefited from her inspiration and leadership, which have been critical in navigating the challenges and milestones of my academic pursuit.

I am deeply indebted to my co-advisor, Jiangguo Liu, for his insightful feedback, constant encouragement, and generous sharing of expertise. His ability to provide constructive criticism while fostering a supportive and motivating environment has greatly enhanced my research experience. I am grateful for his patience and for the numerous discussions that have significantly enriched my understanding and helped me navigate complex challenges.

I extend my heartfelt appreciation to my committee members, Dr. Travis Bailey, and Dr. Claudia Gentry-Weeks for their constructive feedback, valuable insights, and for dedicating their time to review and provide guidance on my research. Their contributions have significantly enriched the quality of this work.

I am grateful to my department, School of Materials Science and Engineering (SMSE), for fostering an intellectually stimulating environment that nurtured my academic and research endeavors. The resources, facilities, and camaraderie within the department were indispensable in my journey. A special thanks to Caro Banuelos for helping me navigate the program. I would like to acknowledge all the facilities from Analytical Resources Core (ARC) for their patience, guidance, and encouragement in the utilization and training of different instruments. Especially, I would like to thank Dr. Roy Geiss, Dr. Karolien Denef, and Dr. Rebecca Miller

My sincere thanks go to my research mates and colleagues for their camaraderie, support, and the countless insightful discussions that have enriched my understanding and fueled my passion for research including Yingli Li, Jesse Heacock, Shuhuai Qin, Naimul Hasan, Bradley Guilliams, . Their friendship has made this journey both rewarding and enjoyable. I am grateful for the collaborative spirit and the willingness to share knowledge, which has been crucial in overcoming obstacles and achieving milestones. The shared experiences, and mutual encouragement have made a significant impact on my work and personal growth. Their contributions have been invaluable, and I am fortunate to have had such a wonderful team by my side. A special thanks to Thomas Tathryn for his help with my academic writing.

Finally, I express my deepest gratitude to my family for their unconditional love, support, and understanding throughout this journey. I am especially thankful to my parents, whose constant encouragement and belief in me have been my pillars of strength, motivating me to strive for excellence. Their patience and sacrifices have made it possible for me to pursue my goals with confidence and determination. My parents' guidance and wisdom have been invaluable, providing me with the foundation to overcome challenges and celebrate successes. I am profoundly thankful for their constant reassurance during difficult times and for celebrating

every achievement along the way. Their faith in my abilities has been a source of immense inspiration, and I am forever indebted to them for their enduring support.

TABLE OF CONTENTS

Chapter 1. Introduction

Since Scottish scientist and Noble laureate Alexander Fleming discovered penicillin in 1928, utilization of antibiotics become an effective medical therapy to treat infectious diseases [1]. Up to now, over 100 different kinds of antibiotics have been found and applied for various bacterial infection treatments [2]. Consequently, drug delivery and its relative research becomes essential in human healthcare. Conventional approaches of drug delivery include oral administration, external applications, inhalation, implant, and intravenous injections [3]. With the development of understanding in human bodies and the advancement of modern medical technologies, however, traditional drug delivery systems have been challenged because there are emerging requirements such as active ingredient chemical modifications, release rate modifications, local irritation reduction, targeted delivery, and drug-device combination [4][5][6][7]. For example, skin wound treatments that are the #1 expenditure of American medical treatment that costs nearly $9.7 billion dollars annually according to American Dermatology Association. Historically, transdermal materials are used for chronic wound treatments. In most cases, conventional wound dressing materials can prevent wounds from external harm and contamination as well as control hemostasis and infection. However, the effects on facilitating wound closure or controlling bacterial infections provided by conventional wound dressing are limited [8]. Therefore, there is a constant need to develop novel drug delivery systems with advanced performance properties which would bring a significant economic benefit. The advanced performance properties in favor of novel wound dressing materials include moisture maintenance, infection monitoring, wound closure facilitation, waterproof, ventilation, and advanced infection control [8][9][10]. As a results of the advancement and innovation of technologies and medicines, there are emerging systems such as

microemulsions, matrix system, solid dispersions, liposomes, nanoparticles, and nanosuspensions developed for drug delivery systems that can be used in novel wound dressing materials [4][11].

Recently, the integration of drug delivery into wound treatment is attractive due to release profiles controlling, precise targeting, cell accessing, and antibiotics bioactivity preserving [4][6][7]. Especially, polymeric nanoparticles made of poly-L-glutamic acid (PGA)-Taxol, N-(2-hydroxypropyl)-methacrylamide copolymer (HPMA)-Doxil, Albumin-Taxol, and Heat Shock Proteins (HSP)-Doxil show a great potential in drug delivery systems, providing advanced properties such as precise targeting, bioactivity preservation, thermal stability, functionality stability and dispersibility [12][13][14][15]. Various drugs, molecules, peptides, and RNA have been loaded into nanoparticles that deliver to human bodies for effective treatments [16]. Because nanoparticles are normally in a dimension range from 70 nm to 3μm that is smaller than the size of human cells that have an average diameter of 30μm [17][18], they have access to cells and blood capillaries, resulting in a drug release inside the cells and hence a significant increase of treatment efficiency with minimum damages of healthy cells [13]. Therefore, utilization of drugs encapsulated nanoparticles as novel drug delivery systems have been an emerging technology in medical treatments such as theragnostic medicine pharmaceuticals, Alzheimer's disease treatments, tissue engineering, and clinic wound treatments [19][20][21]. For example, the treatment of Alzheimer's Disease (AD) and brain cancers requires a precise targeting drug delivery system that has access to cells and hence deliver drugs effectively [14][22]. Conventional cancer treatments require patients to take chemotherapeutics drugs orally which results into side effects such as low treatment efficiency, emesis, anorexia, alopecia and so on. A novel treatment offered by mesoporous silica-based nanoparticles delivers a controlled

sustainable release which can improve the hyaluronic acid efficiency of cancer therapy and reduce the side effects as well [23]. Another example is that skin irritation could be effectively reduced by lipid nanoparticles encapsulated with retinoic acid [24]. Because chemical compounds can be encapsulated within nanoparticles for delivery, applying nanoparticles as drug delivery system for developing novel wound dressing materials will be a promising research topic. Drugs encapsulated PLGA nanoparticles incorporated fiber scaffolds will be able to delivery antibiotics for infection control, local skin irritation reduction, and facilitate wound healing. Therefore, incorporating antibiotics loaded nanoparticles into nanofiber scaffolds is feasible to develop novel wound dressing materials [25][26].

Among different polymer-based nanoparticle drug delivery systems, Poly (lactic-co-glycolic acid) (PLGA) that is a biocompatible and biodegradable polymer has been of great interest in developing nanoparticles for drug delivery applications. This proposed project is focused on the application of PLGA nanoparticles to develop novel drug delivery systems potentially for smart wound dressing materials. The novel wound dressing material is illustrated in Fig. 1. PLGA nanoparticles are synthesized via a double emulsion evaporation method, and the antibiotic loaded nanoparticles will be incorporated into PU/PEO monolithic nanofiber scaffolds via electrospinning. Co-axial electrospinning is applied for developing core-shell fiber scaffolds in which PLGA nanoparticles are primarily loaded in the core fibers. Because of core-shell scaffolds advantages such as antibiotic bioactivity preservation, contamination prevention, open-sites for modification, cost materials reduction, and burst release controlling, the scaffolds will be developed into core-shell fibrous scaffolds. The rest of this report are organized as follows: Chapter 2 focusing on **Incorporation of Gentamicin Encapsulated PLGA Nanoparticles into PU/PEO Nanofiber Scaffolds for Biomedical Applications fully**

illustrates the synthesis method and properties of PLGA nanoparticles incorporated PU/PEO nanofiber scaffolds. Gentamicin, a wide spectrum antibiotic, will be encapsulated in PLGA nanoparticles via a double emulsion solvent evaporation method, and electrospinning can be used for incorporating PLGA nanoparticles into PEO/PU monolithic nanofiber scaffolds. Polyurethane (PU) and polyethylene oxide (PEO) are the primary choices used for fiber supporting materials because of their biocompatibility and biodegradability. Properties of gentamicin loaded PLGA nanoparticles will be evaluated to optimize nanofiber scaffold antibacterial activities. Chapter 3 **Mathematical Modeling and Numerical Simulations for Drug Release from PLGA Nanoparticles** demonstrates the application of Fick's 2nd law and Darcy law in finite difference for release profile mathematical developing. Utilization of finite difference method and its variants, likely finite volume difference analysis, to construct mechanisms-based models shows its accuracy in release rate predictions. Therefore, developing mathematical models to correctly predict release profiles becomes a critical research topic for wound dressing optimization. Mutually, results calculated from mathematical models will be used in comparison with experimental data to verify model accuracy. Chapter 4 **Enhanced Transdermal Medication Delivery: Core-Shell Nanofiber Scaffolds with Antibiotic-encapsulated Poly (lactic acid-co-glycolic acid) Nanoparticles Applications** discusses synthesis and characterization methods for core-shell fibers. Gentamicin loaded PLGA nanoparticles will be incorporated into core-shell fiber scaffold via co-axial electrospinning. PLGA nanoparticles are primarily incorporated into PEO nanofibers which are used as the core, and shell fibers are made of PU/PEO. The core-shell scaffolds are characterized to study morphologies, release profiles, dimension distributions, and antibacterial activity. Chapter 5 **Machine Learning Integrated with In Vitro Experiments for Study of Drug Release from**

Poly (Lactic-co-Glycolic Acid) Particles presents machine learning algorithms including linear regression, principal component analysis, Gaussian process regression, and artificial neural networks are applied to develop mathematical models to investigate factor effects of release matrix pH value, particle size distributions, drug solubilities, and molecular weights on drug release profiles. The established models will be validated via experimental data to improve their accuracy for release profile predications.

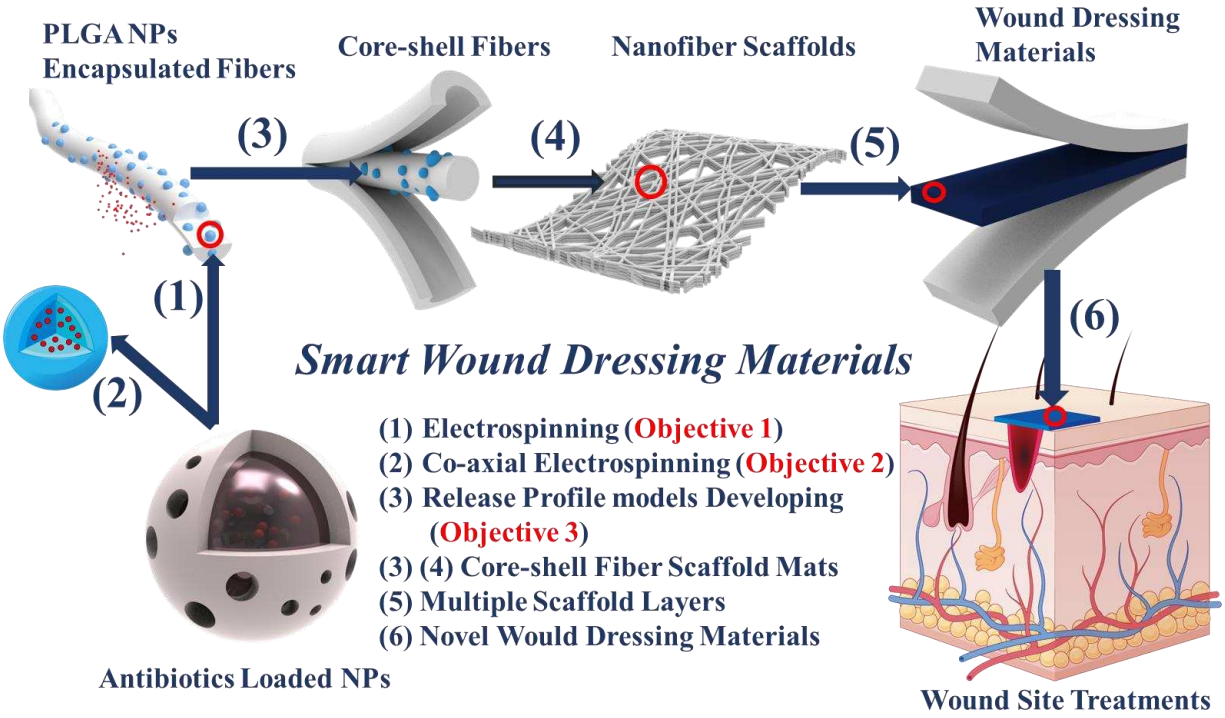

Fig 1. Antibiotics encapsulated PLGA NPs incorporated nanofiber scaffolds can be used as a novel drug delivery system as smart wound dressing materials for skin wound diseases.

1.2 Hypothesis

1. Antibiotics encapsulated PLGA NPs can be integrated into monolithic nanofibers via electrospinning.
2. Antibiotics encapsulated PLGA NPs incorporated monolithic fiber scaffolds can be developed into core-shell fiber scaffolds via co-axial electrospinning.

3. The computational approaches including numerical methods and machine learning can be applied to analysis release profiles of drugs.

1.3 Project Objectives

1.3.1 Objective 1

The main goal of this project is to develop a novel drug delivery system in which antibiotics are encapsulated in nanoparticles incorporated monolithic nanofiber scaffolds for controlled release. Poly lactic-co-glycolic acid (PLGA) is used for synthesizing gentamicin encapsulated PLGA nanoparticles via a double emulsion evaporation method due to its biocompatibility and biodegradability. Electrospinning is the nanofiber fabrication technique for incorporating PLGA nanoparticles into polyurethane (PU)- polyethylene oxide (PEO) nanofiber scaffolds where PU and PEO are biocompatible and biodegradable polymers. The resulting gentamicin-encapsulated PLGA nanoparticles and the nanoparticles-loaded nanofiber scaffolds are characterized to study morphologies, size and size distributions, drug release profiles, and antibacterial activities via scanning electron microscopy (SEM), dynamic light scattering (DLS), ultraviolet-visible spectrophotometers (UV-vis), and a disk diffusion antibacterial testing.

Specific Aims 1

(1) PLGA nanoparticles will be synthesized while gentamicin is encapsulated in the particles via a double emulsion evaporation method and the resulting particles will be characterized to study particle morphologies and drug release properties.

(2) The gentamicin encapsulated PLGA nanoparticles will be incorporated into nanofiber scaffolds made of PU and PEO and the resulting nanofiber scaffolds will be characterized to study fiber morphologies and drug release properties.

(3) PLGA nanoparticle – loaded monolithic nanofiber scaffolds will be evaluated using an antibacterial testing method to investigate the potential of using the scaffolds in smart wound dressing materials.

1.3.2 Objective 2

The main goal of this project is to develop a core-shell nanofiber scaffold to significantly improve the performance of controlled drug release by the nanofibers. In the design of the core-shell structure, PLGA nanoparticles are loaded only in the core of the nanofibers made of PEO, while the shell of the nanofibers made by PU/PEO will protect the fiber core. A co-axial electrospinning method will be utilized to develop this core-shell structure in the nanofiber scaffolds. The core-shell nanofiber scaffolds are characterized using SEM, DLS and UV-vis to determine fiber morphologies, fiber size and size distributions, gentamicin release profiles, and antibacterial properties.

Specific Aim 2

(1) Gentamicin loaded PLGA nanoparticles encapsulated PEO-PU core-shell nanofiber scaffolds will be fabricated via co-axial electrospinning, and the resulting scaffolds will be characterized to study morphologies and release profiles.

(2) PLGA nanoparticles loaded core-shell fiber scaffold antibacterial activity will be determined with an antibacterial test method to evaluate core-shell scaffold potential in developing smart wound dressing materials.

1.3.3 Objective 3

The main goal of this project is to develop mathematical models of PLGA nanoparticles for diffusion, convection and swelling via finite volume-controlled and machine learning

methods. Multiple release mechanisms are involved throughout the PLGA nanoparticle release process. There are usually four main release mechanisms, which are (1) diffusion through porous shell, (2) diffusion through polymers, (3) osmotic pumping, and (4) release of degradation. In this project, mathematical models derived from Fick's 2nd law, Darcy law, and volume conservation law are constructed to simulate release mechanisms caused by diffusion, convection and swelling, respectively. However, degradation kinetics and number of degraded PLGA nanoparticles are difficult to be determined, and hence machine learning algorithms including linear regression, principal component analysis, Gaussian process regression and artificial neural networks are adopted to develop mathematical models. Experimental data of drug release profiles will be used to validate the computational results, providing verification evaluation of the mathematical models.

Specific Aim 3

(1) Fick's 2nd law in finite difference analysis will be used to develop a mathematical model to fit the release mechanism of diffusion through polymers.
(2) Machine learning algorithms including linear regression, principal component analysis, Gaussian process regression, and artificial neural networks will be applied to develop computational model for drug release profile predictions.
(3) Experimental data will be compared with computational results to validate and improve accuracy of these model

1.4 References

[1] Bennett, J. W., & Chung, K.-T. (2011). Alexander Fleming and the discovery of Penicillin. *Germ Theory*, 265–293. https://doi.org/10.1128/9781555817220.ch13

[2] Nigam, A., Gupta, D., & Sharma, A. (2014). Treatment of infectious disease: Beyond antibiotics. *Microbiological Research*, *169*(9-10), 643–651. https://doi.org/10.1016/j.micres.2014.02.009

[3] Anselmo, A. C., & Mitragotri, S. (2014). An overview of clinical and commercial impact of Drug Delivery Systems. *Journal of Controlled Release*, *190*, 15–28. https://doi.org/10.1016/j.jconrel.2014.03.053

[4] Wen, H., Jung, H., & Li, X. (2015). Drug delivery approaches in addressing clinical pharmacology-related issues: Opportunities and challenges. *The AAPS Journal*, *17*(6), 1327–1340. https://doi.org/10.1208/s12248-015-9814-9

[5] Silva, P., Bonifácio, B., Ramos, M., Negri, K., Maria Bauab, T., & Chorilli, M. (2013). Nanotechnology-based drug delivery systems and Herbal Medicines: A Review. *International Journal of Nanomedicine*, 1. https://doi.org/10.2147/ijn.s52634

[6] Khafagy, E.-S., Morishita, M., Onuki, Y., & Takayama, K. (2007). Current challenges in non-invasive insulin delivery systems: A comparative review. *Advanced Drug Delivery Reviews*, *59*(15), 1521–1546. https://doi.org/10.1016/j.addr.2007.08.019

[7] Sultana, A., Zare, M., Thomas, V., Kumar, T. S. S., & Ramakrishna, S. (2022). Nano-based drug delivery systems: Conventional drug delivery routes, recent developments and future prospects. *Medicine in Drug Discovery*, *15*, 100134. https://doi.org/10.1016/j.medidd.2022.100134

[8] Dong, R., & Guo, B. (2021). Smart wound dressings for wound healing. *Nano Today*, *41*, 101290. https://doi.org/10.1016/j.nantod.2021.101290

[9] Holmes, S. P., Rivera, S., Hooper, P. B., Slaven, J. E., & Que, S. K. (2022). Hydrocolloid dressing versus conventional wound care after dermatologic surgery. *JAAD International*, *6*, 37–42. https://doi.org/10.1016/j.jdin.2021.11.002

[10] Yue, Y., Gong, X., Jiao, W., Li, Y., Yin, X., Si, Y., Yu, J., & Ding, B. (2021). In-situ electrospinning of thymol-loaded polyurethane fibrous membranes for waterproof, breathable, and antibacterial wound dressing application. *Journal of Colloid and Interface Science*, *592*, 310–318. https://doi.org/10.1016/j.jcis.2021.02.048

[11] Jain, N., Valli, K. S., & Devi, V. K. (2010). Importance of novel drug delivery systems in Herbal Medicines. *Pharmacognosy Reviews*, *4*(7), 27. https://doi.org/10.4103/0973-7847.65322

[12] Cho, K., Wang, X., Nie, S., Chen, Z. (G., & Shin, D. M. (2008). Therapeutic nanoparticles for drug delivery in cancer. *Clinical Cancer Research*, *14*(5), 1310–1316. https://doi.org/10.1158/1078-0432.ccr-07-1441

[13] Bamrungsap, S., Zhao, Z., Chen, T., Wang, L., Li, C., Fu, T., & Tan, W. (2012). Nanotechnology in therapeutics: A focus on nanoparticles as a drug delivery system. *Nanomedicine*, *7*(8), 1253–1271. https://doi.org/10.2217/nnm.12.87

[14] Masood, F. (2016). Polymeric nanoparticles for targeted drug delivery system for cancer therapy. *Materials Science and Engineering: C*, *60*, 569–578. https://doi.org/10.1016/j.msec.2015.11.067

[15] Choudhury, H., Pandey, M., Lim, Y. Q., Low, C. Y., Lee, C. T., Marilyn, T. C., Loh, H. S., Lim, Y. P., Lee, C. F., Bhattamishra, S. K., Kesharwani, P., & Gorain, B. (2020). Silver nanoparticles: Advanced and promising technology in diabetic wound therapy. *Materials Science and Engineering: C*, *112*, 110925. https://doi.org/10.1016/j.msec.2020.110925

[16] ALMEIDA, A., & SOUTO, E. (2007). Solid lipid nanoparticles as a drug delivery system for peptides and proteins☆. *Advanced Drug Delivery Reviews*, *59*(6), 478–490. https://doi.org/10.1016/j.addr.2007.04.007

[17] Hu, C.-M. J., Fang, R. H., Luk, B. T., Chen, K. N., Carpenter, C., Gao, W., Zhang, K., & Zhang, L. (2013). 'marker-of-self' functionalization of nanoscale particles through a top-down cellular membrane coating approach. *Nanoscale*, *5*(7), 2664. https://doi.org/10.1039/c3nr00015j

[18] Sun, Y., Bhattacharjee, A., Reynolds, M., & Li, Y. V. (2021). Synthesis and characterizations of gentamicin-loaded poly-lactic-co-glycolic (PLGA) nanoparticles. *Journal of Nanoparticle Research*, *23*(8). https://doi.org/10.1007/s11051-021-05293-3

[19] Al-Jamal, W. T., & Kostarelos, K. (2011). Liposomes: From a clinically established drug delivery system to a nanoparticle platform for Theranostic Nanomedicine. *Accounts of Chemical Research*, *44*(10), 1094–1104. https://doi.org/10.1021/ar200105p

[20] Jin, S., Xia, X., Huang, J., Yuan, C., Zuo, Y., Li, Y., & Li, J. (2021). Recent advances in PLGA-based biomaterials for bone tissue regeneration. *Acta Biomaterialia*, *127*, 56–79. https://doi.org/10.1016/j.actbio.2021.03.067

[21] Anand, U., Carpena, M., Kowalska-Góralska, M., Garcia-Perez, P., Sunita, K., Bontempi, E., Dey, A., Prieto, M. A., Proćków, J., & Simal-Gandara, J. (2022). Safer plant-based nanoparticles for combating antibiotic resistance in bacteria: A comprehensive review on its potential applications, recent advances, and future perspective. *Science of The Total Environment*, *821*, 153472. https://doi.org/10.1016/j.scitotenv.2022.153472

[22] Anand, B., Wu, Q., Nakhaei-Nejad, M., Karthivashan, G., Dorosh, L., Amidian, S., Dahal, A., Li, X., Stepanova, M., Wille, H., Giuliani, F., & Kar, S. (2022). Significance of native

PLGA nanoparticles in the treatment of alzheimer's disease pathology. *Bioactive Materials*, *17*, 506–525. https://doi.org/10.1016/j.bioactmat.2022.05.030

[23] Yu, M., Jambhrunkar, S., Thorn, P., Chen, J., Gu, W., & Yu, C. (2013). Hyaluronic acid modified mesoporous silica nanoparticles for targeted drug delivery to CD44-overexpressing cancer cells. *Nanoscale*, *5*(1), 178–183. https://doi.org/10.1039/c2nr32145a

[24] Castro, G. A., Coelho, A. L., Oliveira, C. A., Mahecha, G. A. B., Oréfice, R. L., & Ferreira, L. A. M. (2009). Formation of ion pairing as an alternative to improve encapsulation and stability and to reduce skin irritation of retinoic acid loaded in solid lipid nanoparticles. *International Journal of Pharmaceutics*, *381*(1), 77–83. https://doi.org/10.1016/j.ijpharm.2009.07.025

[25] Chereddy, K. K., Her, C.-H., Comune, M., Moia, C., Lopes, A., Porporato, P. E., Vanacker, J., Lam, M. C., Steinstraesser, L., Sonveaux, P., Zhu, H., Ferreira, L. S., Vandermeulen, G., & Préat, V. (2014). PLGA nanoparticles loaded with host defense peptide LL37 promote wound healing. *Journal of Controlled Release*, *194*, 138–147. https://doi.org/10.1016/j.jconrel.2014.08.016

[26] Akolpoğlu Başaran, D. D., Gündüz, U., Tezcaner, A., & Keskin, D. (2021). Topical delivery of heparin from PLGA nanoparticles entrapped in nanofibers of sericin/gelatin scaffolds for wound healing. *International Journal of Pharmaceutics*, *597*, 120207. https://doi.org/10.1016/j.ijpharm.2021.120207

[27] Byeon, Y., Lee, J.-W., Choi, W. S., Won, J. E., Kim, G. H., Kim, M. G., Wi, T. I., Lee, J. M., Kang, T. H., Jung, I. D., Cho, Y.-J., Ahn, H. J., Shin, B. C., Lee, Y. J., Sood, A. K., Han, H. D., & Park, Y.-M. (2018). CD44-targeting plga nanoparticles incorporating paclitaxel and FAK Sirna overcome chemoresistance in epithelial ovarian cancer. *Cancer Research*, *78*(21), 6247–6256. https://doi.org/10.1158/0008-5472.can-17-3871

Chapter 2

Manuscript: Incorporation of Gentamicin-Encapsulated Poly (lactic-co-glycolic acid) Nanoparticles into Polyurethane/Poly (ethylene oxide) Nanofiber Scaffolds for Biomedical Applications*

Overview

The development of novel wound-dressing materials has attracted significant research interests in recent years. With the advancement of nanofabrication, the application of nanoparticles (NPs) in drug delivery systems has become feasible. However, most existing work focuses on incorporation of metal, metal/semi-metal oxide, or organic particles into nanofiber scaffolds. There has been a lack of work on incorporation of drug-encapsulated polymeric particles into nanofiber scaffolds. In this study, gentamicin-encapsulated poly (lactic-co-glycolic acid) (PLGA) NPs were synthesized via a double emulsion solvent evaporation method. Electrospinning was used to incorporate gentamicin-encapsulated PLGA NPs into nanofiber scaffolds. Atomic force microscopy (AFM), dynamic light scattering, scanning electron microscopy (SEM), ultraviolet-visible spectroscopy (UV-vis), and an agar diffusion method were utilized to characterize the morphologies, release profiles, and antibacterial activities of various gentamicin-loaded PLGA NPs incorporated nanofiber scaffolds. The results indicated the PLGA NPs had a spherical morphology with an average diameter of 130nm. Purification of PLGA NPs was essential to eliminate the residual polyvinyl alcohol (PVA) and to prevent particle agglomeration. The purified PLGA NPs were uniformly and individually incorporated into the polyurethane (PU)/ poly ethenyl oxide (PEO) or PEO-only nanofiber scaffolds, but nearly none into the PU-only fiber scaffolds. PEO served as a continuous phase in the PU/PEO mixture,

* The manuscript has been published by ACS Applied Nano Materials, Aug 2023

which significantly improved the compatibility of PLGA NPs and PU, resulting in a well dispersed distribution of PLGA NPs in the monolithic nanofiber scaffolds. Excellent antibacterial properties against *E.coli* were found in both PU/PEO and PEO nanofiber scaffolds. This study of incorporating gentamicin-encapsulated PLGA NPs into fiber scaffolds provides insights for achieving successful incorporation of drugs-encapsulated polymeric NPs into fiber scaffolds. This offers a promising microfabrication technology for delivery of therapeutic molecules with controlled release for biomedical applications.

Keywords: Double emulsion evaporation, Electrospinning, Poly-lactic-co-glycolic acid (PLGA) nanoparticles, Polyurethane (PU), Poly (ethylene oxide) (PEO), Purification, Wound-dressing materials.

2.1 Introduction

Antibacterial infection treatment on wounds has been of great importance in healthcare and medicines. The application of antibiotics is the most common in wound management [1]. One common approach is topical application because the topical antibiotics act on only the wound sites and result in minimal side effects. Topical antibiotics have usually been paired with wound dressing that helps maximize efficacy of antibacterial activities [2]. Traditional wound dressing is made of woven or nonwoven gauze based on natural and synthetic fibers, providing contamination prevention, hemostasis control, moist maintenance, bacterial infection control, and promotion of wound healing [2][3][4]. With the development of nanotechnology, it demonstrated that molecules and cells have properties of high selectivity and sensitivity, and electrospun nanofibers have been used to create extracellular matrix at the structural and functional levels in which targeted growth factors can be delivered for different cell types to control bacterial infection and retain cellular structures and functions [5][6][7].Recently, an

innovative approach of integration of antibacterial nanoparticles into monolithic nanofiber scaffolds has been investigated due to its advantages of cost-effectiveness, quick response, and structural simplicity. Metal (Cu, Au) [8][9][10][11], metallic oxide (Fe_3O_4, glass particles) [12][13], or extracted bioparticles such as cellulose nanocrystal particles [14][15] incorporated monolithic fiber scaffolds for controlled drug delivery has aroused great interest. For example, silver nanoparticles were incorporated into cotton fibers, which demonstrated great antibacterial activities [16][17][18][19]. Silica nanoparticles encapsulating fluorescein and rhodamine B were integrated into PLGA fibrous scaffolds, demonstrating controlled release of drugs [20][21][22]. Results from Xing's study showed lysophosphatidic acid and zinc oxide nanoparticles were successfully incorporated into nanofibers [23]. However, only a few papers reported incorporation of artificial drug-encapsulated polymeric nanoparticles into monolithic fibers. Many polymers including poly-lactic-co-glycolic acid (PLGA), poly (ethylene oxide) (PEO), polyethylene glycol (PEG), polycaprolactone (PCL), ammonio methacrylate copolymer and polyvinyl alcohol (PVA) have been used in developing nanoparticles and fibrous scaffolds for skin therapeutic treatments due to their distinct advantages such as controlled release rates, contamination prevention, targeted area treatments, and hemostasis control [24][25][26][27][28][29][30]. The primary advantage of polymeric nanoparticles are biocompatibility and biodegradability. Polymeric particles can be decomposed into water and carbon dioxide after being introduced into human metabolism and hence cause no harm to human body. Therefore, polymeric nanoparticles become promising candidates for incorporation with monolithic fibrous scaffolds for wound treatments over inorganic particles or extracted bioparticles.

Double emulsion solvent evaporation and double emulsification-solvent extraction methods have been widely adopted to prepare polymeric particles [31][32][33]. PLGA nanoparticles are attractive owing to their biodegradability, biocompatibility, and nontoxicity [43]. PLGA nanoparticles have been reported in encapsulation of antibiotics, proteins, and small molecules for medical treatment of bacterial infection, cancer, and Alzheimer disease (AD) [28][34][35]. While applications of both nanoparticles and fibrous scaffolds are respectively growing, the integration of nanoparticles into fibrous scaffolds is a novel approach for enhancing drug delivery systems intended for controlled release. For example, Chen et al. reported that Chitosan nanoparticles containing siRNA were integrated into PLGA fibrous scaffolds and investigated their applications in gene disease treatment [36]. Another example is that heparin-encapsulated PLGA nanoparticles with an average size of 100 nm were synthesized and successfully incorporated into sericin/gelatin scaffolds [37].

Although the approach of integrating drug-encapsulated nanoparticles into fibrous scaffolds is attractive, it is yet challenging due to the complexity of microfabrication, particularly at the nanoscale. Morphological results from these studies on incorporation of polymeric particles into fibers were unclear to show either uniform distribution of particles incorporated into fibers, or few particles found on the fiber surfaces. The lack of uniform particle distribution on fibrous scaffolds can significantly reduce the effectiveness of drug delivery and wound management. The challenges lie mainly in synthesis of drug encapsulated nanoparticles within the range of 100 nm, particle purification, and separation after synthesis for nanoparticles well distribution in fibrous scaffolds.

In this paper, we repot a novel microfabrication method derived from Iqbal's work [32] for developing gentamicin- encapsulated PLGA nanoparticles with a range of diameter from 59

nm – 259 nm and an average size of 130 nm, and furthermore uniform incorporation of the nanoparticles into PU/PEO nanofiber scaffolds [30]. Gentamicin is a wide spectrum antibiotic and hence chosen as a model antibiotic in our study. PU has been widely used in developing nanofiber scaffolds for modern wound dressing applications, owing to its excellent biocompatibility and biodegradability [24]. Both the gentamicin-encapsulated PLGA nanoparticles and the PU/PEO nanofiber scaffolds showed controlled release of gentamicin, while the uniform incorporation of the nanoparticle into nanofiber scaffolds was able to prolong the release of gentamicin, suggesting enhanced controlled release profiles. In addition, the nanofiber scaffolds demonstrated significant antibacterial properties against *E. coli* in comparison with control groups. The success of incorporating gentamicin-encapsulated PLGA nanoparticles into nanofiber scaffolds requires precise control of three factors: (1) nanoparticle size; (2) nanoparticle purification; and (3) a continuous phase of nanofibers during the particle synthesis and fiber fabrication. The successful completion of the multi-component system relies on four key steps:

(1) Control of diameters of PLGA NPs (spheres) and nanofiber scaffolds (cylinders);

(2) Purification of PLGA NPs to prevent formulation of nanoparticles clusters;

(3) Incorporation of antibiotics-loaded polymeric PLGA NPs into nanofiber scaffolds;

(4) Dispersion of PLGA NPs on the fiber surface for better uniformity.

2.2 Experimental Section

2.2.1 Materials

Poly (D, L-lactide-co-glycolic acid) (PLGA, lactide: glycolic 75:25, Mw 4000~15000, Sigma-Aldrich) and polyvinyl alcohol（PVA, 99+%, MW 89000~98000, Sigma-Aldrich）were

used in nanoparticle synthesis. Gentamicin sulfate salt (99+%, Sigma-Aldrich) was encapsulated in PLGA nanoparticles. Polyurethane (PU, 90%-100%, SG80A, Lubrizol Corporation) and Poly (ethylene oxide) (PEO, ≥99%, Mw=5000000, Sigma-Aldrich) were used as matrix polymers in electrospinning. Dichloromethane (DCM, Mw=84.93, ≥99.8%, Sigma-Aldrich) was an organic solvent used to create an oil phase in nanoparticles synthesis. Deionized water (Fisher Scientific) was used as an aqueous phase in nanoparticle synthesis as well as in electrospinning. Luria broth (LB), BBL Muller Hinton II Agar, used to grow *E.coli,* was purchased from Becton, Dickinson and Company, Spark, MD. *E.coil* (7.1×10^3 CFU/pellet, ATCC 25922), purchased from MicroBiologics. NaCl (SX0420-1, M=58.44g/mol, Supelco), was used as the dialysis solution. Dialysis tubing (UG281774, 3500 MWCO, 3.7ml/cm) was purchased from SnakeSkin.

2.2.2 Synthesis of PLGA Nanoparticles

A double emulsion solvent evaporation method reported by Sun et al. [38] was adopted to prepare gentamicin-encapsulated PLGA nanoparticles. 200mg PLGA powder in 4ml dichloromethane (DCM), 45mg gentamicin in 0.5ml DI water, and 3% PVA solution were used to form a water-oil-water nanodroplet dispersion. The solution was sonicated and titrated into 25ml 0.1% PVA solution, resulting in an opaque solution. PLGA nanoparticles precipitated after 8-hour solvent evaporation. PVA having hydrophilic and hydrophobic function groups makes it reduce surface tension between phases. In PLGA nanoparticle synthesis, PLGA dissolved in DCM and gentamicin dissolved in water were two immiscible solutions, so it was essential to introduce PVA to reduce surface tension resulting in nanodroplet dispersion. The synthesis procedures with details can be found in Supporting Information S1 and Figure. S1. The obtained PLGA nanoparticles were examined using a scanning electron microscope (SEM, JEOL JSM-6500) to investigate particle morphologies.

2.2.3 PLGA Nanoparticle Purification and Characterizations

The gentamicin-encapsulated PLGA nanoparticles were suspended in the resulting solution likely containing residual PVA and PLGA after the synthesis. Therefore, a purification step was necessary to clean and separate the particles from the suspension. Based on this unique system, a four-step purification method was developed to be able to successfully purify and separate PLGA nanoparticles. DCM was added to the condensed PLGA nanoparticle solution, and the mixture was centrifuged resulting in a multiple phase-separation solution. A detailed description of the purification method can be found in Supporting Information S2. The obtained PLGA nanoparticles were characterized using a Scanning Electron Microscopy (SEM, JEOL JSM-6500), an Atomic Force Microscopy (AFM, XE-70, Park System), and a Dynamic Light Scattering (DLS, Malvern Zetasizer ZS, 633nm red-laser) to examine particle morphology, particle sizes, and size distribution. The purification process was validated via determining the composition of residual solution after purification. Fourier transform infrared (FTIR, Cary 630, Agilent) was used to determine chemical compositions of unpurified PLGA nanoparticle solution, upper and bottom solutions of purified PLGA nanoparticle solution, and pure PVA solution.

2.2.4 Incorporation of PLGA Nanoparticles into Nanofiber Scaffolds

For incorporation of nanoparticles with fibrous scaffolds, electrospinning was an effective approach [20][36][37][38][39]. Therefore, electrospinning was adopted in our experiments to incorporate PLGA nanoparticles with fibers as shown in Figure 2(A). 0.35g of PU was first dissolved in 10ml DCM and 0.2g of PEO was dissolved in 10ml DCM. The PU and PEO solutions were placed on a hot plate with a stirring rate of 450 rads/min overnight, resulting in a

fully combined PU/PEO solution. The PU/PEO solution was then mixed with the PLGA nanoparticle solution with 10 minutes sonication to yield a uniform emulsion solution.

Table 1. Electrospinning solution formulas: #1, purified PLGA NPs + PU; #2, unpurified PLGA NPs + PU; #3, purified PLGA NPs + PU + PEO with a PU/PEO ratio of 0.175; #4, purified PLGA NPs + PU + PEO with a PU/PEO ratio of 0.117; #5, purified PLGA NPs + PEO.

Spinning solution	0.035g/ml PU (ml)	0.2g/ml PEO (ml)	DCM (ml)	Purified PLGA NPs (ml)	Unpurified PLGA NPs (ml)	PU/PEO ratio
#1	5	-	-	3	-	-
#2	5	-	-	-	3	-
#3	5	5	-	3	-	0.175
#4	4	6	-	3	-	0.117
#5	-	5	5	3	-	-

Five emulsion solutions with different compositions shown in Table 1 have been tested for loading efficiency of PLGA nanoparticles into nanofiber scaffolds via electrospinning. The electrospinning with details is described in Supporting Information S3.

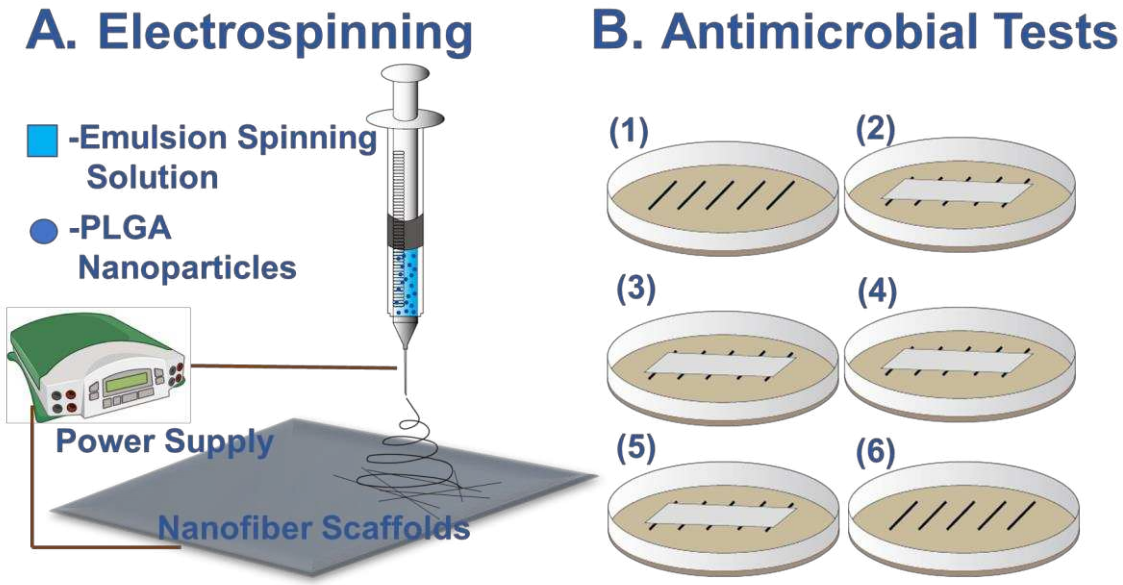

Figure 2. (A) The electrospinning diagram. PLGA nanoparticles mixed with PU/PEO emulsion spinning solution. The spinning parameters were: 20kv spinning voltage, 0.45ml/hour injection rate; 20cm spinning distance. (B) gentamicin encapsulated PLGA nanoparticles incorporated nanofiber scaffolds antibacterial activity tests. (1) *E.coil* controlled samples; (2) aluminum foil controlled sample; (3) PU/PEO nanofiber; (4) PU/PEO-purified particles nanofiber; (5) PEO-purified particles. (6) pure gentamicin-controlled sample.

2.2.5 Gentamicin Release Profiles from Nanoparticles and Nanofiber Scaffolds

Ultraviolet-visible spectroscopy was used for detecting PLGA nanoparticles release profiles [40][41][42][43][44][45]. In the measurement of release profile, a nanoparticle solution was equally distributed into 12 testing tubes. The gentamicin-encapsulated PLGA nanoparticles in each testing tube were allowed to degrade for a given time interval (every hour up to 12 hours). The upper solution was used to be measured at 220 nm using a UV-vis (Agilent Cary 4000) that can determine gentamicin concentrations in the solution. A plot of released gentamicin concentration as a function of time was obtained to demonstrate release profiles of gentamicin. A similar method was used to determine the release profiles of gentamicin from nanofiber scaffolds as well. Five samples of scaffolds with the same mass (0.075g) were prepared. Each sample was fully immersed in a testing tube. After testing tubes were centrifuged, the upper solution in each tube was taken to measure accumulative concentrations of gentamicin. The testing time intervals for scaffold samples were designed at 3 hours, 6 hours, 9 hours, 12 hours, and 18 hours.

2.2.6 Antibacterial Testing

An agar diffusion method derived from the AATCC 100 antimicrobial test method for textile was used to determine the antibacterial properties of the nanofiber scaffolds against *E. coli*. The growth of *E.coli* ATCC25922 is described in details in Supporting Information.

Scaffold samples were prepared first along with a controlled sample which was an aluminum foil specimen without fibers. Scaffold specimens with a dimension of 60mm×10mm and a weight of 0.05g were prepared. 1ml of the 24 hour-broth *E. coil* culture was diluted with 9ml distilled water in a test tube. *E. coil* culture solution was transferred by an inoculum inoculating loop to the sterile agar plate. The loop was swiped over five streaks which were about 60mm in length and 10mm apart from each other covering the central area of the LB-Agar broth petri dishes. Then the fiber specimen was gently pressed transversely across the five inoculum streaks as shown in Figure 2 (B). The petri dishes were placed in an incubator for 18 hours at 37°C. The antibacterial activities of fibers can be measured by the interruption of growth along the streaks of inoculum beneath the specimen, or rather, the clear zone of inhibition beyond its edge. The average width of a zone of inhibition along a streak on each side of the test specimen was calculated using the following equation:

$$W = \frac{T-D}{2} \qquad \text{Equation (1)}$$

where W is the width of clear zone of inhibition, T is the diameter of clear zone of fiber specimen, D is the diameter of the fiber specimen (in mm).

The morphologies of those tested fiber strips were explored via SEM and their properties were compared.

2.3. Results & Discussion

2.3.1 Characterizations of PLGA Nanoparticles

2.3.1.1 Nanoparticle Purification

Nanoparticle purification played an important role in the gentamicin-encapsulated PLGA nanoparticle synthesis. It was challenging to examine unpurified individual nanoparticles in

SEM. The nanoparticles without purification significantly aggregated, resulting in large particle clusters that contained PVA residues on particles surfaces as shown in Figure 3. The PLGA nanoparticles were embedded in the PVA films as shown in Figure 3 (A). Figure 3 (B) illustrates the PLGA nanoparticles embedded in PVA films, resulting in a large cluster. Therefore, the removal of PVA residues from the PLGA nanoparticles was an essential step for further experiments.

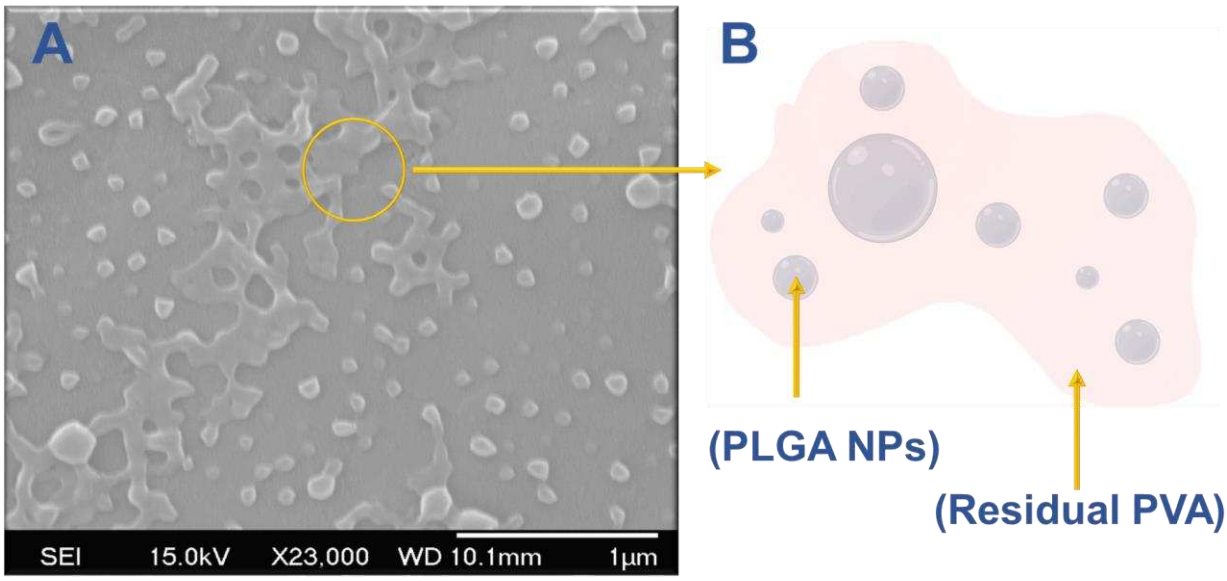

Figure 3. (A) PLGA nanoparticles were embedded in PVA after double emulsion synthesis; (B) PLGA nanoparticles were embedded in PVA films.

Previous studies suggest that centrifugation is usually used to promote clean nanoparticles by facilitating particle precipitation [46][47][48]. However, no precipitation was found in the gentamicin-encapsulated PLGA nanoparticle solutions using centrifugation only as shown in Figure 4 (A)(B), suggesting that nanoparticles were still suspended in the milky solutions. It is likely because the PLGA nanoparticles synthesized in our experiments were too small to be separated from PVA residues only by centrifugal forces.

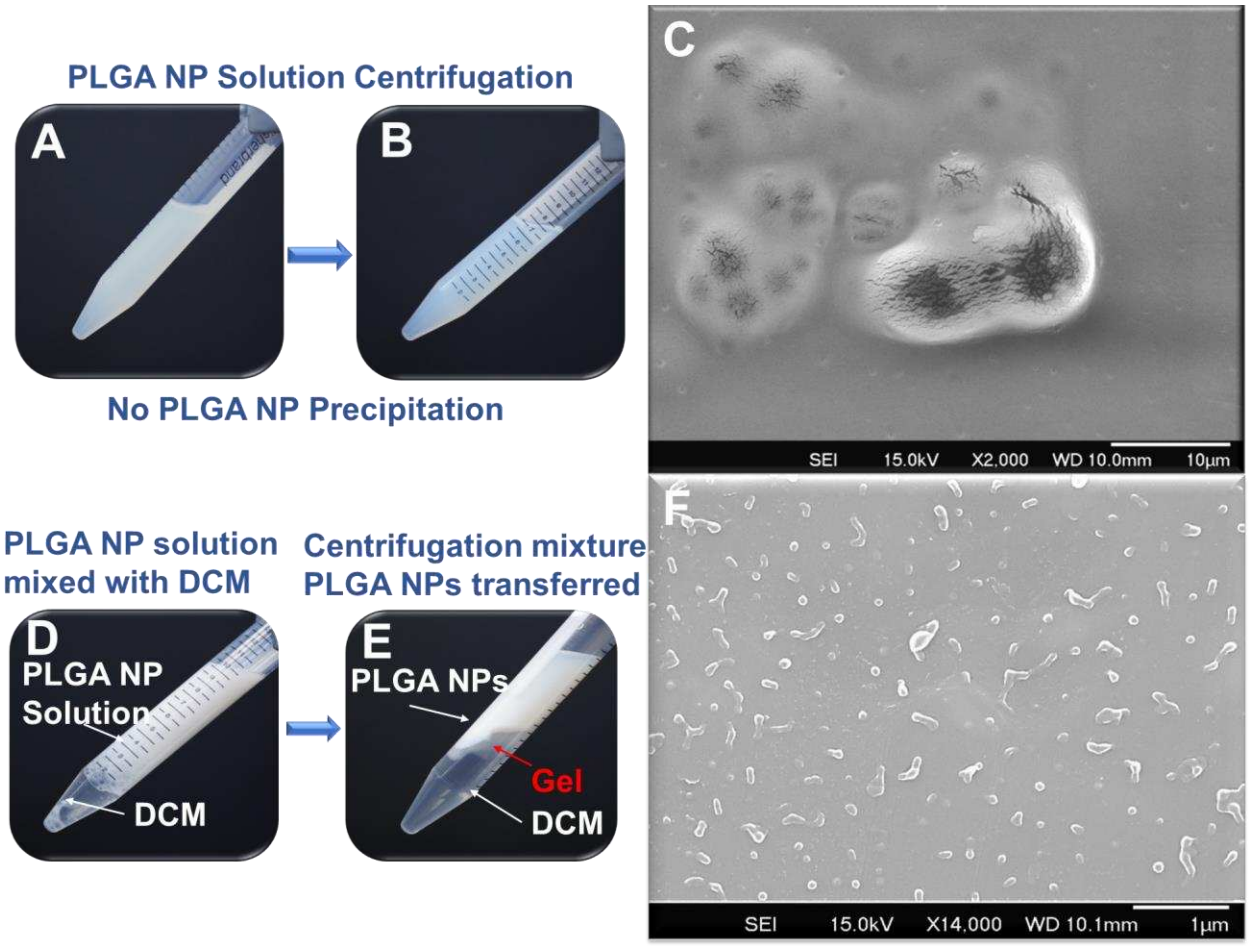

Figure 4. (A)(B) PLGA nanoparticles cannot be separated from the solution via centrifugation due to PLGA nanoparticle small size. (C) SEM image of un-purified PLGA nanoparticles embedded in PVA film. PLGA nanoparticles were piled up into clusters. (D)(E) PLGA nanoparticle solution can be purified via adding DCM to the condensed PLGA nanoparticle solution. The purified particles were in the top layer. (F) SEM image of purified PLGA nanoparticles, PLGA nanoparticles were well dispersed, and most PVA was gotten rid.

When the PVA residues remained in the solution, the PVA formed a film that covered PLGA nanoparticle clusters after water evaporated as shown in Figure 4 (C). The particles clusters were significantly big (approximately 10 µm), which prevented the nanoparticles from being well dispersed in the electrospinning solution and eventually caused a failure of nanoparticle incorporation into fibrous scaffolds. Therefore, the removal of PVA residues from PLGA nanoparticles is necessary for our further experiments. Very few methods have been reported to purify PLGA nanoparticles, especially for gentamicin-encapsulated PLGA

nanoparticles. After a few trials of experiments described in detail in Supporting Information S2 were conducted, a four-step purification method was developed to successfully obtain clean PLGA nanoparticles. The particle solutions after synthesis were first condensed by water evaporation and dialysis. Then, DCM was added to the highly condensed nanoparticle solution and the mixture was centrifuged. Phase separation occurred in the solution, resulting in three layers: DCM layer at the bottom; gel-like PVA layer in the middle; PLGA nanoparticles in aqueous layer on the top, as shown in Figure 4 (D)(E). Individual PLGA nanoparticles were clearly found in SEM images (Figure 4 (F)), suggesting PVA residues were nearly completely removed and hence the PLGA nanoparticles were no longer hidden in clusters, but individually observed in SEM.

Figure 5 showed FTIR spectra analysis confirming that PVA was removed from PLGA nanoparticle solution after going through the four-step purification step. The PVA spectrum showed that PVA had -C-O stretching, -CH bending, -CH stretching, and -OH functional groups which have wavenumber at $1100cm^{-1}$, $1700cm^{-1}$, $2900cm^{-1}$, and $3300cm^{-1}$ respectively. These peaks were found in the particle samples before purification. After purification process, the upper solution which was purified PLGA nanoparticle solution did not show -C-O- stretching and -CH stretching, but the middle solution still had those four function groups. Consequently, PVA can be removed from the PLGA nanoparticle solution after the purification process.

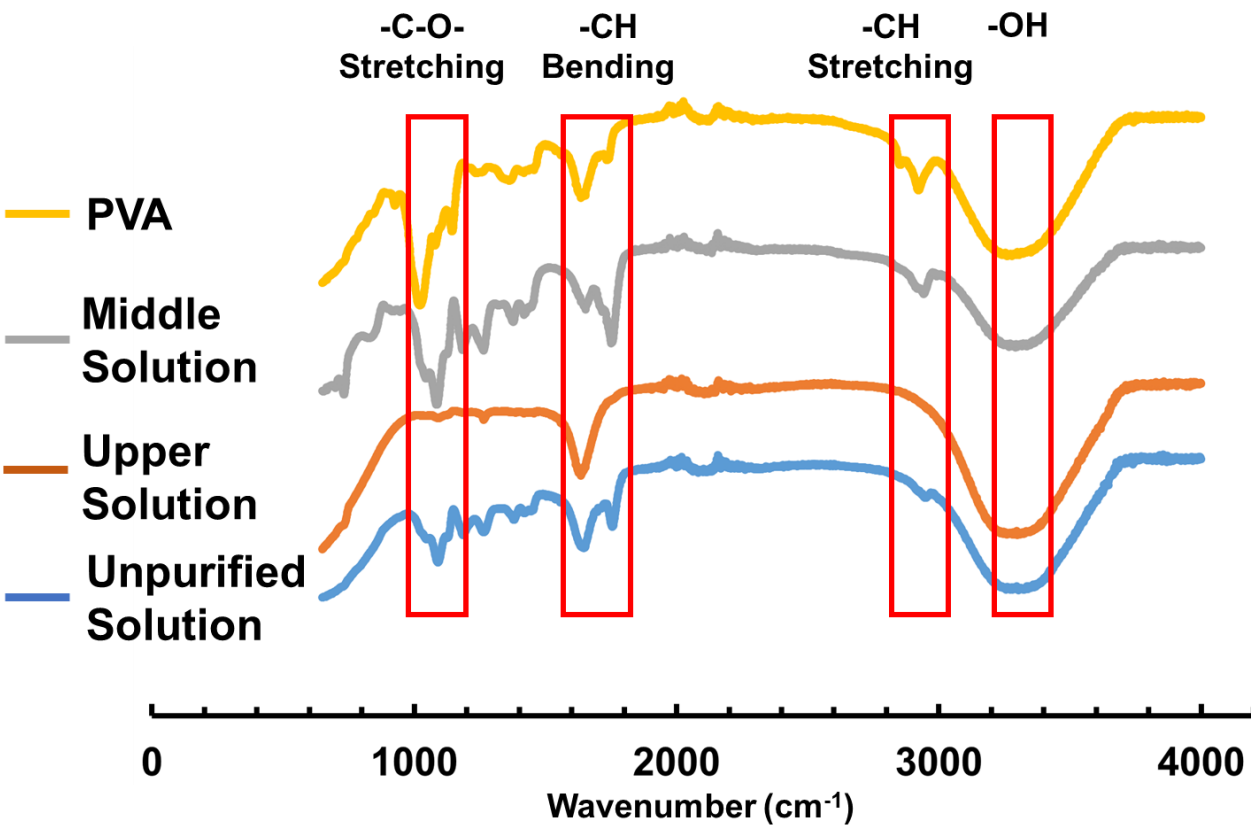

Figure 5. FTIR spectra of unpurified PLGA nanoparticle solution shown as blue line; upper layer solution (purified PLGA nanoparticle solution) shown as orange line; middle layer solution (PVA hydrogel) shown as grey line; pure PVA solution shown as yellow line.

2.3.1.2 Nanoparticle Size Distribution and Morphology

Clean gentamicin-encapsulated PLGA nanoparticles were observed in SEM images as shown in Figure 6 (A)(B). Compared to SEM image, the AFM image provides a high resolution of PLGA nanoparticles, and more information can be acquired. Figure 6 (C) showed a 3-dimensional image of the nanoparticles using an AFM, suggesting spherical structures of the nanoparticles, and most particles have a diameter around 132nm, which agreed with the date acquired from DLS. Particle size distributions of the PLGA nanoparticles obtained from DLS were presented in Figure 6 (D), which was calculated based on the intensity percentage. The particles had a median size of 130 nm and a normal distribution of size ranging from 59 nm to

295 nm with a mode of 132 nm (17 %). The sizes observed in SEM and AFM were in good agreement with DLS measurements. The same synthesis method of spherical gentamicin-encapsulated PLGA nanoparticles was previously reported, however, the particle size was relatively bigger (average 1.2μm) and the particle surface was porous [29]. The porous structure was not visible in the PLGA nanoparticles in the current study likely because either there were no pores, or the pores were too small to be seen.

Molecular weight and monomer ratio of the precursors have been reported to significantly affect nanoparticle size and size distributions [49] [50]. The ratios between oil phase and water phase in the current synthesis method had a great effect on the particle sizes. When the amount of PVA was increased from 2ml to 8ml, the obtained PLGA nanoparticles became bigger, with a size distribution ranging from 120nm to 2μm.

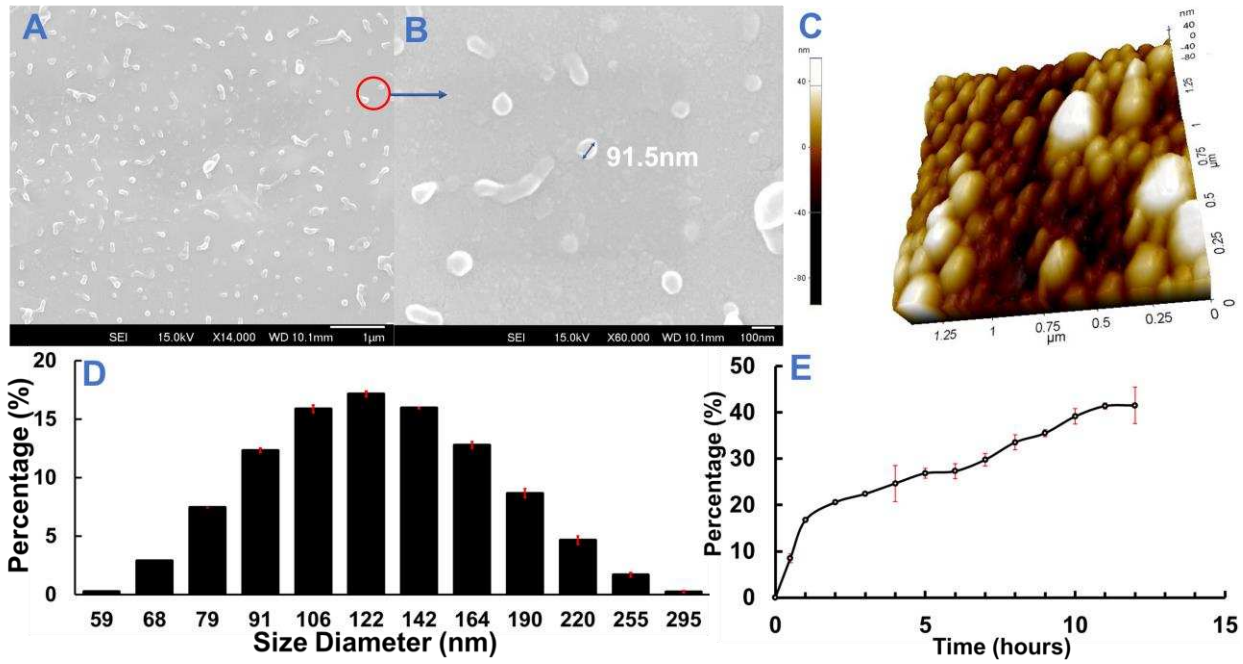

Figure 6. (A) and (B) SEM image of PLGA nanoparticles. PLGA nanoparticles were spherical and not unified. Most particles had a size around 122nm. (C) PLGA nanoparticle 3D structure explored via AFM. (D) PLGA nanoparticles had a wide range of diameter, and the average size of PLGA nanoparticle was 130nm. Most PLGA nanoparticles had a size around 122nm accounting for 17.2%. (E) Accumulative gentamicin amount percentage diagram. At the first 1 hours, 16.7% of gentamicin was released.

2.3.1.3 Profiles of Gentamicin Release from PLGA Nanoparticles

A gentamicin release profile is presented in Figure 6 (E). It shows the accumulative amount of the released gentamicin in 12 hours. The profile showed that about 16.7% of gentamicin was released during the first 1 hour, which was considered as the burst effect. A slow increase continued after the burst, followed by a plateau of release rate. The release profile was in good agreement with the results previously reported [38]. There are four widely accepted hypothesized release mechanisms which are diffusion, convection, osmotic pumping, and degradation. According to literature, a considerable amount of gentamicin was released at the early release stage due to the burst effect, and a controlled release profile was followed. In the first one and half hours, the release profile had a zero-order release, which was ascribed to the releasing of gentamicin on particle surfaces and large concentration of difference between core of particle and outer matrix [51][52].

The results demonstrated that the gentamicin was successfully encapsulated in PLGA nanoparticles that provided controlled release of gentamicin.

2.3.2 Nanofiber Scaffolds Incorporated with PLGA Nanoparticles

Successful incorporation of drugs into nanofibers is critical in developing fibrous dressing materials as an effective topical approach of wound care and management. The incorporation of particles into fibers in our study was focused on introducing gentamicin-encapsulated PLGA nanoparticles into nanofiber scaffolds made by biodegradable and biocompatible polyurethane (PU) and polyethylene oxide (PEO).

2.3.2.1 PU + PLGA Nanoparticles

Gentamicin-encapsulated PLGA nanoparticles with purification and without purification were mixed with PU solutions, respectively, to be fabricated via electrospinning. Figure 7

showed the morphology of the electrospun PU fibers. First, significant particle clusters were found on the irregular fibers that were obtained when unpurified PLGA nanoparticles were used, as shown in Figure 7 (A)(B). It was because unpurified PLGA nanoparticles were in cluster due to PVA residue covering on surface, which was discussed in the previous section of nanoparticle purification. The relatively big size of particle clusters (around 10μm) prevented incorporation of particles into the fibers. Particle clusters were found on the electrospinning collector, rather than on fibers.

Figure 7 (C)(D) showed the fiber morphology when purified PLGA nanoparticles were used in the electrospinning, for which more regular fibers were obtained (both size and surface morphology). However, unfortunately, no PLGA nanoparticles were found to be incorporated with fibers (inside or on fiber surface). A significant number of particles were found on the fiber collector. The fibers were smaller in diameter (1.5μm) than those obtained with unpurified nanoparticles. The purification step primarily removed extra PVA residue covering on the particles after the synthesis, resulting in clean PLGA nanoparticles in an aqueous solution. When the particle aqueous solution was mixed with the PU that was dissolved in DCM for electrospinning, significant phase separation occurred due to no surfactant in the electrospinning solution. PLGA nanoparticles were not compatible with PU solution even after the mixture was sonicated for 15 minutes. The upper PLGA nanoparticle solution formed into about 1mm droplets floating in the PU solution after sonication. When the PU was stretched into fibers, the PLGA nanoparticles were not incorporated with PU fibers. Therefore, it is critical to improve the compatibility between PLGA nanoparticles and PU fibers. Previous studies suggested that a continuous phase could be added in electrospinning solutions to improve compatibility between polymeric nanoparticles and nanofibers [53][54]. The continuous phase is able to reduce surface

tension between the aqueous and oil phases, which was essential for incorporating particles with fibers.

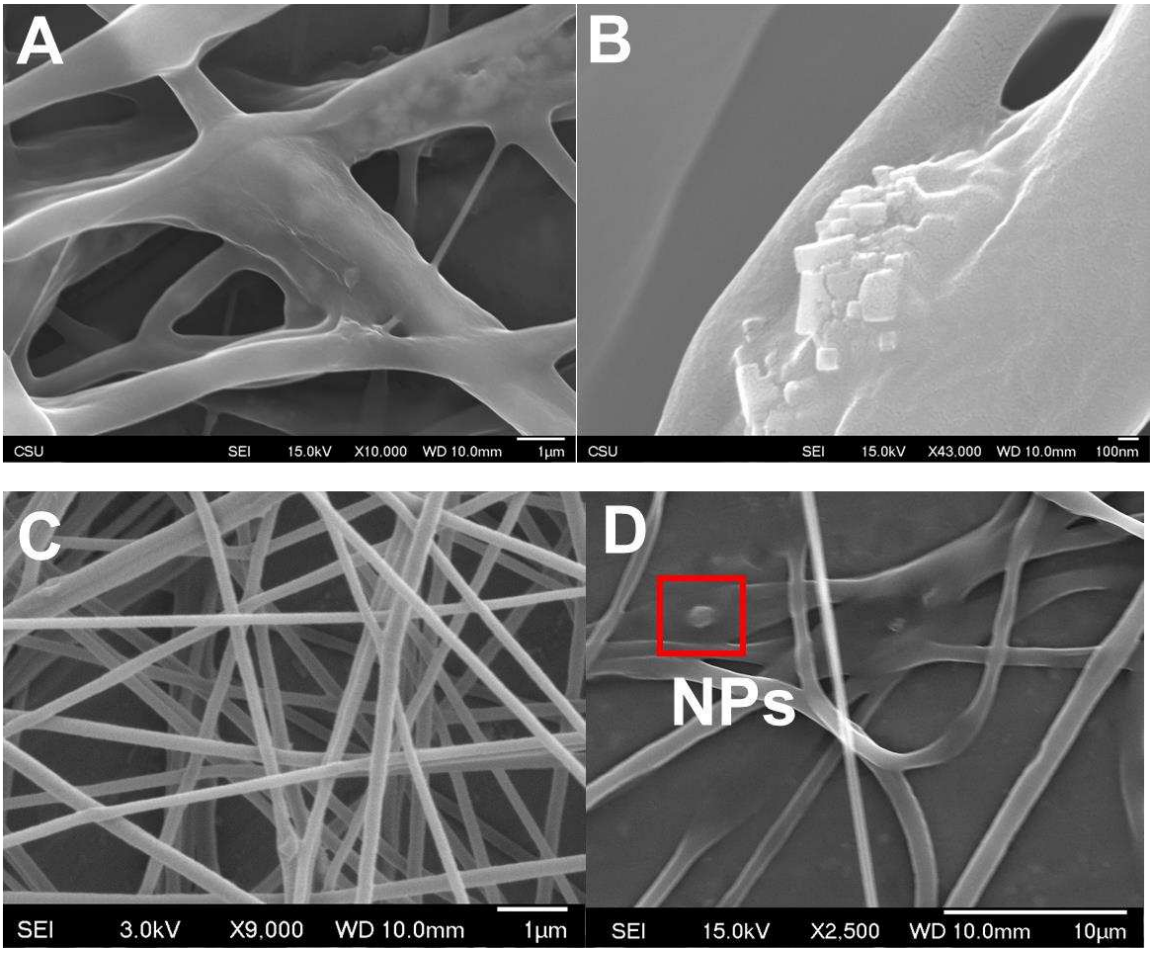

Figure 7. (A) and (B) PU-unpurified PLGA nanoparticle fiber. The spinning solution consisted of 10ml of 0.035g/ml PU solution mixed with 5ml PLGA nanoparticle solution which had residual PVA. PLGA nanoparticles were piled up into clusters. (C) and (D) SEM images of PU- purified PLGA nanoparticle fibers. The spinning solution consisted of 5ml of 0.035g/ml PU solution mixed with 3ml extracted PLGA nanoparticle solution. No PLGA nanoparticles incorporated with fibers.

2.3.2.2 PU/PEO + Purified PLGA Nanoparticles

electrospinning as a continuous phase to fabric nanofiber composites [56]. Therefore, PEO was chosen to be the continuous phase for the PU and PLGA nanoparticle solution used in electrospinning. Figure 8(A)(B) showed the fiber morphology, suggesting a significant improvement was made for incorporating PLGA nanoparticles into the nanofiber scaffolds.

PLGA nanoparticles were visibly distributed in the PU-PEO fibers that were uniform and had an average diameter around 1.5μm.

No visible droplets were found on the collected nanofiber mats, suggesting the majority of the nanoparticles were incorporated with fibers. When the ratio of PEO to PU in the spinning solution was increased (the ratio of PU to PEO decreased from 0.175 to 0.117 as shown in Figure 7), the PLGA nanoparticle loading efficiency was increased, resulting in more particles in the fibers with large diameter (2.5μm) as shown in Figure 7 (C)(D). Therefore, the increase of PEO in the spinning solution was able to improve the loading efficiency of PLGA nanoparticles into nanofiber scaffolds.

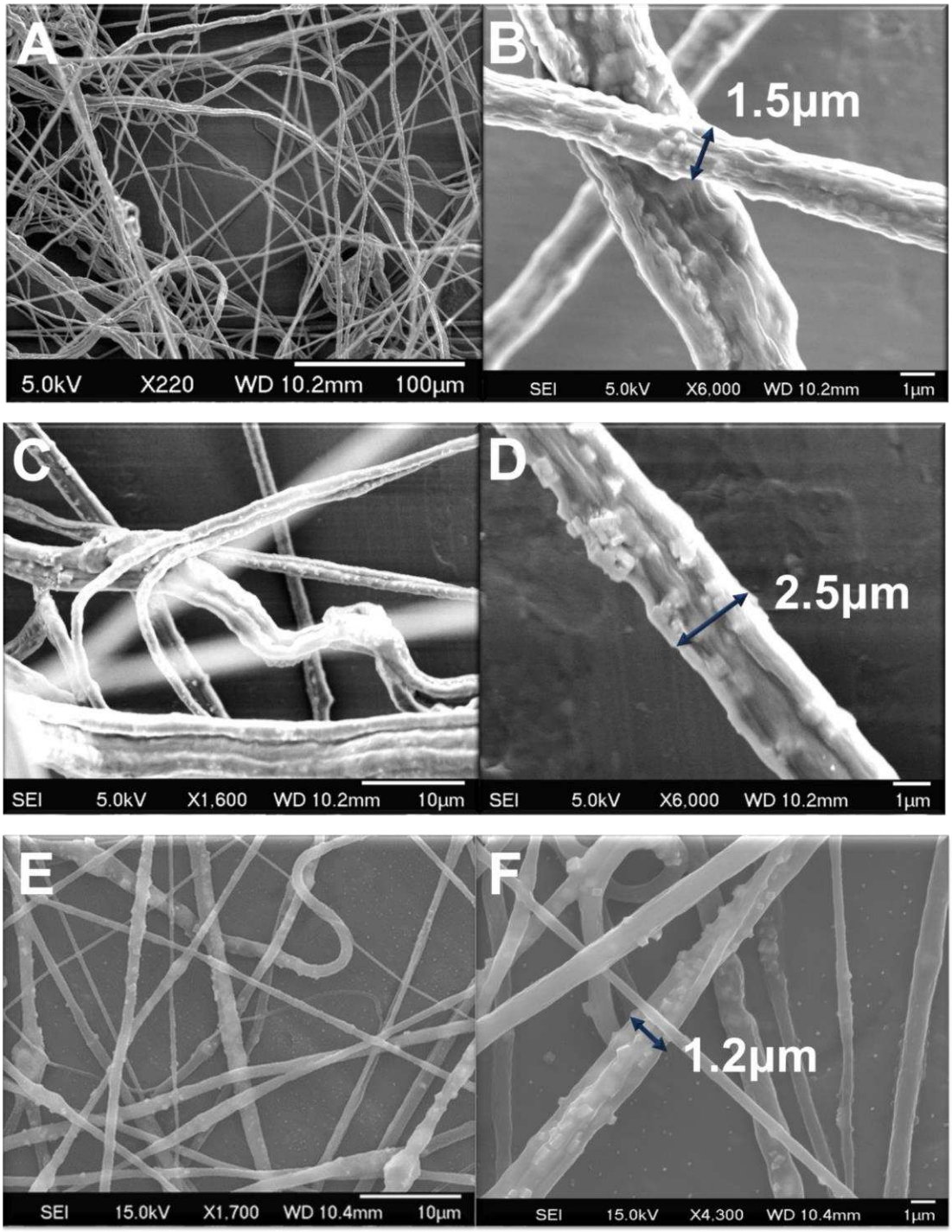

Figure 8. (A) and (B) 0.175 (PU/PEO)-Purified PLGA nanoparticle nanofiber scaffolds. PLGA nanoparticles were incorporated with fibers of which had a diameter of 1.5µm. (C) and (D) 0.117 (PU/PEO)- Purified PLGA nanoparticles nanofiber scaffolds. Plenty of PLGA nanoparticles were incorporated with fibers of which had a diameter of 2.5µm. Load efficiency increased with diameter increasing. (E) and (F) PEO-Purified PLGA Nanoparticle nanofiber scaffolds. PLGA nanoparticles were incorporated and well distributed. Scaffolds had an average size of 1.2µm.

2.3.3 Profiles of Gentamicin Release from Nanofiber Scaffolds

The gentamicin release profile of the PU/PEO fibers obtained using 4ml of 0.035g/ml PU, 6ml of 0.2g/ml PEO, and 3ml purified PLGA nanoparticles solution was presented by the accumulative concentration of gentamicin as shown in Figure 9.

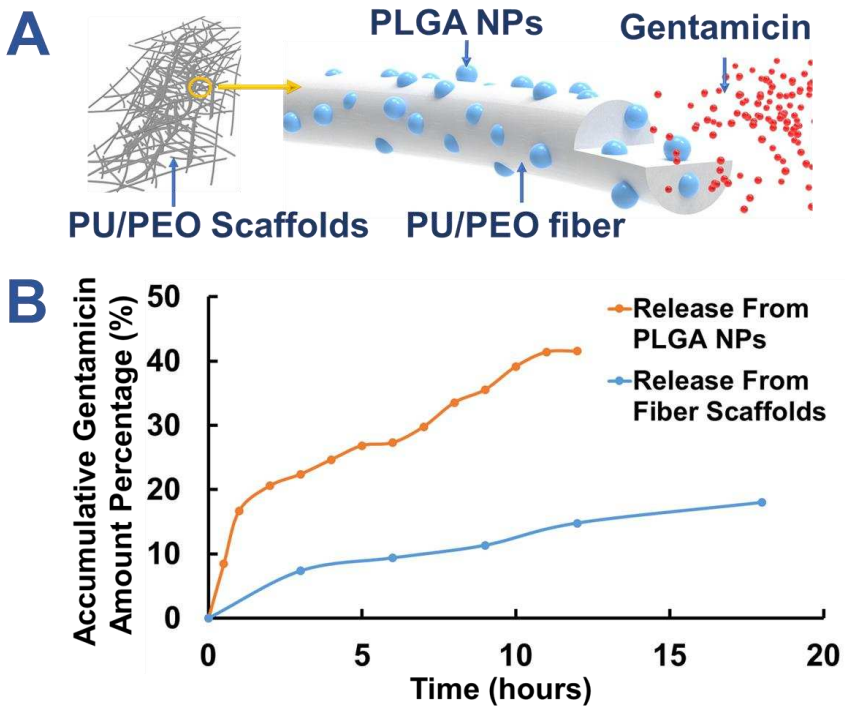

Figure 9. (A) A 3D diagram showed gentamicin release from the PLGA nanoparticle incorporated fibers. (B) Release profile of fibers. Accumulative gentamicin amount percentage released from NPs and fibers scaffolds at different time.

Figure 9(A) showed a diagram of gentamicin released from the PLGA nanoparticles incorporated fiber scaffolds. 7.37% gentamicin released during the first 3 hours due to the burst effect in Figure 9 (B). The increase of concentration slowed down after 3 hours. At 20 hours approximately, the accumulated gentamicin concentration was 16.7%, equivalent to that of the gentamicin-encapsulated PLGA nanoparticles at the first 1 hour shown in Figure 6 (E). Compared with the release profile of gentamicin-encapsulated PLGA nanoparticles, the release rate of the nanofiber scaffolds was prolonged, suggesting enhanced controlled release rates

which could be of great interest in chronic wound care and treatment. The promising results suggested that the strategy of incorporating gentamicin-encapsulated PLGA nanoparticles into nanofiber scaffolds was effective for controlled release of drugs. According to literature, a considerable amount of gentamicin should be released to control bacterial infection. Therefore, focusing on the first 12-hour release profile instead of studying the whole release process is meaningful and helpful for improving PLGA nanoparticle loaded nanofiber scaffold properties.

2.3.4 Antibacterial Activities

Antibacterial activities were measured by quantification of bacterial inhibition using an agar diffusion method in petri dishes where different nanofiber scaffolds were tested. Bacterial inhibition was virtually shown in Figure 10-(A) and was quantified in Figure 10-(B). The three controlled samples are *E. coil* growing in a petri dish (Figure 10-A-(1), *E. coli* growing on aluminum foil (Figure 10-A-(2)), and no *E. coli* growing on gentamicin-coated surface (Figure 10-A-(6)). The nanofiber scaffolds for testing included PU/PEO fibers without PLGA nanoparticles (Figure 10-A-(3)), PU/PEO fibers with PLGA nanoparticles (Figure 10-A-(4)), and PEO fibers with PLGA nanoparticles (Figure 10-A-(5)). When no PLGA nanoparticles were incorporated in PU/PEO fibers, such fibers had no ability to control bacterial growth, as shown in Figure 10-A-(3).

In a comparison, Figure 10-A-(4) and Figure 10-A-(5) illustrated significant bacterial inhibition indicated by clear zones next to the nanofiber scaffolds. Figure 10-(B) shows, the average diameter of the clear zone for PU-PEO with PLGA nanoparticles (gentamicin) and PEO with PLGA nanoparticles (gentamicin) were 5.17mm and 7.16mm, respectively, suggesting that the PEO nanofibers had a better antibacterial activity than the PU-PEO nanofibers. An observation relevant to the better antibacterial activity was that the majority of PEO fibers were

dissolved. It was because PEO is highly hydrophilic and easily dissolved in water that is present in the LB medium used in *E. coli* growth. When the fibers dissolved, gentamicin was quickly released, resulting in high bacterial inhibition.

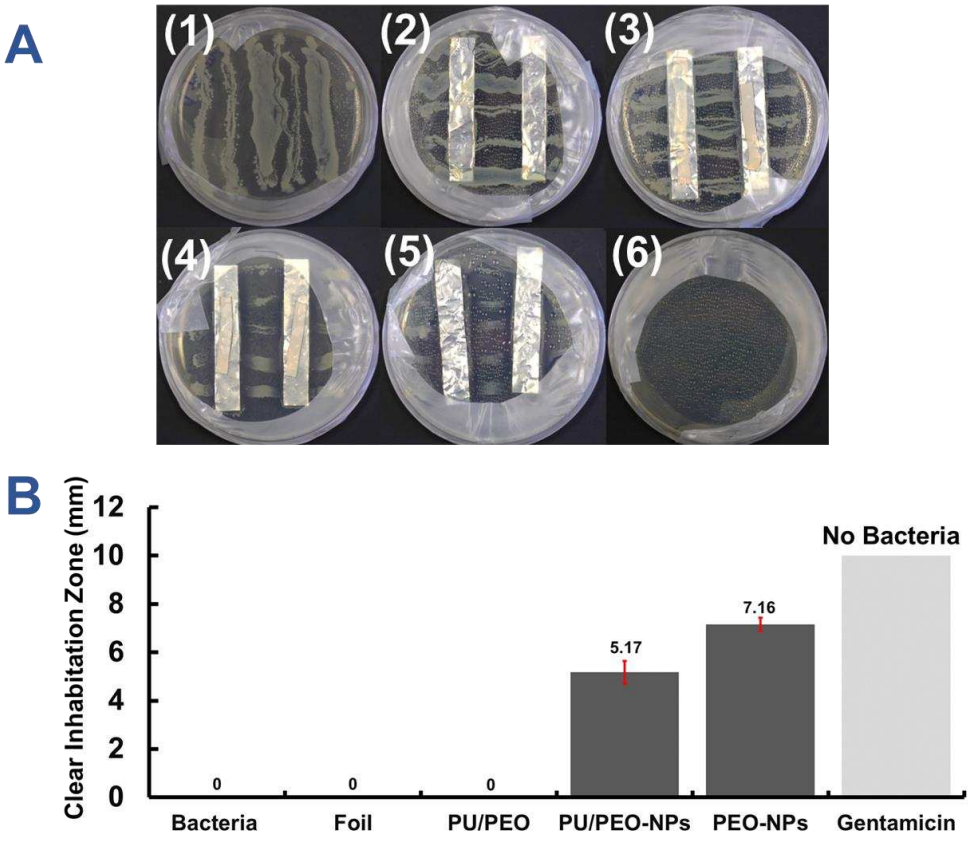

Figure 10. (A) Antibacterial activity tests. (1) *E.coil* controlled sample; (2) Aluminum foil controlled sample; (3) PU/PEO controlled sample; (4) PU/PEO-PLGA Nanoparticles; (5) PEO-PLGA Nanoparticles; (6) pure gentamicin controlled sample. (B) The average inhabitation diameter of each sample.

The current antibacterial testing results suggested that gentamicin can be released from PLGA nanoparticles incorporated PU/PEO fiber scaffolds for controlling *E. coli* affections. However, quantitative analysis for bacterial affection controlling such as the minimum inhibitory concentration (MIC) and the minimum bactericidal concentration (MBC) will be studied in our future work.

2.4 Conclusions

In this paper, a facile but effective fabrication procedure of multifunctional and antibacterial nanofiber scaffolds along with biomedical applications is presented. This involves gentamicin-loaded PLGA NPs being incorporated into PU/PEO nanofiber scaffolds via electrospinning. Gentamicin-loaded PLGA NPs with an average diameter of 130 nm were prepared via a double emulsion solvent evaporation method. A purification process was performed to remove PVA residuals and hence prevent PLGA NPs agglomeration on fiber scaffolds. PEO was chosen as a continuous phase in the electrospinning solution, which provided a compatible environment for PU and PLGA NPs and helped stabilize the incorporation process. Release profiles and antibacterial tests proved that gentamicin released from PLGA NPs (incorporated with PU/PEO fiber scaffolds) was able to inhibit *E.coli* growth. It was also observed antibiotics release rates were well controlled.

The work presented in this paper has significantly extended the usage of polymeric particles as drug carriers, compared to the existing work that used only metal, metal/semi-metal oxide, or organic particles. The described methodology and procedure enable us to incorporate drug-encapsulated PLGA particles into PU/PEO fiber scaffolds at the nano-meter scale. As is well known, PU is a readily available and widely used polymer. Our findings are expected to promote development of cost-effective drug delivery systems for smart wound-dressing materials and broader biomedical applications.

Loading efficiency and capacity of gentamicin or other drugs are affected by various factors. Quantification of these aspects will be helpful for further medical applications. This will be reported in our future work. Release profiles of gentamicin from PLGA NPs in our *in vivo* experiments demonstrate some burst effects in the early stage. Further study of release

mechanisms and characterizations of drug release from PLGA NPs is an interesting topic, especially when it is integrated with the *in silico* approach that involves mathematical modeling and numerical simulations.

2.5 References

[1] Stebbins, N. D., Ouimet, M. A., & Uhrich, K. E. (2014). Antibiotic-containing polymers for localized, sustained drug delivery. *Adv. Drug Deliv. Rev.*, *78*, 77–87. https://doi.org/10.1016/j.addr.2014.04.006

[2] Farahani, M., & Shafiee, A. (2021). Wound healing: From passive to smart dressings. *Adv. Healthc. Mater.*, *10*(16), 2100477. https://doi.org/10.1002/adhm.202100477

[3] Stashak, T. S., Farstvedt, E., & Othic, A. (2004). Update on wound dressings: Indications and best use. *Clin. Tech. Equine Pract.*, *3*(2), 148–163. https://doi.org/10.1053/j.ctep.2004.08.006

[4] Boateng, J. S., Matthews, K. H., Stevens, H. N. E., & Eccleston, G. M. (2008). Wound healing dressings and Drug Delivery Systems: A Review. *J. Pharm. Sci.*, *97*(8), 2892–2923. https://doi.org/10.1002/jps.21210

[5] Khalil, H., Cullen, M., Chambers, H., Carroll, M., & Walker, J. (2015). Elements affecting wound healing time: An evidence-based analysis. *Wound Repair Regen.*, *23*(4), 550–556. https://doi.org/10.1111/wrr.12307

[6] Chouhan, D., Dey, N., Bhardwaj, N., & Mandal, B. B. (2019). Emerging and innovative approaches for wound healing and skin regeneration: Current status and advances. *Biomaterials*, *216*, 119267. https://doi.org/10.1016/j.biomaterials.2019.119267

[7] Ashok, K., Babu, M., Kavitha, G., Jeyanthi, R., Ladchumananandasivam, R., da Silva, O., & Manikandan, E. (2022). Fabrication of textile-based scaffolds using electrospun nanofibers for biomedical applications. Jayakumar, R. *Electrospun Polymeric Nanofibers: Insight into fabrication techniques and biomedical applications,* Cham, Switzerland, April.

[8] Fan, J., Cheng, Y., & Sun, M. (2020). Functionalized gold nanoparticles: Synthesis, properties and biomedical applications. *Chem. Rec.*, *20*(12), 1474–1504. https://doi.org/10.1002/tcr.202000087

[9] Pourjavadi, A., Doroudian, M., Ahadpour, A., & Azari, S. (2019). Injectable Chitosan/κ-carrageenan hydrogel designed with au nanoparticles: A conductive scaffold for tissue engineering demands. *Int. J. Bio. Macromol.*, *126*, 310–317. https://doi.org/10.1016/j.ijbiomac.2018.11.256

[10] Liverani, L., Reiter, T., Zheng, K., Neščáková, Z., & Boccaccini, A. R. (2022). Copper-doped cotton-like malleable electrospun bioactive glass fibers for wound healing applications. *Mater. Lett.: X*, *14*, 100133. https://doi.org/10.1016/j.mlblux.2022.100133

[11] Noori, F., Neree, A. T., Megoura, M., Mateescu, M. A., & Azzouz, A. (2021). Insights into the metal retention role in the antibacterial behavior of montmorillonite and cellulose tissue-supported copper and silver nanoparticles. *RSC Adv.*, *11*(39), 24156–24171. https://doi.org/10.1039/d1ra02854e

[12] Zhang, H., Xia, J., Pang, X., Zhao, M., Wang, B., Yang, L., Wan, H., Wu, J., & Fu, S. (2017). Magnetic nanoparticle-loaded electrospun polymeric nanofibers for tissue engineering. *Mater. Sci. Eng. C*, *73*, 537–543. https://doi.org/10.1016/j.msec.2016.12.116

[13] Luginina, M., Schuhladen, K., Orrú, R., Cao, G., Boccaccini, A. R., & Liverani, L. (2020). Electrospun PCL/PGS composite fibers incorporating bioactive glass particles for soft tissue engineering applications. *Nanomater.*, *10*(5), 978. https://doi.org/10.3390/nano10050978

[14] Seddiqi, H., Oliaei, E., Honarkar, H., Jin, J., Geonzon, L. C., Bacabac, R. G., & Klein-Nulend, J. (2021). Cellulose and its derivatives: Towards biomedical applications. *Cellulose*, *28*(4), 1893–1931. https://doi.org/10.1007/s10570-020-03674-w

[15] Norrrahim, M. N., Nurazzi, N. M., Jenol, M. A., Farid, M. A., Janudin, N., Ujang, F. A., Yasim-Anuar, T. A., Syed Najmuddin, S. U., & Ilyas, R. A. (2021). Emerging development of nanocellulose as an antimicrobial material: An overview. *Mater. Adv.*, *2*(11), 3538–3551. https://doi.org/10.1039/d1ma00116g

[16] Chen, C.-Y., & Chiang, C.-L. (2008). Preparation of cotton fibers with antibacterial silver nanoparticles. *Mater. Lett.*, *62*(21-22), 3607–3609. https://doi.org/10.1016/j.matlet.2008.04.008

[17] Perelshtein, I., Applerot, G., Perkas, N., Guibert, G., Mikhailov, S., & Gedanken, A. (2008). Sonochemical coating of silver nanoparticles on textile fabrics (nylon, polyester and cotton) and their antibacterial activity. *Nanotechnology*, *19*(24), 245705. https://doi.org/10.1088/0957-4484/19/24/245705

[18] Ravindra, S., Murali Mohan, Y., Narayana Reddy, N., & Mohana Raju, K. (2010). Fabrication of antibacterial cotton fibres loaded with silver nanoparticles via "Green approach." *Colloids Surf. A: Physicochem. Eng. Asp.*, *367*(1-3), 31–40. https://doi.org/10.1016/j.colsurfa.2010.06.013

[19] Qian, Y., Zhou, X., Zhang, F., Diekwisch, T. G., Luan, X., & Yang, J. (2019). Triple PLGA/PCL scaffold modification including silver impregnation, collagen coating, and electrospinning significantly improve biocompatibility, antimicrobial, and osteogenic properties for orofacial tissue regeneration. *ACS Appl. Mater. Interfaces*, *11*(41), 37381–37396. https://doi.org/10.1021/acsami.9b07053

[20] Song, B., Wu, C., & Chang, J. (2012). Dual drug release from Electrospun Poly (lactic-co-glycolic acid)/mesoporous silica nanoparticles composite mats with distinct release profiles. *Acta Biomater.*, *8*(5), 1901–1907. https://doi.org/10.1016/j.actbio.2012.01.020

[21] Su, X., Kuang, L., Battle, C., Shaner, T., Mitchell, B. S., Fink, M. J., & Jayawickramarajah, J. (2014). Mild two-step method to construct DNA-conjugated silicon nanoparticles: Scaffolds for the detection of MicroRNA-21. *Bioconjug. Chem.*, *25*(10), 1739–1743. https://doi.org/10.1021/bc5004026

[22] Carpenter, A. W., Slomberg, D. L., Rao, K. S., & Schoenfisch, M. H. (2011). Influence of scaffold size on bactericidal activity of nitric oxide-releasing silica nanoparticles. *ACS Nano*, *5*(9), 7235–7244. https://doi.org/10.1021/nn202054f

[23] Xing, D., Zuo, W., Chen, J., Ma, B., Cheng, X., Zhou, X., & Qian, Y. (2022). Spatial delivery of triple functional nanoparticles via an extracellular matrix-mimicking coaxial scaffold synergistically enhancing bone regeneration. *ACS Appl. Mater. Interfaces*, *14*(33), 37380–37395. https://doi.org/10.1021/acsami.2c08784

[24] Kamble, P., Sadarani, B., Majumdar, A., & Bhullar, S. (2017). Nanofiber based drug delivery systems for skin: A promising therapeutic approach. *J. Drug Deliv. Sci. Tech.*, *41*, 124–133. https://doi.org/10.1016/j.jddst.2017.07.003

[25] Evrova, O., Hosseini, V., Milleret, V., Palazzolo, G., Zenobi-Wong, M., Sulser, T., Buschmann, J., & Eberli, D. (2016). Hybrid randomly electrospun poly (lactic-*co*-glycolic acid):poly(ethylene oxide) (PLGA:PEO) fibrous scaffolds enhancing myoblast differentiation and alignment. *ACS Appl. Mater. Interfaces*, *8*(46), 31574–31586. https://doi.org/10.1021/acsami.6b11291

[26] Kamyar, N., Greenhalgh, R. D., Nascimento, T. R., Medeiros, E. S., Matthews, P. D., Nogueira, L. P., Haugen, H. J., Lewis, D. J., & Blaker, J. J. (2018). Exploiting inherent instability of 2D black phosphorus for controlled phosphate release from blow-spun poly(lactide-*co*-glycolide) nanofibers. *ACS Appl. Nano Mater.*, *1*(8), 4190–4197. https://doi.org/10.1021/acsanm.8b00938

[27] Kaur, J., Singh, R. R., Khan, E., Kumar, A., & Joshi, A. (2021). Piperine-loaded plga nanoparticles as cancer drug carriers. *ACS Appl. Nano Mater.*, *4*(12), 14197–14207. https://doi.org/10.1021/acsanm.1c03664

[28] Ambrogio, M. W., Toro-González, M., Keever, T. J., McKnight, T. E., & Davern, S. M. (2020). Poly(lactic-*co*-glycolic acid) nanoparticles as delivery systems for the improved administration of Radiotherapeutic Anticancer Agents. *ACS Appl. Nano Mater.*, *3*(11), 10565–10570. https://doi.org/10.1021/acsanm.0c02350

[29] Zafar, N., Bitar, A., Valour, J. P., Fessi, H., & Elaissari, A. (2016). Elaboration of ammonio methacrylate copolymer based spongy cationic particles via double emulsion solvent evaporation process. *Mater. Sci. Eng. C*, *61*, 85–96. https://doi.org/10.1016/j.msec.2015.12.017

[30] Iqbal, M., Valour, J.-P., Fessi, H., & Elaissari, A. (2015). Preparation of biodegradable PCL particles via double emulsion evaporation method using ultrasound technique. *Colloid Polym. Sci.*, *293*(3), 861–873. https://doi.org/10.1007/s00396-014-3464-9

[31] Zafar, N., Agusti, G., Fessi, H., & Elaissari, A. (2016). Elaboration of sponge-like biodegradable cationic particles via double-emulsion solvent evaporation. *J. Dispers. Sci. Technol.*, *38*(4), 577–583. https://doi.org/10.1080/01932691.2016.1182923

[32] Iqbal, M., Zafar, N., Fessi, H., & Elaissari, A. (2015). Double emulsion solvent evaporation techniques used for drug encapsulation. *Int. J. Pharm.*, *496*(2), 173–190. https://doi.org/10.1016/j.ijpharm.2015.10.057

[33] Baena-Aristizábal, C. M., Fessi, H., Elaissari, A., & Mora-Huertas, C. E. (2016). Biodegradable microparticles preparation by double emulsification—solvent extraction method: A systematic study. *Colloids Surf. A: Physicochem. Eng. Asp.*, *492*, 213–229. https://doi.org/10.1016/j.colsurfa.2015.11.067

[34] Anand, B., Wu, Q., Nakhaei-Nejad, M., Karthivashan, G., Dorosh, L., Amidian, S., Dahal, A., Li, X., Stepanova, M., Wille, H., Giuliani, F., & Kar, S. (2022). Significance of native PLGA nanoparticles in the treatment of alzheimer's disease pathology. *Bioact. Mater.*, *17*, 506–525. https://doi.org/10.1016/j.bioactmat.2022.05.030

[35] Byeon, Y., Lee, J.-W., Choi, W. S., Won, J. E., Kim, G. H., Kim, M. G., Wi, T. I., Lee, J. M., Kang, T. H., Jung, I. D., Cho, Y.-J., Ahn, H. J., Shin, B. C., Lee, Y. J., Sood, A. K., Han, H. D., & Park, Y.-M. (2018). CD44-targeting plga nanoparticles incorporating paclitaxel and FAK Sirna overcome chemoresistance in epithelial ovarian cancer. *Cancer Res.*, *78*(21), 6247–6256. https://doi.org/10.1158/0008-5472.can-17-3871

[36] Chen, M., Gao, S., Dong, M., Song, J., Yang, C., Howard, K. A., Kjems, J., & Besenbacher, F. (2012). Chitosan/siRNA nanoparticles encapsulated in PLGA nanofibers for siRNA delivery. *ACS Nano*, *6*(6), 4835–4844. https://doi.org/10.1021/nn300106t

[37] Akolpoğlu Başaran, D. D., Gündüz, U., Tezcaner, A., & Keskin, D. (2021). Topical delivery of heparin from PLGA nanoparticles entrapped in nanofibers of sericin/gelatin scaffolds for wound healing. *Int. J. Pharm.*, *597*, 120207. https://doi.org/10.1016/j.ijpharm.2021.120207

[38] Sun, Y., Bhattacharjee, A., Reynolds, M., & Li, Y. V. (2021). Synthesis and characterizations of gentamicin-loaded poly-lactic-co-glycolic (PLGA) nanoparticles. *J. Nanopart. Res.*, *23*(8). https://doi.org/10.1007/s11051-021-05293-3

[39] Tyo, K. M., Lasnik, A. B., Zhang, L., Mahmoud, M., Jenson, A. B., Fuqua, J. L., Palmer, K. E., & Steinbach-Rankins, J. M. (2020). Sustained-release Griffithsin nanoparticle-fiber composites against HIV-1 and HSV-2 infections. *J. Cont. Rel.*, 321, 84–99. https://doi.org/10.1016/j.jconrel.2020.02.006

[40] Chigumira, W., Maposa, P., Gadaga, L. L., Dube, A., Tagwireyi, D., & Maponga, C. C. (2015). Preparation and evaluation of pralidoxime-loaded PLGA nanoparticles as potential carriers of the drug across the Blood Brain Barrier. *J. Nanomater.*, *2015*, 1–5. https://doi.org/10.1155/2015/692672

[41] Wiegand, I., Hilpert, K., & Hancock, R. E. (2008). Agar and broth dilution methods to determine the minimal inhibitory concentration (MIC) of antimicrobial substances. *Nat. Protoc.*, *3*(2), 163–175. https://doi.org/10.1038/nprot.2007.521

[42] Pillai, R. R., Somayaji, S. N., Rabinovich, M., Hudson, M. C., & Gonsalves, K. E. (2008). Nafcillin-loaded plga nanoparticles for treatment of osteomyelitis. *Biomed. Mater.*, *3*(3), 034114. https://doi.org/10.1088/1748-6041/3/3/034114

[43] Posadowska, U., Brzychczy-Wloch, M., & Pamula, E. (2015). Injectable gellan gum-based nanoparticles-loaded system for the local delivery of vancomycin in osteomyelitis treatment. *J. Mater Sci: Mater. Med.*, *27*(1). https://doi.org/10.1007/s10856-015-5604-2

[44] Vidawati, S., Barbosa, S., Taboada, P., Villar, E., Topete, A., & Mosquera, V. (2018). Study of human serum albumin-spions loaded plga nanoparticles for protein delivery. *Adv. Biol. Chem.*, *08*(05), 91–100. https://doi.org/10.4236/abc.2018.85008

[45] Harguindey, A., Domaille, D. W., Fairbanks, B. D., Wagner, J., Bowman, C. N., & Cha, J. N. (2017). Synthesis and assembly of Click-nucleic-acid-containing peg–plga nanoparticles for DNA delivery. *Adv. Mater.*, *29*(24), 1700743. https://doi.org/10.1002/adma.201700743

[46] Gaumet, M., Gurny, R., & Delie, F. (2007). Fluorescent biodegradable PLGA particles with narrow size distributions: Preparation by means of selective centrifugation. *Int. J. Pharm.*, *342*(1-2), 222–230. https://doi.org/10.1016/j.ijpharm.2007.05.001

[47] Pieper, S., & Langer, K. (2017). Doxorubicin-loaded PLGA nanoparticles - A systematic evaluation of preparation techniques and parameters∗. *Mater. Today Proc.*, *4*. https://doi.org/10.1016/j.matpr.2017.09.185

[48] McCall, R. L., & Sirianni, R. W. (2013). PLGA nanoparticles formed by single- or double-emulsion with Vitamin E-TPGS. *J. Vis. Exp.*, (82). https://doi.org/10.3791/51015

[49] Park, K., Skidmore, S., Hadar, J., Garner, J., Park, H., Otte, A., Soh, B. K., Yoon, G., Yu, D., Yun, Y., Lee, B. K., Jiang, X., & Wang, Y. (2019). Injectable, long-acting PLGA formulations: Analyzing PLGA and understanding Microparticle Formation. *J. Cont. Rel.*, *304*, 125–134. https://doi.org/10.1016/j.jconrel.2019.05.003

[50] Kohno, M., Andhariya, J. V., Wan, B., Bao, Q., Rothstein, S., Hezel, M., Wang, Y., & Burgess, D. J. (2020). The effect of PLGA molecular weight differences on risperidone release from Microspheres. *Int. J. Pharm.*, *582*, 119339. https://doi.org/10.1016/j.ijpharm.2020.119339

[51] Narasimhan, B., & Langer, R. (1997). Zero-order release of micro- and macromolecules from polymeric devices: The role of the burst effect. *J. Cont. Rel.*, *47*(1), 13–20. https://doi.org/10.1016/s0168-3659(96)01611-2

[52] Huang, X., & Brazel, C. S. (2001). On the importance and mechanisms of burst release in matrix-controlled drug delivery systems. *J. Cont. Rel.*, *73*(2–3), 121–136. https://doi.org/10.1016/s0168-3659(01)00248-6

[53] Cho, H. K., Cho, K. S., Cho, J. H., Choi, S. W., Kim, J. H., & Cheong, I. W. (2008). Synthesis and characterization of PEO–PCL–peo triblock copolymers: Effects of the PCL chain length on the physical property of W1/o/W2 multiple emulsions. *Colloids Surf. B: Biointerfaces*, *65*(1), 61–68. https://doi.org/10.1016/j.colsurfb.2008.02.017

[54] Zou, S., Lv, R., Tong, Z., Na, B., Fu, K., & Liu, H. (2019). In situ hydrogen-bonding complex mediated shape memory behavior of PAA/PEO blends. *Polymer*, *183*, 121878. https://doi.org/10.1016/j.polymer.2019.121878

[55] Alexandridis, P., & Alan Hatton, T. (1995). Poly (ethylene oxide)・poly (propylene oxide)・poly (ethylene oxide) block copolymer surfactants in aqueous solutions and at interfaces: Thermodynamics, structure, dynamics, and modeling. *Colloids Surf. A: Physicochem. Eng. Asp.*, *96*(1-2), 1–46. https://doi.org/10.1016/0927-7757(94)03028-x

[56] Xu, Y., Zou, L., Lu, H., & Kang, T. (2017). Effect of different solvent systems on PHBV/PEO electrospun fibers. *RSC Adv.*, *7*(7), 4000–4010. https://doi.org/10.1039/c6ra26783a

[57] Darvish, A., Goyal, G., Aneja, R., Sundaram, R. V., Lee, K., Ahn, C. W., Kim, K.-B., Vlahovska, P. M., & Kim, M. J. (2016). Nanoparticle mechanics: Deformation Detection

Via Nanopore resistive pulse sensing. *Nanoscale*, *8*(30), 14420–14431. https://doi.org/10.1039/c6nr03371g

Chapter 3

Manuscript: Mathematical Modeling and Numerical Simulations for Drug Release from PLGA Particles *

Overview

Poly lactic-co-glycolic acid (PLGA) is a copolymer that has demonstrated great potential in the development of novel drug delivery systems. This paper first discusses synthesis procedures and properties of PLGA micro/nanoparticles (MPs/NPs) and then examines mechanisms of drug release from PLGA particles. For the core-shell structure of reservoir-type PLGA MPs/NPs, diffusion through the polymeric shell is identified as the main mechanism of drug release. A time-dependent diffusion equation is used to model release from homogeneous spherical particles. Finite volume schemes are developed for the radial diffusion model. Numerical results and in vitro experiment data are discussed.

Keywords: Core-shell structure; Diffusion; Drug release; Finite volume schemes; Microparticles and nanoparticles; PLGA (poly lactic-co-glycolic acid)

3.1 Introduction

Polymers have been used in the pharmaceutical industry for several decades due to their biocompatible, biodegradable, and nontoxic properties [1,3,5,7,9,19,22]. A considerable amount of research has been devoted to the roles of poly-lactic-co-glycolic-acid (PLGA), poly-ethylene-oxide (PEO), and polyethylene glycol (PEG) in drug delivery. PLGA has shown great potential in making drug delivery systems. It was approved by FDA as a material for therapeutic devices

*The manuscript has been published by International Conference on Computational Science 2023, Prague Czechia.

due to its biocompatibility and biodegradability [2,10,15,24]. After PLGA is introduced to the human metabolism system, it can decompose into carbon dioxide and water, causing no harm to human bodies.

PLGA can be formed into particles at the micro- or nano-meter level and various shapes, e.g., slabs, cylinders, or spheres with therapeutic agents (drugs) encapsulated. The drugs will be released later in a controlled manner. Applications of PLGA MPs/NPs for control of bacterial infection and cures of Alzheimer's disease and breast cancer can be found in [2,10,15].

Four major mechanisms and three main release stages have been identified for drug release from PLGA micro- or nanoparticles [16,17,18].

(1) Diffusion through the polymeric shell.

(2) Convection through the pores in the polymeric shell.

(3) Osmotic pumping.

(4) Degradation.

Diffusion is the major mechanism observed in the early stage [14]. Development of mathematical models for drug release from porous polymer systems dates back to the early 1980s, see [6] and references therein. Back then, the focus was on finding series solutions and then approximation for short time behaviors, usually under the perfect sink condition, see [12] and references therein. Effects of variable boundary conditions and distribution of particle size on release behaviors were also investigated [12]. For diffusion-controlled release from reservoir or matrix systems, a summary of the series solutions was given in [14] for slabs, cylinders, and spheres. This approach is still very useful as demonstrated in a recent work [4] using series expansion in terms of eigenfunctions to investigate drug delivery from a multilayer spherical

capsule. Finite element methods were investigated in [20,23] for diffusional drug release from complex matrix systems. All these demonstrate that mathematical models are helpful for the design of new drug delivery systems [11].

The rest of this paper is organized as follows. Section 2 briefly describes a procedure for synthesis of PLGA particles and how drug, e.g., gentamicin, is encapsulated into PLGA MPs/NPs. Section 3 discusses properties of PLGA particles and commonly observed release mechanisms of drug release from PLGA MPs/NPs. Section 4 examines mathematical modeling for drug release from PLGA particles. Section 5 develops a numerical method for the radial diffusion equation that models release from spherical particles with the core-shell structure. Section 6 discusses numerical results and experimental data. The paper is concluded with some remarks in Section 7.

3.2 PLGA Nanoparticles Synthesis and Drug Encapsulation

Various techniques have been used in preparation of PLGA MPs/NPs and encapsulation of drugs [3,7,10,22]. Gentamicin is a commonly used drug encapsulated in PLGA particles. This is finished through a synthesis procedure based on a double emulsion evaporation method [16] as shown in Figure 13. Different solutions for emulsion are prepared first. These include, for instance,

—— 100 mg PLGA dissolved in 6 ml dichloromethane (DCM) as the oil phase;

—— 20 mg gentamicin dissolved in water as the aqueous phase 1;

——12% PVA solution as the aqueous phase 2.

The synthesis procedure contains 4 steps.

(i) Oil phase (PLGA/DCM) was mixed with aqueous phase 1 (gentamicin/water), yielding a primary emulsion solution.

(ii) Sonication was applied to the mixture for 3 minutes with a 35% amplitude.

(iii) Double-emulsion nano-droplets were formed via mixing primary emulsion solution with aqueous phase 2 (PVA/water);

(iv) The double-emulsion nano-droplet solution was allowed to evaporate for 6 hours, then PLGA NPs precipitated.

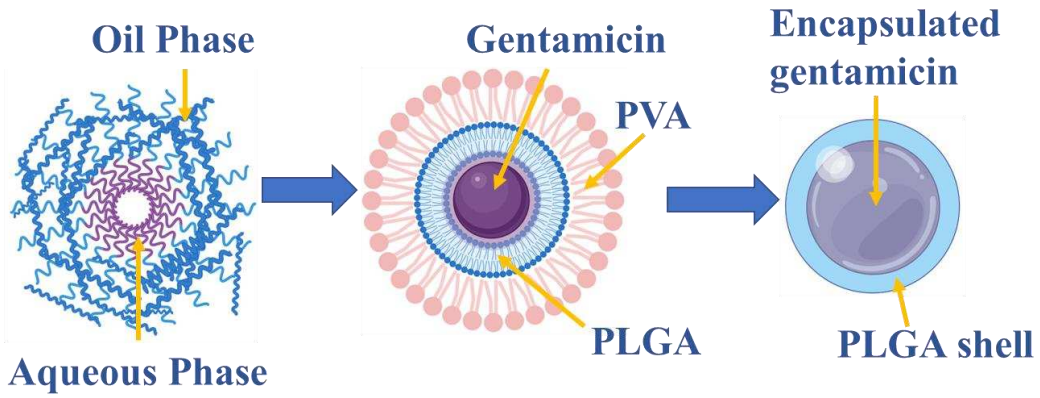

Fig. 13. An illustration of synthesis PLGA micro-/nano-particles and encapsulation of drug gentamicin.

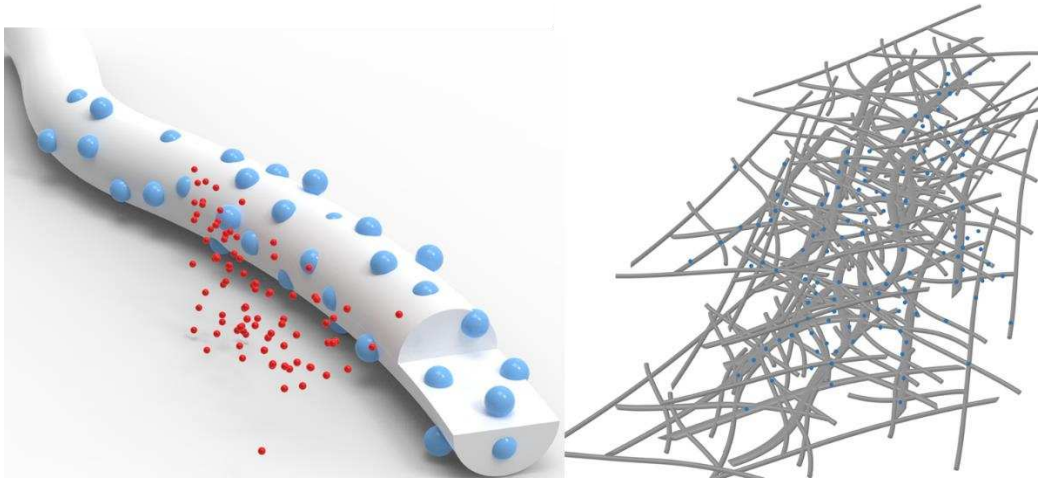

Fig. 14. An illustration of drug gentamicin being encapsulated in PLGA nanoparticles (PU-PEO nanofiber scaffolds).

Electron-spinning is an effective way to incorporate NPs into fibers as shown in Figure 14. Solutions of 0.35g PU dissolved in 10ml DCM and 0.2g PEO dissolved in 10ml DCM are prepared first. Then PU and PEO solution were mixed with PLGA NP solutions for 10-minute sonication to yield an emulsion solution. A scanning electron microscopy (SEM) image of gentamicin-encapsulated PLGA NPs is shown in Figure 15. The core-shell structure and porous shells can be clearly observed.

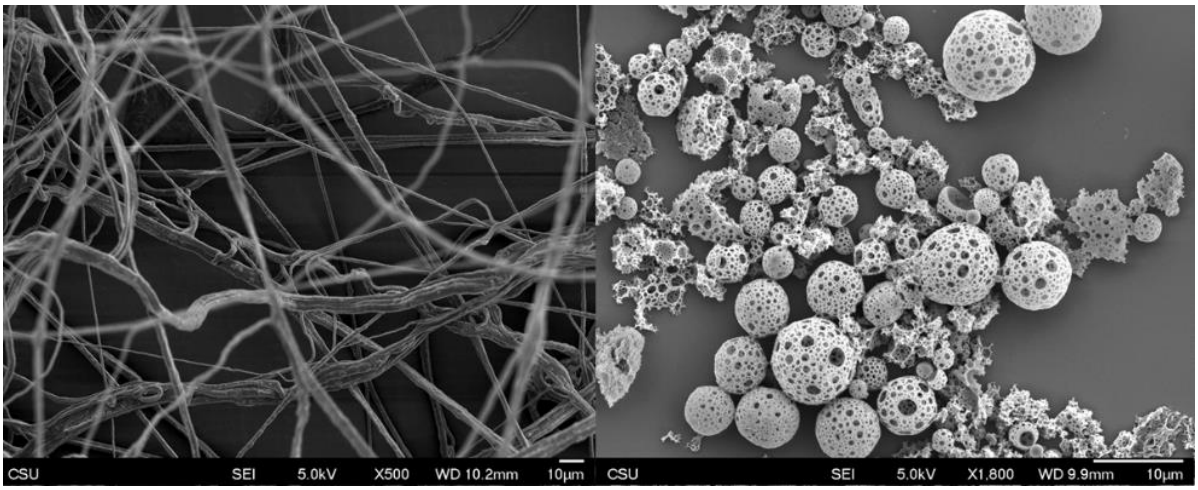

Fig. 15. *Left panel*: A scanning electron microscopy (SEM) image of gentamicin encapsulated PLGA NPs with PU-PEO fiber; *Right panel*: An SEM image of PLGA NPs with porous shells.

According to SEM images, PLGA nanoparticles had three different morphologies on PU-PEO nanofiber scaffolds, which were in the fibers, on the fibers, and partially inlay the fibers.

3.3 Properties and Release Mechanisms of PLGA NPs

With the synthesis procedure discussed in Section 2, PLGA particles are mostly in the spherical shape, as shown in Figure 3 right panel. Shown in Figure 16 is a distribution of the diameters of PLGA particles from a particular experiment when the PLGA concentration was at 16.7 mg/ml.

A summary of PLGA particles average size, thickness, number of PLGA MPs/NPs and estimated loading gentamicin concentration is given in Table 2. Major mechanisms of drug release from PLGA particles, as listed in Table 3 have been identified in the literature [16-18]. An illustration of the major mechanisms in the process of drug release from PLGA particles is also provided in Figure 17.

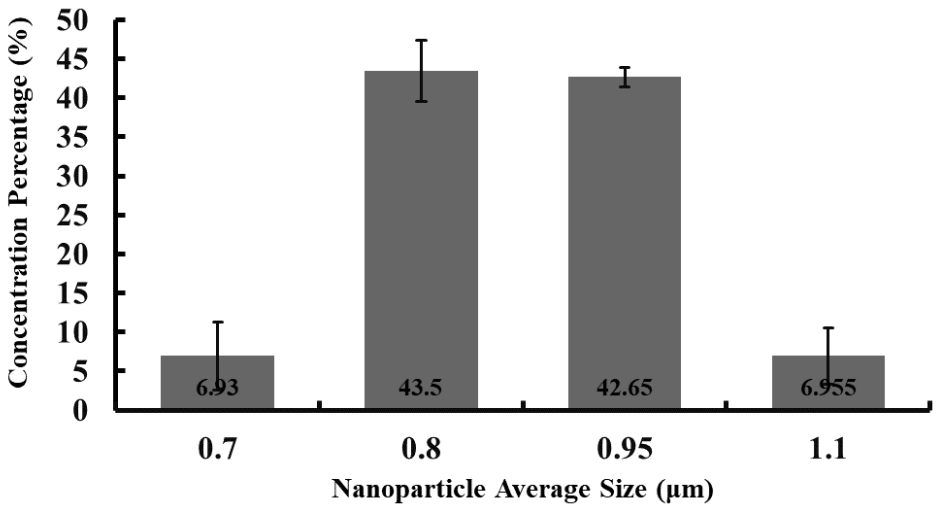

Fig. 16. Size (diameter) distribution of PLGA particles from an *in vitro* experiment.

A summary of PLGA nanoparticles average size, thickness, number of PLGA NPs and estimated loading gentamicin concentration is shown in Table 1.

Table 2. Properties of PLGA particles & drug gentamicin observed in five experiments

PLGA concentration (m*g/ml*)	Yield rate (%)	Average diameter (μm)	Thickness (μm)	PLGA NPs (#)	Gentamicin initial concentration (mg/ml)
13.3	68.34%	1.5	0.21	5.78×10^7	0.0768
15.0	58.89%	1.6	0.48	3.58×10^7	0.0621
16.7	96.33%	1.0	0.06	4.77×10^8	0.0177
18.3	32.12%	1.8	0.17	6.19×10^7	0.0297
20.0	38.16%	2.4	0.20	3.18×10^7	0.0224

Table 3. Summary of drug release mechanisms from PLGA particles

Mechanisms	Description
Diffusion thru polymeric shell	Early stage of release process, burst effect
Convection thru pores	Through the porous shells
Osmotic pumping	Due to concentration gradient
Degradation	Degradation of NPs

Major mechanisms of drug release from PLGA particles, as listed in Table 3 have been identified in the literature [16-18]. An illustration of the four major mechanisms in the process of drug release from PLGA particles is also provided in Figure 17.

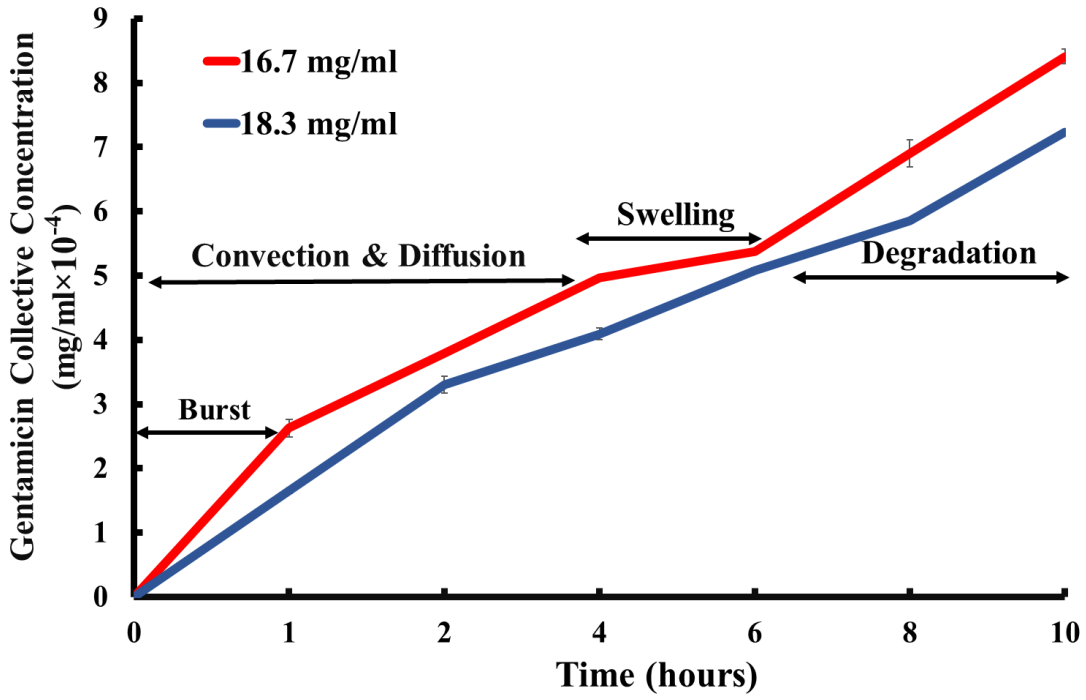

Fig. 17. An illustration of major mechanisms for drug release from PLGA particles.

3.4 Mathematical Modeling for Drug Release from PLGA Nanoparticles

3.4.1 A Model for Radial Diffusion in Polymeric Shells

We follow the approaches and major assumptions in [14]. Specifically,

(i) PLGA MPs/NPs are formed as reservoir devices for drug delivery;

(ii) The drug solution inside the core is a **constant activity resource**;

(iii) The PLGA MPs/NPs have a core-shell structure, in particular, the inner and outer radius are r_a; r_b;

(iv) The polymeric shell is porous and homogeneous, drug is diffused through this shell, the diffusivity is a positive constant D;

(v) For the early stage of the diffusion process, the drug concentration at the inner membrane (r_a) is maintained as a constant;

Shown in Figure 18 is an illustration of the spherical core-shell structure of a typical PLGA particle.

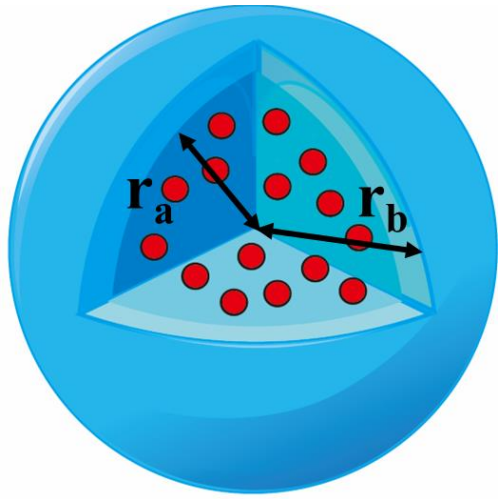

Fig. 18. An illustration of the spherical core-shell structure of a typical PLGA particles

Based on Fick's 2nd law [13-14], we write down a time-dependent diffusion equation in the radial direction with a constant diffusivity as below.

$$\begin{cases} \dfrac{\partial c}{\partial t} = \dfrac{D}{r^2}\dfrac{\partial}{\partial r}\left(r^2\dfrac{\partial c}{\partial r}\right), r \in [r_a, r_b], t \in (0, T] \\ Boundary\ Conditions \\ Initial\ Conditions \end{cases} \quad (2)$$

For the above simple model, the early work focused on finding series solutions. For a special case with a constant initial condition and a constant Dirichlet boundary condition, see [12] for a series solution. [14] summarized the classical work up to Year 2012 and provided a nice overview of various models of dosage forms and their series solutions.

As in vitro experiments for investigation of drug-release from PLGA particles are expensive and vary with lab conditions, the *in-silico* approach with numerical simulations will offer meaningful alternative/supplementary data to experiment results. This relies on accurate and efficient numerical methods for solving the differential equations boundary initial value problems.

3.4.2 Other Existing Mathematical Models

There exist a good number of mathematical models for drug release from PLGA or more generally polymeric devices, depending on what mechanisms are being considered, e.g., diffusion, convection, swelling, and degradation. The popular ones are the 0th order, 1st order, Higuchi, and Korsmeyer-Peppas models, according to ChatGPT.

The Peppas equation shown below applies to non-swellable matrix systems in the early stage [11-12]:

$$\frac{M_t}{M_\infty} = At^\beta \quad (3)$$

where M_t is the accumulative mass of the drug released up to time t, M_∞ is the total mass released up to time infinity, A; β are positive constants. In particular, β = 0.50 for slabs, β = 0.45

for cylindrical particles, β = 0.43 for spherical particles. It is also mentioned that, if 0.50/0.45/0.43 < β < 1.00, the diffusion is anomalous, i.e., non-Fickian. This simple exponential relation was elaborated in [12] and further justified in [11].

For drug release from non-swellable polymeric devices (reservoir or matrix), a summary of mathematical models can be found in [14]. In particular, for a spherical particle of the reservoir type with a core-shell structure under the assumption of constant activity source, there holds:

$$M_t = 4\pi DKc_s \frac{r_a r_b}{r_b - r_a} t \qquad (4)$$

where D is the drug diffusivity, K is a drug partition parameter, c_s is the solubility concentration, r_a; r_b are the inner and outer radii, respectively, and t is time. See [14] p.355. We will fit our experimental data with this model later.

3.5 Numerical Simulations for Diffusion-controlled Release

In this section, we develop efficient numerical schemes for solving the radial diffusion equation that models drug diffusion through the polymeric shell of sphere-shaped PLGA particles.

3.5.1 Node-oriented Finite Volume Schemes for Spherical Diffusion

In this subsection, we develop a mass-conservative scheme for the spherical diffusion problem, which was motivated by the control volume method in [21]. We consider a constant radial diffusion equation with a source term.

$$\frac{\partial u}{\partial t} = \frac{D}{r^2}\frac{\partial}{\partial r}\left(r^2 \frac{\partial u}{\partial r}\right) + f(r,t) \qquad (5)$$

which can be rewritten as

$$r^2\frac{\partial u}{\partial t} - D\frac{\partial}{\partial r}\left(r^2\frac{\partial u}{\partial r}\right) = r^2 f(r,t) \qquad (6)$$

Let $0 < r_a < r_b$ be the inner and outer radii of a spherical shell. Consider a uniform partition $r_a = r_1 < \cdots < r_n = r_b$ with $h = (r_a - r_b)/(n-1)$ being the mesh size. For node r_i, we consider the control volume $[r_i - \frac{h}{2}, r_i + \frac{h}{2}]$. This will be a half volume when $i = 1$ or $i = n$.

Integrating the LHS of Equation (6) over the control volume, we obtain

$$\int_{r_{i-\frac{1}{2}}}^{r_{i+\frac{1}{2}}} r^2\frac{\partial u}{\partial t}dr = \frac{\partial}{\partial t}\left(\int_{r_{i-\frac{1}{2}}}^{r_i} r^2 u dr + \int_{r_i}^{r_{i+\frac{1}{2}}} r^2 u dr\right) \qquad (7)$$

Consider the integrand $w(r) = r^2u(r,t)$ in the above integrals. We approximate its derivatives in the half volumes $[r_i - \frac{h}{2}, r_i]$ and $[r_i, r_i + \frac{h}{2}]$, respectively, to obtain:

$$w'(r_i) \approx \frac{r_i^2 u_i - r_{i-1}^2 u_{i-1}}{h}, \quad w'(r_i) \approx \frac{r_{i+1}^2 u_{i+1} - r_i^2 u_i}{h} \qquad (8)$$

The Taylor expansion in these two half volumes takes the forms shown below.

$$w(r) = r^2u = r_i^2 u_i + (r - r_i) + \frac{r_i^2 u_i - r_{i-1}^2 u_{i-1}}{h} + \vartheta(h^2) \quad (9-1)$$

$$w(r) = r^2u = r_i^2 u_i + (r - r_i) + \frac{r_{i+1}^2 u_{i+1} - r_i^2 u_i}{h} + \vartheta(h^2) \qquad (9-2)$$

Plugging these back into Equation (7) yields.

$$\int_{r_{i-\frac{1}{2}}}^{r_{i+\frac{1}{2}}} r^2 \frac{\partial u}{\partial t} dr = h \frac{\partial}{\partial t}\left[\frac{1}{8} r_{i-1}^2 u_{i-1} + \frac{6}{8} r_i^2 u_i + \frac{1}{8} r_{i+1}^2 u_{i+1} + \vartheta(h^2)\right] \quad (10)$$

Similar formulas can be established for the half volumes related to $i = 1, n$.

Now we check the diffusion term on the LHS of Equation (6). The integral is treated by the Fundamental Theorem of Calculus cancellation.

$$\int_{r_{i-\frac{1}{2}}}^{r_{i+\frac{1}{2}}} D \frac{\partial}{\partial r}(r^2 \frac{\partial u}{\partial r}) dr = D \int_{r_{i-\frac{1}{2}}}^{r_i} \frac{\partial}{\partial r}(r^2 \frac{\partial u}{\partial r}) dr + D \int_{r_i}^{r_{i+\frac{1}{2}}} \frac{\partial}{\partial r}(r^2 \frac{\partial u}{\partial r}) dr$$

$$= D r_{i+\frac{1}{2}}^2 \frac{\partial u}{\partial r}|_{r_{i+\frac{1}{2}}} - D r_{i-\frac{1}{2}}^2 \frac{\partial u}{\partial r}|_{r_{i-\frac{1}{2}}}$$

$$= \frac{D}{h}\left(r_{i-\frac{1}{2}}^2 u_{i-1} - \left(r_{i-\frac{1}{2}}^2 + r_{i+\frac{1}{2}}^2\right) u_i + r_{i+\frac{1}{2}}^2 u_{i+1}\right) + \vartheta(h^2) \quad (11)$$

As for the two special cases $i = 1, n$, one has

$$\int_{r_1}^{r_{\frac{3}{2}}} D \frac{\partial}{\partial r}(r^2 \frac{\partial u}{\partial r}) dr \approx \frac{D}{h}(-(r_{\frac{3}{2}}^2 - r_{\frac{1}{2}}^2) u_1 + (r_{\frac{3}{2}}^2 - r_{\frac{1}{2}}^2) u_2 \quad (12-1)$$

$$\int_{r_{1-\frac{1}{2}}}^{r_n} D \frac{\partial}{\partial r}(r^2 \frac{\partial u}{\partial r}) dr \approx \frac{D}{h}(-(r_n^2 - r_{n-\frac{1}{2}}^2) u_{n-1} + (r_n^2 - r_{n-\frac{1}{2}}^2) u_n) \quad (12-2)$$

For the RHS of Equation (3), we use the midpoint quadrature to obtain

$$\int_{r_{i-\frac{1}{2}}}^{r_{i+\frac{1}{2}}} f r^2 dr = h r_i^2 f_i + \vartheta(h^3), \quad 2 \le i \le (n-1) \quad (13)$$

For the special cases $i = 1$ and $i = n$, we have

$$\int_{r_1}^{r_{\frac{3}{2}}} fr^2 dr = \frac{h}{2} r_1^2 f_1, \quad \int_{r_{n-\frac{1}{2}}}^{r_n} fr^2 dr = \frac{h}{2} r_n^2 f_n \qquad (14)$$

Let $\boldsymbol{v}(t) = [v_1(t), v_2(t), \ldots, v_n(t)]^T$ be the dim-n column vector consisting of the numerical solution nodal values. An ODE system can be obtained:

$$\boldsymbol{M}\frac{d\boldsymbol{v}}{dt} + \boldsymbol{S}\boldsymbol{v} = \boldsymbol{g} \qquad (15)$$

Where $\boldsymbol{S}$ and $\boldsymbol{M}$ are the stiffness and mass matrices, respectively.

$$\boldsymbol{S} = \frac{D}{h}\begin{bmatrix} r_{\frac{3}{2}}^2 - r_1^2 & -\left(r_{\frac{3}{2}}^2 - r_1^2\right) & \cdots & \cdots & \cdots \\ \cdots & \cdots & \cdots & \cdots & \cdots \\ \cdots & -r_{i-\frac{1}{2}}^2 & r_{i-\frac{1}{2}}^2 + r_{i+\frac{1}{2}}^2 & -r_{i+\frac{1}{2}}^2 & \cdots \\ \cdots & \cdots & \cdots & r_n^2 - r_{n-\frac{1}{2}}^2 & -\left(r_n^2 - r_{n-\frac{1}{2}}^2\right) \end{bmatrix} \qquad (16)$$

$$\boldsymbol{M} = \frac{h}{8}\begin{bmatrix} 3r_1^2 & r_2^2 & 0 & 0 & & 0 & 0 & 0 \\ r_1^2 & 6r_2^2 & r_3^2 & 0 & \cdots & 0 & 0 & 0 \\ 0 & r_2^2 & 6r_3^2 & r_4^2 & & 0 & 0 & 0 \\ & \vdots & & & \ddots & & \vdots & \\ 0 & 0 & 0 & 0 & & r_{n-2}^2 & 6r_{n-1}^2 & r_n^2 \\ 0 & 0 & 0 & 0 & \cdots & 0 & r_{n-1}^2 & 3r_n^2 \end{bmatrix} \qquad (17)$$

Vector g corresponds to the source term.

The linear ODE system in Equation (13) can be solved using the implicit Euler or Crank-Nicolson methods. Let $\Delta t = T/m$ and $0 = t_0 < \cdots < t_{j-1} < t_j < \cdots < t_m = T$ be a uniform temporal partition. Let $\boldsymbol{v}^{(j)}$ the fully discretized numerical solution at time t_j. Then the implicit Euler discretization yields

$$\boldsymbol{M}\frac{\boldsymbol{v}^{(j+1)}-\boldsymbol{v}^{(j)}}{\Delta t}+\boldsymbol{S}v^{(j+1)}=\boldsymbol{g}^{(j+1)}, \qquad (18)$$

And hence

$$(\boldsymbol{M}+\Delta t\boldsymbol{S})v^{(j+1)}=\boldsymbol{M}v^{(j)}+\Delta t\boldsymbol{g}, \quad j=0,1,2,\dots,(m-1) \qquad (19)$$

After modification by boundary conditions, the above linear system can be solved by a standard linear solver. This offers a well-defined time-marching scheme.

For better approximation accuracy of the numerical solution, we could also use the Crank-Nicolson discretization.

$$\boldsymbol{M}\frac{\boldsymbol{v}^{(j+1)}-\boldsymbol{v}^{(j)}}{\Delta t}+\boldsymbol{S}\frac{\boldsymbol{1}}{\boldsymbol{2}}(\boldsymbol{v}^{(j+1)}+\boldsymbol{v}^{(j)})=\frac{1}{2}(\boldsymbol{g}^{(j+1)}+\boldsymbol{g}^{(j)}), \qquad (20)$$

Which leads to another time-marching scheme,

$$\left(\boldsymbol{M}+\frac{\Delta t}{2}\boldsymbol{S}\right)\boldsymbol{v}^{(j+1)}=\left(\boldsymbol{M}-\frac{\Delta t}{\boldsymbol{2}}\boldsymbol{S}\right)v^{(j)}+\frac{\Delta t}{2}\left(\boldsymbol{g}^{(j+1)}+\boldsymbol{g}^{(j)}\right),$$

$$For\ j=0,1,2,\dots,(m-1) \qquad (21)$$

3.5.2 Computation of Mass and Fluxes

For the above numerical schemes, we can compute (mass) fluxes at the two radial ends r_a and r_b, which correspond to the interior and exterior shells for the core-shell structure of spherical PLGA MPs/NPs.

At a typical time, moment t_j $(j=0,1,\dots,m)$, the numerical solution $v^{(j)}(r)$ is a continuous piecewise linear polynomial determined by its nodal values. The numerical total mass in the radial interval [r_a, r_b] is, by direct calculations,

$$M_j = \sum_{i=1}^{n-1} \int_{r_i}^{r_{i+1}} v^{(j)}(r) r^2 dr = \int_{r_i}^{r_{i+1}} \left(v_i^{(j)} \frac{r_{i+1} - r}{h} + v_{i+1}^{(j)} \frac{r - r_i}{h} \right) r^2 dr$$

$$= \sum_{i=1}^{n-1} \left(v_i^{(j)} r_{i+1} - v_{i+1}^{(j)} r_i \right) \frac{1}{3h} (r_{i+1}^3 - r_i^3) \qquad (22)$$

$$= \sum_{i=1}^{n-1} \left(v_i^{(j)} - v_{i+1}^{(j)} \right) \frac{1}{4h} (r_{i+1}^4 - r_i^4), \qquad j = 0, 1, \dots, m$$

The outflow fluxes at r_b and r_a, (for $j = 0, 1, \dots, m$) are respectively,

$$F_j^b = -\frac{D}{2} \left(\frac{v_{N_r}^{(j)} - v_{N_r-1}^{(j)}}{h} + \frac{v_{N_r}^{(j-1)} - v_{N_r-1}^{(j-1)}}{h} \right) r_b^2 \Delta t \qquad (23-1)$$

$$F_j^b = \frac{D}{2} \left(\frac{v_2^{(j)} - v_1^{(j)}}{h} + \frac{v_2^{(j-1)} - v_2^{(j-1)}}{h} \right) r_a^2 \Delta t \qquad (24-2)$$

Since there is no source in this case, mass conservation for the numerical solution takes the following form:

$$M_j - M_{j-1} = F_j^a + F_j^b, j = 1, \dots, m \qquad (25)$$

3.5.3 Nondimensionalization

The numerical solvers discussed in the previous subsection could produce simulation results for release from single PLGA particle once the model parameters, e.g., diffusivity *D*, the inner and outer radii r_a; r_b, are provided. For units of parameters or variables, we follow [4]. See Table 4.

Table 4. Variables units and meanings

Variabl	Uni	Meaning

es	ts	
D	$cm^2 s^{-1}$	Diffusion coefficient
c	mg/ml	Concentration
r_a; r_b; r	cm	Radial positions
t	s	Time

For better performance of numerical simulations, we introduce new dimensionless parameters and variables $\widehat{\boldsymbol{D}}, \hat{\boldsymbol{t}}, \hat{\boldsymbol{r}}, \hat{\boldsymbol{c}}$ so that:

$$\widehat{\boldsymbol{D}} = \frac{\boldsymbol{D}}{\boldsymbol{D_0}}, \hat{\boldsymbol{t}} = \frac{\boldsymbol{t}}{\boldsymbol{T_0}}, \hat{\boldsymbol{r}} = \frac{\boldsymbol{r}}{\boldsymbol{r_b}}, \hat{\boldsymbol{c}} = \frac{\boldsymbol{c}}{\boldsymbol{C_0}} \qquad (25)$$

where D_0; T_0; C_0 are chosen according to experiment data. Let $H_0 = (r_b - r_a)/r_b$ be the thickness of the polymeric shell. Then the nondimensionalized diffusion problem takes the form

$$\begin{cases} \dfrac{\partial \hat{c}}{\partial \hat{t}} = \dfrac{T_0 D_0}{r_b^2} \dfrac{\widehat{D}}{\widehat{r^2}} \dfrac{\partial}{\partial \hat{r}} \left(\widehat{r^2} \dfrac{\partial \hat{c}}{\partial \hat{r}} \right), \hat{r} \in [1 - H_0, 1], \hat{t} \in (0,1] \\ Boundary\ Conditions \\ Initial\ Conditions \end{cases} \qquad (26)$$

The source term does not exist for drug release from PLGA particles.

3.6 Experimental and Numerical Results

Note that in vitro experiment data varies. For our experiments gentamicin encapsulated in PLGA particles, three sets of radii are recorded as follows.

Case 1: $r_a = 0.7\ \mu m = 7.0 \times 10^{-5} cm$, $r_b = 0.8\ \mu m = 8{:}0 \times 10^{-5}$ cm;

Case 2: $r_a = 0{:}8\ \mu m = 8.0 \times 10^{-5} cm$, $r_b = 1.0\ \mu m = 1{:}0 \times 10^{-5}$ cm;

Case 3: r_a = 1:8 μm = 1.8×10^{-4}cm, r_b = 2.0 μm = $2{:}0 \times 10^{-4}$ cm.

This indicates the relative thickness $H_0 = (r_b - r_a)/r_b$ is in the range 0.10−0.20. The observation time T_0 could be chosen as 1hr - 2 hrs, namely, 3600 - 7200 seconds, to focus on the early (burst) stage.

The diffusivity parameter D is difficult to obtain. An empirical formula was proposed in [13] based on data fitting and knowledge from series solutions of similar problems. For the *in-silico* approach, one may consider a baseline value for D0 and vary it up or down for several magnitudes in numerical simulations.

For our five in vitro experiments with gentamicin encapsulated in PLGA particles, we recorded the accumulative percentage of gentamicin released versus time. As shown in Table 5, about 20% of total gentamicin was released after about 2 hours; about 60% of total gentamicin was released after about 10 hours.

Table 5. Accumulative percentage of gentamicin release in five experiments

PLGA/DCM (mg/ml) concentration	13.3	15.0	16.7	18.3	20.0
Time (hours)	Accumulative % of gentamicin released				
1 hour	11.54%	12.86%	15.77%	9.92%	9.41%
2 hour	21.71%	22.29%	22.73%	19.82%	17.92%
4 hour	26.03%	28.15%	29.81%	24.56%	23.51%
6 hour	31.04%	31.68%	32.25%	30.47%	30.88%
8 hour	36.11%	37.99%	41.43%	35.09%	33.58%
10 hour	44.34%	46.11%	50.46%	43.37%	42.97%

The raw data suggests that we should focus on the 1st hour for a potential stage of burst. Following the discussion in [14] Fig.16, we fit the model \reservoir devices with constant activity source" (Eqn.(8) therein) using our experimental data for the 1st 60 min with 2-min sampling as shown in Figure 19. Linear regression yields:

$$M_t = 4.2 \times 10^{-3} t$$

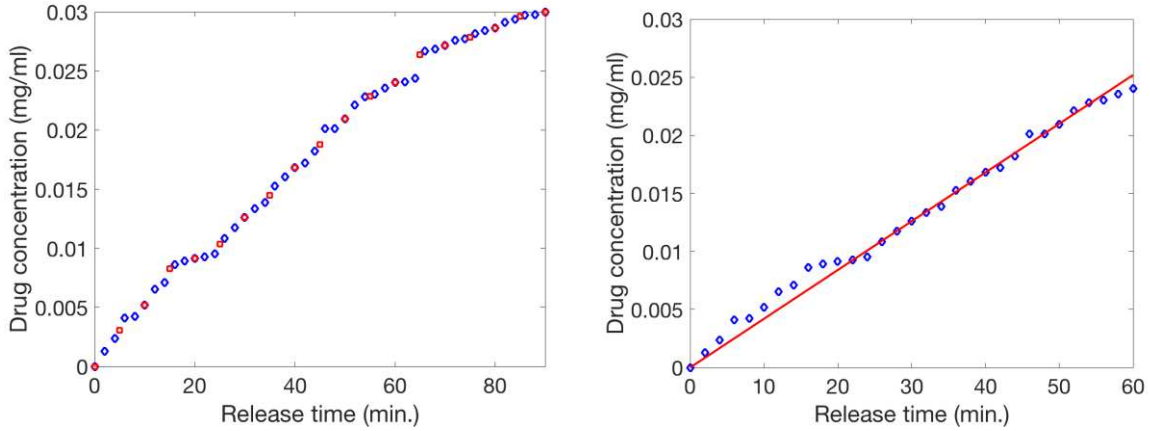

Fig. 19. Experimental data fitting for gentamicin release from PLGA particles. Blue dots for 2-min samples; red dots for 5-min samples; red line for the fitted model (a) Raw data showing the accumulative concentration of released drug during the 1st 90 minutes; (b) The red line represents the fitting model $M_t = 4.2 \times 10^{-3} t$ for $t \in [0; 60]$ min.

3.7 Concluding Remarks

This paper investigates mathematical modeling and numerical simulations for drug release from PLGA particles as our exploratory efforts in this interdisciplinary approach. Based on examination of data obtained from in vitro experiments, our focus is placed on modeling the early stage of release with assumptions of no swelling of the porous shell, homogeneity of the shell, and the perfect sink condition, a radial direction diffusion equation is adopted. Finite volume schemes have been developed for this model. Matlab code modules along with in silico results will be incorporated in our code package DarcyLite [8].

Due to the pores on the polymeric shells of PLGA MPs/NPs, a time-dependent convection-diffusion equation would be more suitable for modeling the drug release process. This is currently under our investigation and will be reported in our future work.

As drug release proceeds, the porous shell is subject to swelling and eventually degrades. Mathematical modeling and numerical simulations for degradation are more challenging. These are under our investigation also.

Simulations of drug release from PLGA MPs/NPs using Molecular Dynamics (MD) seem too expensive and hence will not be our pursuit. Our goal is to develop efficient simulation code modules that can run on laptops or low configuration desktop computers. These code modules will be based on the mathematical equations that characterize transport through porous media.

3.7 References

[1] Darvish, A., Goyal, G., Aneja, R., Sundaram, R. V., Lee, K., Ahn, C. W., Kim, K.-B., Vlahovska, P. M., & Kim, M. J. (2016). Nanoparticle mechanics: Deformation Detection Via Nanopore resistive pulse sensing. *Nanoscale*, *8*(30), 14420–14431. https://doi.org/10.1039/c6nr03371g

[2] Howard, G. T. (2002). Biodegradation of polyurethane: A Review. *International Biodeterioration & Biodegradation*, *49*(4), 245–252. https://doi.org/10.1016/s0964-8305(02)00051-3

[3] Crank, J. (1975). The mathematics of diffusion, Clarendon Press, Oxford, 2nd ed.

[4] Zhou, Y., & Wu, X. Y. (1997). Finite element analysis of diffusional drug release from Complex Matrix Systems. i. *Journal of Controlled Release*, *49*(2-3), 277–288. https://doi.org/10.1016/s0168-3659(97)00103-x

[5] Siepmann, J., & Siepmann, F. (2012). Modeling of Diffusion Controlled Drug Delivery. *Journal of Controlled Release*, *161*(2), 351–362. https://doi.org/10.1016/j.jconrel.2011.10.006

[6] Zeng, Y., Albertus, P., Klein, R., Chaturvedi, N., Kojic, A., Bazant, M. Z., & Christensen, J. (2013). Efficient conservative numerical schemes for 1D nonlinear spherical diffusion equations with applications in battery modeling. *Journal of The Electrochemical Society*, *160*(9). https://doi.org/10.1149/2.102309jes

[7] Peppas, N. A., & Narasimhan, B. (2014). Mathematical models in drug delivery: How modeling has shaped the way we design New Drug Delivery Systems. *Journal of Controlled Release*, *190*, 75–81. https://doi.org/10.1016/j.jconrel.2014.06.041

[8] Ojha, V. K., Jackowski, K., Abraham, A., & Snasel, V. (2015). Dimensionality reduction, and function approximation of poly(lactic-co-glycolic acid) micro- and nanoparticle dissolution rate. *International Journal of Nanomedicine*, 1119. https://doi.org/10.2147/ijn.s71847

[8] Busatto, C., Pesoa, J., Helbling, I., Luna, J., & Estenoz, D. (2018). Effect of particle size, Polydispersity and polymer degradation on progesterone release from PLGA microparticles: Experimental and mathematical modeling. *International Journal of Pharmaceutics*, *536*(1), 360–369. https://doi.org/10.1016/j.ijpharm.2017.12.006

[9] Spiridonova, T. I., Tverdokhlebov, S. I., & Anissimov, Y. G. (2019). Investigation of the size distribution for diffusion-controlled drug release from Drug Delivery Systems of various geometries. *Journal of Pharmaceutical Sciences*, *108*(8), 2690–2697. https://doi.org/10.1016/j.xphs.2019.03.036

[10] Ghitman, J., Biru, E. I., Stan, R., & Iovu, H. (2020). Review of hybrid plga nanoparticles: Future of Smart Drug Delivery and Theranostics medicine. *Materials & Design*, *193*, 108805. https://doi.org/10.1016/j.matdes.2020.108805

[11] Lagreca, E., Onesto, V., Di Natale, C., La Manna, S., Netti, P. A., & Vecchione, R. (2020). Recent advances in the formulation of PLGA microparticles for controlled drug delivery. *Progress in Biomaterials*, *9*(4), 153–174. https://doi.org/10.1007/s40204-020-00139-y

[12] Jain, A., McGinty, S., Pontrelli, G., & Zhou, L. (2022). Theoretical model for diffusion-reaction based drug delivery from a multilayer spherical capsule. *International Journal of Heat and Mass Transfer*, *183*, 122072. https://doi.org/10.1016/j.ijheatmasstransfer.2021.122072

[13] Fredenberg, S., Wahlgren, M., Reslow, M., & Axelsson, A. (2011). The mechanisms of drug release in poly(lactic-co-glycolic acid)-based drug delivery systems—a review. *International Journal of Pharmaceutics*, *415*(1-2), 34–52. https://doi.org/10.1016/j.ijpharm.2011.05.049

[14] Ficheux, M.-F., Bonakdar, L., Leal-Calderon, F., & Bibette, J. (1998). Some stability criteria for double emulsions. *Langmuir*, *14*(10), 2702–2706. https://doi.org/10.1021/la971271z

[15] Busatto, C., Pesoa, J., Helbling, I., Luna, J., & Estenoz, D. (2018). Effect of particle size, Polydispersity and polymer degradation on progesterone release from PLGA microparticles: Experimental and mathematical modeling. *International Journal of Pharmaceutics*, *536*(1), 360–369. https://doi.org/10.1016/j.ijpharm.2017.12.006

[16] Casalini, T., Rossi, F., Lazzari, S., Perale, G., & Masi, M. (2014). Mathematical modeling of PLGA microparticles: From polymer degradation to drug release. *Molecular Pharmaceutics*, *11*(11), 4036–4048. https://doi.org/10.1021/mp500078u

[17] Faisant, N., Siepmann, J., & Benoit, J. P. (2002). PLGA-based microparticles: Elucidation of mechanisms and a new, simple mathematical model quantifying drug release. *European Journal of Pharmaceutical Sciences*, *15*(4), 355–366. https://doi.org/10.1016/s0928-0987(02)00023-4

[18] Ghitman, J., Biru, E. I., Stan, R., & Iovu, H. (2020). Review of hybrid plga nanoparticles: Future of Smart Drug Delivery and Theranostics medicine. *Materials & Design*, *193*, 108805. https://doi.org/10.1016/j.matdes.2020.108805

[19] Grassi, M., Lamberti, G., Cascone, S., & Grassi, G. (2011). Mathematical modeling of simultaneous drug release and in vivo absorption. *International Journal of Pharmaceutics*, *418*(1), 130–141. https://doi.org/10.1016/j.ijpharm.2010.12.044

[20] Jain, A., McGinty, S., Pontrelli, G., & Zhou, L. (2022). Theoretical model for diffusion-reaction based drug delivery from a multilayer spherical capsule. *International Journal of Heat and Mass Transfer*, *183*, 122072. https://doi.org/10.1016/j.ijheatmasstransfer.2021.122072

[21] Jusu, S. M., Obayemi, J. D., Salifu, A. A., Nwazojie, C. C., Uzonwanne, V., Odusanya, O. S., & Soboyejo, W. O. (2020). Drug-encapsulated blend of PLGA-peg microspheres: In vitro and in vivo study of the effects of localized/targeted drug delivery on the treatment of triple-negative breast cancer. *Scientific Reports*, *10*(1). https://doi.org/10.1038/s41598-020-71129-0

[22] Klose, D., Siepmann, F., Elkharraz, K., Krenzlin, S., & Siepmann, J. (2006). How porosity and size affect the drug release mechanisms from PLGA-based microparticles. *International Journal of Pharmaceutics*, *314*(2), 198–206. https://doi.org/10.1016/j.ijpharm.2005.07.031

[23] Korsmeyer, R. W., Gurny, R., Doelker, E., Buri, P., & Peppas, N. A. (1983). Mechanisms of solute release from porous hydrophilic polymers. *International Journal of Pharmaceutics*, *15*(1), 25–35. https://doi.org/10.1016/0378-5173(83)90064-9

[24] Lagreca, E., Onesto, V., Di Natale, C., La Manna, S., Netti, P. A., & Vecchione, R. (2020). Recent advances in the formulation of PLGA microparticles for controlled drug delivery. *Progress in Biomaterials*, *9*(4), 153–174. https://doi.org/10.1007/s40204-020-00139-y

Chapter 4

Manuscript: Enhanced Transdermal Medication Delivery: Core-Shell Nanofiber Scaffolds with Antibiotic-encapsulated Poly (lactic acid-co-glycolic acid) Nanoparticles Applications *

Overview

The development of novel nanostructured materials has sparked considerable interest in transdermal medication research. Leveraging nanotechnology, the utilization of nanoparticles (NPs) and nanofabrication techniques has dramatically advanced drug delivery systems in recent years. Among these advancements, core-shell nanofiber scaffolds (CSNS) incorporating drug carriers have emerged as particularly promising for the development of innovative transdermal materials due to its properties of (i) sustainable release profiles, (ii) modifiable open-sites, and (iii) expensive material replacements. While existing research has predominantly focused on incorporation of inorganic NPs (metals, metal/semi-metal oxides, and drug-only) into CSNS, there remains a notable gap in the literature regarding integration of polymeric NPs. In this study, a double emulsion solvent evaporation method was employed to synthesize gentamicin (Gen) - encapsulated poly (lactic acid-co-glycolic acid) (PLGA) NPs. These Gen/PLGA NPs were then incorporated into polyurethane (PU) / poly (ethylene oxide) (PEO) CSNS using a coaxial electrospinning technique. Characterization of the fabricated CSNS was conducted using Fourier transform infrared spectrometer (FTIR), Scanning Electron Microscopy (SEM), Transmission Electron Microscopy (TEM), Ultraviolet-Visible spectroscopy (UV-Vis), and an agar diffusion method for antimicrobial testing. The results indicated successful incorporation of Gen/PLGA

NPs (with an average diameter of 130 nm) into PU/PEO CSNS. The resulting CSNS exhibited an inner and outer diameter of 1.38μm and 2.22μm, respectively. Utilization of PEO in the shell spinning solution was found to effectively mitigate immiscibility between core and shell solutions, while also facilitating the controlled release of gentamicin. Drug release profiles and antimicrobial tests further supported the efficacy of Gen/PLGA NPs-PU/PEO CSNS in inhibiting *E.coli* growth, demonstrating sustained release of gentamicin over time. Overall, the study showcases a microfabrication approach for integration of Gen/PLGA NPs into PU/PEO CSNS, offering a promising strategy for (i) long-term therapeutic drug delivery with (ii) controlled release rates compared to monolithic fibrous scaffolds, and (iii) effective antimicrobial activity against *E.coli* affections. These findings underscore the potential of this methodology for advancing the development of innovative transdermal materials.

Keywords: Core-shell nanofiber scaffolds (CSNS), Coaxial-electrospinning, Poly (lactic acid-co-glycolic acid) (PLGA), Nanoparticles (NPs), Polyurethane (PU), Poly (ethylene oxide) (PEO), Wound-dressing transdermal, Drug delivery systems

4.1 Introduction

In recent years, the applications of nanomaterials in many fields such as tissue engineering, biomaterials manufacturing, and vascular bioengineering have garnered significant interest, driving the exploration of novel nanomaterials and synthesis approaches [1]. Various nanofabrication methods, including self-assembly, electrospinning, phase separation, and lithography, have been employed to produce a diverse range of nanomaterials such as nanorods, foams, spheres, micelles, nanofiber webs, and core-shell nanofiber scaffolds for numerous biomedical applications [2][3][4][5]. Core-shell nanofiber scaffolds (CSNS) have emerged as

particularly promising, owing to their exceptional properties including controlled drug release, incorporation of unstable components, mechanical reinforcements, minimization of decomposition, surface modification capabilities, and cost effectiveness [6][7][8][9][10][11]. Therefore, the utilization of CSNS represents a compelling avenue for the advancement of novel transdermal materials.

Compared to conventional wound dressing materials, which typically consist of monolithic fiber structures, CSNS offers many advantages. These include high encapsulation efficiency, precise control over drug release rates, open sites for modification, effective incorporation of incompatible material, protection of fragile agents, and cost-effectiveness, particularly with expensive materials [12][13]. For example, achieving controlled release of bioactive agents has long been a challenge in transdermal material development. Previous studies have demonstrated that CSNS effectively regulated the release of metoclopramide hydrochloride, particularly in the burst-release phase [14]. In another example, carbide/nitride fibers can be enveloped by heterogeneous graphene using coaxial wet spinning, resulting in core-shell fibers with exceptional performance in thermal protection, oil/water separation, and oxidation isolation. [15].

Various methods are available for creating CSNS, with electrospinning being a commonly employed technique due to its simplicity and efficiency [16][17]. Many biocompatible and biodegradable polymers, including poly (ethylene oxide) (PEO), poly (vinyl acetate) (PVA), and poly (ethylene glycol) (PEG), poly (DL-lactic acid) (PDLLA), and poly (glycerol sebacate) (PGS), have been utilized in development of CSNSs for transdermal medication applications [18][19][20][21][22][23]. For example, a CSNS with poly (DL-lactic acid) (PDLLA) core and a poly-(3-hyroxy butyrate) (PHB) shell exhibited remarkable thermal resistance for thermal

protection materials [23]. Another example involves a CSNS comprising a poly (vinyl alcohol) (PVA) core and a poly-L-lactide (PLA) shell, demonstrating significant enhancements in controlled drug delivery compared to monolithic PVA fibers [24]. On the other hand, core-shell scaffolds have showed great potentials for incorporating NPs such as ZnO, Fe_3O_4, Ag, and silica NPs [25][26][27][28], as well as drugs like antibiotics, for various biomedical applications. For example, Ag NPs were incorporated into PCL/PEG CSNS where Ag NPs were loaded in the shell layer resulting in a controlled release of Ag NPs over two weeks [28]. In another study, paclitaxel was successfully loaded into PLGA-Caprolactone CSNS, enabling a long-term delivery of paclitaxel over a month [29], which could be beneficial for chronic disease treatments and preventing side effects caused by medicine overdose. Although existing research on incorporating NPs or small molecules into CSNS has been primarily focused on inorganic particles or antibiotics-only, organic or polymeric particles have not been extensively studied in integration into CSNS. However, polymeric NPs such as poly (lactic-co-glycolic acid) (PLGA), polycaprolactones (PCL), poly (ortho esters) (POEs) and poly(alkyl cyanoacrylates) (PACAs) have gained widespread use in nanomedicine development due to their unique advantages, including controlled release, targeted delivery, high surface-to-volume ratios, protection of agent bioactivity, biodegradability, and biocompatibility [30][31][32][33]. These polymeric NPs can be metabolized into carbon and water upon introduction to the human body, leaving no hazardous waste. Various substances such as drugs, genes, growth factors, antibiotics, and peptides have been encapsulated into NPs, leading to the development of numerous nanomedicines for advanced drug delivery applications. For instance, Sun reported that gentamicin loaded PLGA NPs could be incorporated into PU/PEO monolithic nanofiber scaffolds, demonstrating controlled release of gentamicin and excellent antimicrobial properties, indicating the promising

potential of NP incorporation into nanofiber scaffolds for novel transdermal material development [34]. However, the study also highlighted some challenges associated with this approach, including immiscible phase incorporation, burst effects, and systems coordination, which remain to be addressed.

This paper presents a novel fabrication method for producing core-shell nanofiber scaffolds (CSNSs) containing gentamicin-loaded PLGA NPs (Gen/PLGA NPs) via coaxial electrospinning. Gentamicin, a wide spectrum antibiotic, was chosen for encapsulation in PLGA NPs. The Gen/PLGA NPs were synthesized using a double emulsion solvent evaporation method followed by a four-step purification process adopted from Sun [34][35]. The CSNSs were composed of polyurethane (PU) and poly (ethylene oxide) (PEO) due to their biodegradable and biocompatible nature, making them suitable for biomedical applications. The resulting fiber scaffolds were analyzed to characterize their morphological properties, gentamicin release profiles, and antimicrobial activities. It was observed that the inclusion of PEO in the core of the CSNSs was crucial as it acted as a stabilizer, ensuring uniform dispersion of Gen/PLGA NPs in the spinning solution, thus facilitating stable and uniform electrospinning of the fiber core. The composition of PU and PEO in the fiber shell enabled sustained release of gentamicin while maintaining fiber scaffolds integrity in moist environment, which is a typical characteristic of wounds. The incorporation of nanoparticle encapsulation and core-shell fabrication effectively mitigated the burst effect in gentamicin release profiles, which is advantageous for wound healing and treatment. The results suggest that CSNSs incorporating gentamicin PLGA nanoparticles offer a promising approach for achieving controlled release and long-term drug delivery. Furthermore, CSNSs incorporating polymeric nanoparticles present a versatile platform

for developing innovative nanostructured materials tailored for efficient transdermal medication applications.

4.2 Experimental Section

4.2.1 Materials

Poly (D, L-lactide-co-glycolic acid) (PLGA, lactide: glycolic 75:25, Mw 4000~15000, Sigma-Aldrich) and polyvinyl alcohol（PVA, 99+%, MW 89000~98000, Sigma-Aldrich）were used in the synthesis of NPs. Gentamicin sulfate salt (99+%, Sigma-Aldrich) was encapsulated within the PLGA NPs. Polyurethane (PU, 90%-100%, SG80A, Lubrizol Corporation) and Poly (ethylene oxide) (PEO, ≥99%, Mw=5000000, Sigma-Aldrich) served as matrix polymers in the electrospinning process. Dichloromethane (DCM, Mw=84.93, ≥99.8%, Sigma-Aldrich) and chloroform (Mw=119.38, ≥99.8%, Sigma-Aldrich) were the organic solvents used for CSNS fabrication and NP synthesis. Deionized water (Fisher Scientific) was employed as the aqueous phase in both NP synthesis and electrospinning. Luria broth (LB) and BBL Muller Hinton II Agar, used for growing *E.coli,* were purchased from Becton, Dickinson and Company, Spark, MD. *E.coil* (4.5×10^3 CFU/pellet, ATCC 25922), obtained from MicroBiologics. NaCl (SX0420-1, M=58.44g/mol, Supelco), was utilized as the dialysis solution, with dialysis tubing (UG281774, 3500 MWCO, 3.7ml/cm) acquired from SnakeSkin (Thermo Scientific™, #68100).

4.2.2 Synthesis & Purification of PLGA NPs

The synthesis of Gen/PLGA NPs followed a double emulsion solvent evaporation method as reported by Sun et al. [35]. Specifically, 100mg of PLGA powder was dissolved in 4ml of dichloromethane (DCM), while 45mg of gentamicin was dissolved in 0.5ml of DI water. Additionally, 8ml of a 3% PVA solution was prepared. These components were mixed to form a water-oil-water nanodroplet dispersion. The solution underwent sonication at 35% amplitude for

15 minutes, resulting in a dispersion solution. The dispersion solution was then titrated into 25ml of a 0.1% PVA solution, yielding an opaque solution. Subsequently, PLGA NPs precipitated after an 8-hour solvent evaporation process. The obtained PLGA NPs underwent purification via a 4-step purification process previously described by Sun. Finally, the morphology of the obtained PLGA NPs was examined using a Transmission Electron Microscope (TEM, JEOL JEM-1400 120KV).

4.2.3 Incorporation of PLGA NPs into Core-Shell Nanofiber Scaffolds

Coaxial electrospinning proved to be an effective method for incorporating NPs into fibrous scaffolds [36][37][38]. Therefore, a coaxial electrospinning was employed to integrate PLGA NPs into core-shell fibers, using various recipes outlined in Table 6. For example, to create the core of the fibers, 0.5g of PEO was dissolved in 10ml of DCM, yielding a spinning solution. Similarly, to form the shell of the fibers, 0.2g of PU was dissolved in 10ml of chloroform, yielding another spinning solution. A batch of purified Gen/PLGA NPs was combined with the PEO core spinning solution to produce fiber sample 5. In the coaxial electrospinning, 3ml of the mixed solution and PU solution were injected into the coaxial spinning needle through the core and shell inlets, as depicted in Figure 20. An electric field was generated by applying a fixed at 10kV power supply, with the spinning distance set at 15cm. The feeding injection rate was maintained at 0.01ml/hour for both core and shell solutions. Various other fiber samples were fabricated under different conditions outlined in Table 6.

Table 6. Core-Shell electrospinning solution formulas: **#1**, PEO (C) + PEO-PU (S); **#2**, Gentamicin-PEO (C) + PEO-PU (S); **#3**, PLGA NPs-PEO (C) + PEO-PU (S); **#4**, Gentamicin-PLGA NPs-PEO (C) + PU (S); **#5** gentamicin-PLGA NPs-PEO (C)+ PEO-PU (S).

	Spinning Solution Composition		PLGA NP	Gentamicin	Comments
Fiber Sample	Core Solution	Shell Solution			

#1	0.05g/ml PEO	0.02g/ml PU-PEO (1:1)	No	No	A controlled sample without any NPs or gentamicin
#2	0.05g/ml PEO	0.02g/ml PU-PEO (1:1)	No	Yes	Gentamicin was loaded within core solution
#3	0.05g/ml PEO	0.02g/ml PU-PEO (1:1)	Yes	No	PLGA NPs did not loaded with gentamicin
#4	0.05g/ml PEO	0.02g/ml PU	Yes	Yes	Gentamicin was encapsulated within PLGA NPs
#5	0.05g/ml PEO	0.02g/ml PU-PEO (1:1)	Yes	Yes	Gentamicin was encapsulated within PLGA NPs

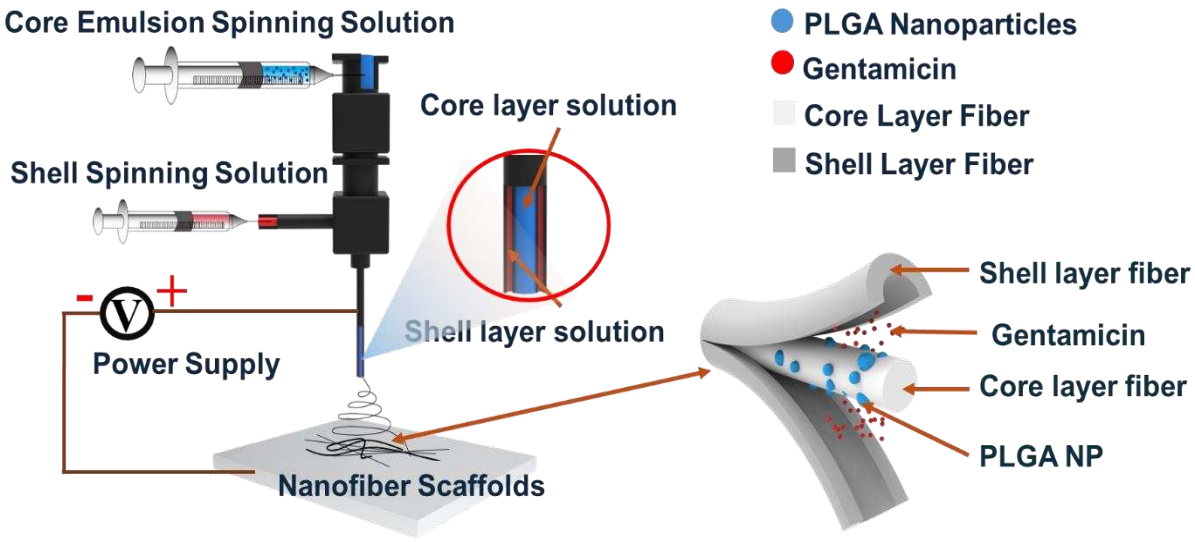

Figure 20. Core-shell fiber scaffolds were fabricated via core-shell electrospinning. The corresponding fiber sample ingredients were presented in **Table 6.** Fiber scaffolds had a core-shell structure where Gen/PLGA NPs were incorporated with core fiber layers. The applied power was 10kV; injection rate fixed at 0.05ml/hour; spinning distance was set at 15cm.

4.2.4 Chemical Analysis

The primary tool utilized for studying the chemical composition of the fabricated fiber scaffolds at different conditions shown in Table 6, as well as each ingredient (PEO, PU, PLGA, and gentamicin) used in the scaffold fabrication, was a Fourier-transform Infrared Spectroscopy

(FTIR, Cary 630 FTIR, Agilent). Each fiber scaffold was cut into a 1cm × 1cm square, and these samples were loaded into an FTIR stage to determine resonance intensity at different wavelengths. FTIR spectra were collected for five fiber samples and the four ingredients to conduct chemical composition analysis.

4.2.5 Morphology Investigation

The electrospun fiber mats were cut into 3cm × 3cm square fiber samples, which were then subjected to examination using Scanning Electron Microscopy (SEM, JEOL JSM-6500) to explore their morphology properties. In addition, the morphologies of core-shell fiber structure were investigated using the TEM. To prepare fiber samples for TEM examination, copper grids were placed beneath the spinning needle for 1 minute to collect fibers. Subsequently, the samples underwent gold-coating before imaging. These prepared fiber samples were then loaded into the TEM for morphological analysis, and relevant information was collected and analyzed.

4.2.6 Gentamicin Release Profiles

Scaffolds samples with equal masses (0.045g) were prepared for determining the gentamicin release profiles. Ultraviolet-visible spectroscopy (UV-Vis, Agilent Cary 4000) was used to measure gentamicin concentration, enabling the plotting of release profiles over time [39][40][41]. Each sample was fully immersed in a testing tube containing 2 ml of water. Gentamicin release measurements were conducted at time intervals of 0.5 hours, 1 hour, 2 hours, 3 hours, 4 hours, 6 hours, 8 hours, 10 hours, 12 hours, 16 hours, 20 hours, and 24 hours. Subsequently, the resulting sample solutions underwent centrifugation, and 3ml of the upper water solutions were collected and analyzed using UV-Vis spectroscopy to determine absorbance at the 220nm wavelength, where a characteristic peak for gentamicin was observed. The absorbance values were compared to a gentamicin calibration curve to determine gentamicin

concentrations, indicating the release rate at various time intervals. Plotting the release rate against the time interval provided insights into the gentamicin release properties of the fiber scaffolds.

4.2.7 Antibacterial Testing

The antibacterial properties of the CSNS against *E. coli* were assessed using an agar diffusion method adapted from the AATCC 100 antimicrobial test method for textiles [34]. First, an *E.coli* culture solution with a concentration of 4.5×10^2 CFU/ml was prepared. Second, 1ml of the 24 hour-broth *E.coli* culture solution was diluted by a factor of 10. Fiber scaffolds sample were then prepared with dimensions of 60 mm × 10 mm and a weight of 0.05 g. An inoculum loop was used to transfer the *E.coli* culture solution onto the sterile agar plates. The loop was passed over five marked lines, each approximately 60 mm in length and spaced 10 mm apart, covering the central area of the LB-Agar broth petri dishes as shown in Figure 21(A). Next, CSNS specimens were gently pressed transversely across the inoculum streaks on the agar surface, as shown in Figure 21(B). The petri dishes were subsequently incubated for 18 hours at 37°C. The antimicrobial activity of the CSNS was assessed by observing the interruption of bacterial growth along the streaks on the inoculum. This interruption was indicated by the presence of clear zones of inhibition along the fiber specimens.

The average width of a zone of inhibition along a streak on each side of the test specimen can be calculated using the following equation:

$$W_{arg} = \frac{\sum_{i=1}^{5}(\frac{T_i - D_i}{2})}{5} \qquad \text{Equation (27)}$$

where W_{arg} represents the average width of the clear zone of inhibition, T_i denotes the diameter of the clear zone for each fiber specimen, and D_i represents the diameter of each fiber specimen (in mm).

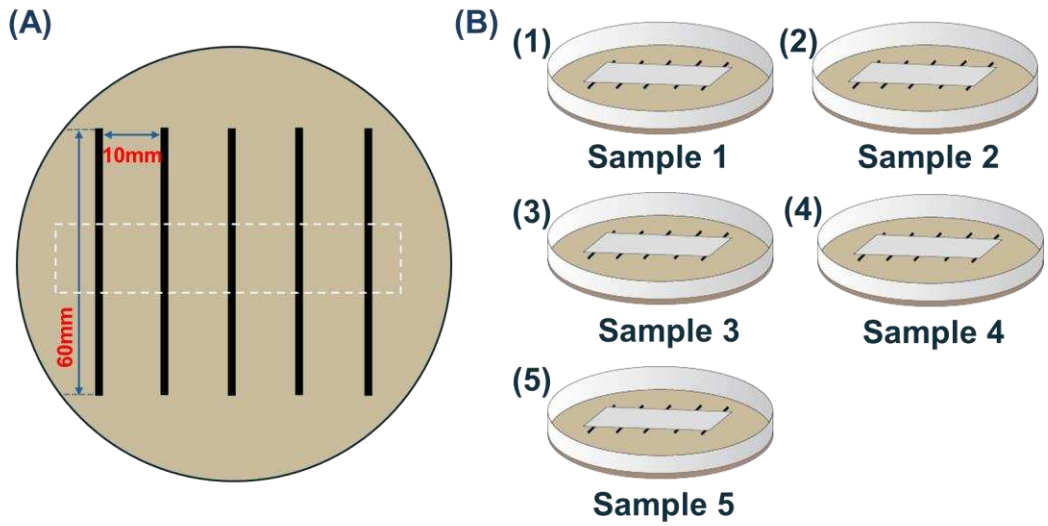

Figure 21. A Drawn mark layout on petri dish for antibacterial activity tests. **Figure 2. B-(1)** PEO (C) + PU-PEO (S); **B-(2)** Gentamicin-PEO (C) + PEO-PU (S) fiber scaffolds; **B-(3)** PLGA NPs-PEO (C) + PEO-PU (S) fiber scaffolds; **B-(4)** Gentamicin-PLGA NPs-PEO (C) + PU (S) fiber scaffolds; **B-(5)** Gentamicin-PLGA NPs-PEO (C) + PU-PEO (S) fiber scaffolds.

4.3. Results & Discussion

4.3.1 Gentamicin-encapsulated PLGA NPs

Gentamicin-encapsulated PLGA NPs played a crucial role in the development of core-shell nanofiber scaffolds for drug delivery systems. The size and distribution of these NPs were particularly important for their incorporation into fibers. It was recommended that the ratio of NP diameter to fiber diameter should be less than ¼ to facilitate incorporation [34]. Additionally, the cleanliness of the resulting PLGA NPs was essential, ideally free from any residual precursors such as PVA. Therefore, a 4-step purification process, adapted from Sun et al., was employed to clean the PLGA NPs [34]. Figure 22-(A) depicts a TEM image of the gentamicin-encapsulated PLGA NPs, while Figure 22-(B) shows the particle size distribution histogram. The particles exhibited an average diameter of 132 ±24.31nm. Previous reports indicated a highly porous structure for gentamicin-loaded PLGA NPs with larger particle sizes ranging from 1μm to 3μm, using a similar synthesis method [35]. A schematic illustration in Figure 22-(A) shows the porous

structure of a PLGA NPs with a core-shell structure where gentamicin is encapsulated within. This structure suggests a porous sphere favorable for drug release applications.

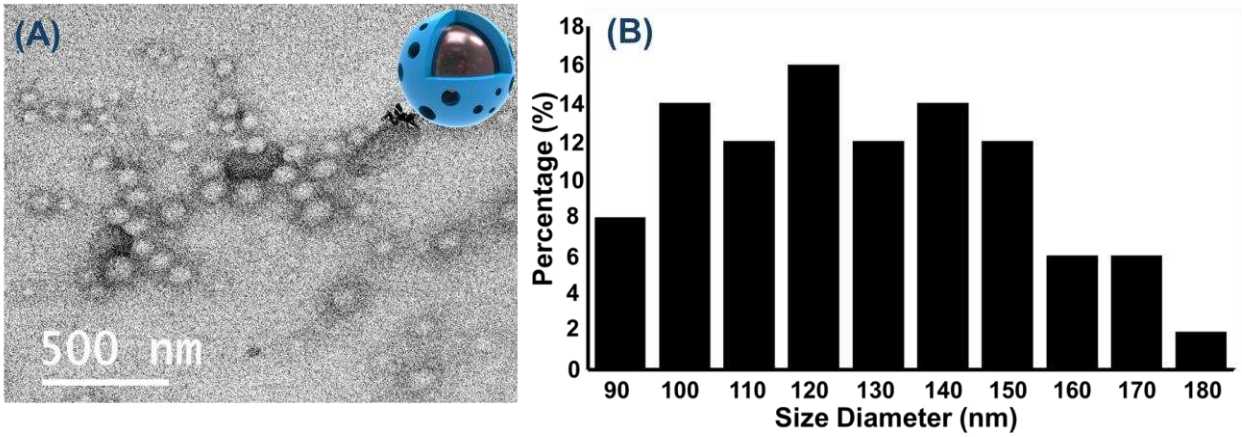

Figure 22. (A) A TEM image of PLGA NPs showed PLGA NPs had a core-shell structure where gentamicin was encapsulated inside presented by a 3D NP model. The PLGA NPs were spherical shapes with a wide range of diameters. **(B)** PLGA NPs had a normalized size distribution with an average dimension at 132±24.31nm after purification.

4.3.2 Chemical Analysis

Chemical analysis via FTIR was conducted on fiber scaffolds prepared using different recipes. Figure 23 showed the FTIR spectra of scaffold samples and individual ingredients, including PEO, PU, PLGA, and gentamicin. The spectra for the five scaffold samples exhibited very similar characteristic peaks such as (C-H bends at 650-850cm-1; -C-O ester at 1080-1180 cm^{-1}; CH2 bends at 1150-1650cm-1; -C=O stretch at 1750cm^{-1}; CH_3 / CH_2 stretch at 2880-3010cm^{-1}. Most of these characteristic peaks were also present in the spectrum obtained for PEO alone, as PEO was used in all scaffold recipes. Additionally, PU, which was used in all recipes, displayed a peak corresponding to C = O stretch at 1750 cm^{-1}, consistent with the spectra of the five scaffold samples. On the other hand, the major characteristic peaks for PLGA and gentamicin were -C=O stretch at 1750 cm-1 and C-H bends at 850cm^{-1}, respectively. These peaks were also present in PEO and PU spectra [42][43][44][45].

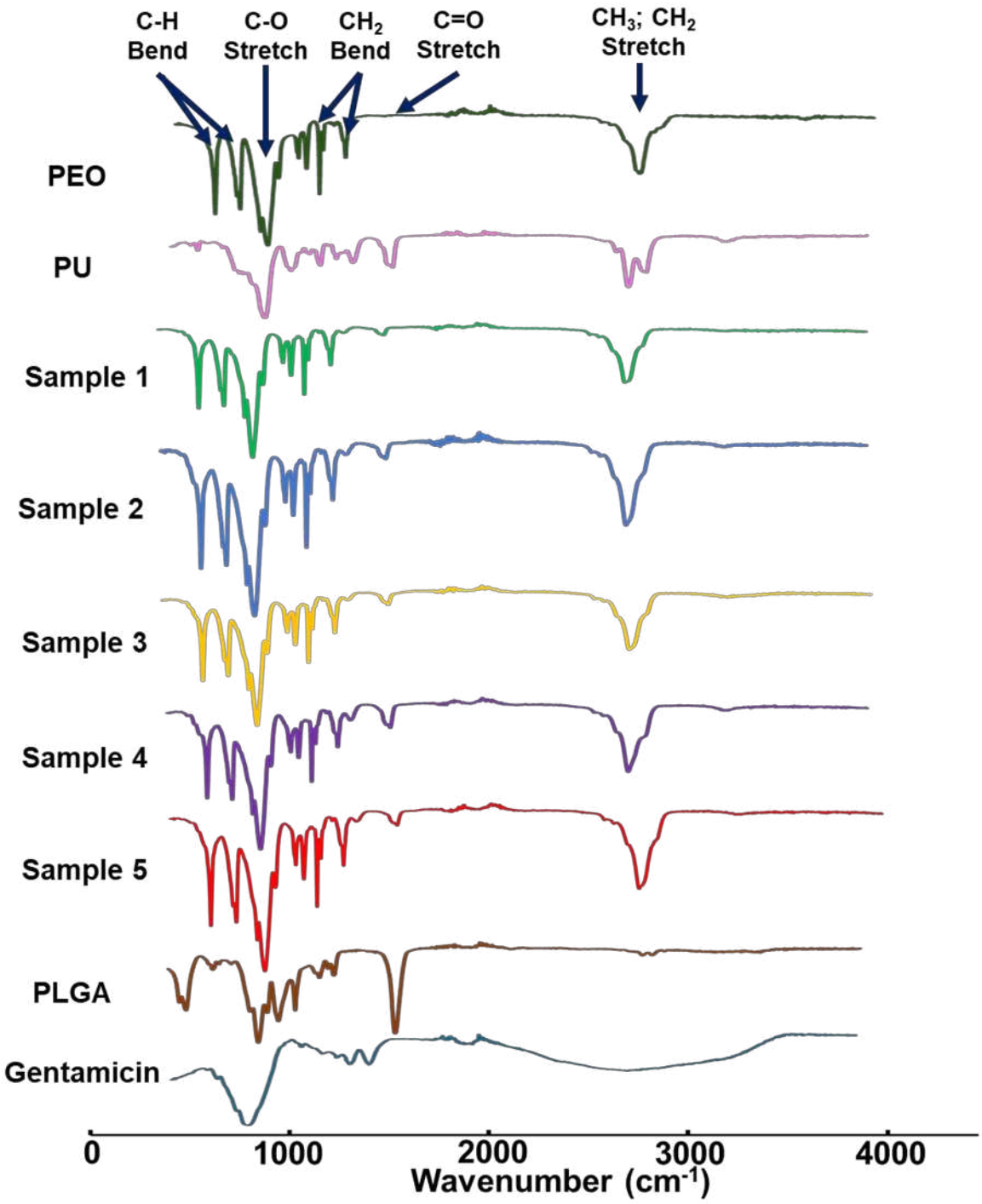

Figure 23. Chemical Analysis of five fiber samples. **Sample 1:** gentamicin-PLGA NPs-PEO (C)+ PEO-PU (S) fiber scaffolds; **Sample 2:** Gentamicin-PEO (C) + PEO-PU (S) fiber scaffolds; **Sample 3:** PLGA NPs-PEO (C) + PEO-PU (S) fiber scaffolds; **Sample 4:** Gentamicin-PLGA NPs-PEO (C) + PU (S) fiber scaffolds; **Sample 5:** PEO (C) + PEO-PU (S) fiber scaffolds. The aiming characteristic peaks of PLGA were fixed C-H bends at 850cm^{-1}; -C-O-C- ether at 1080-1180cm^{-1}; -C=O stretch at 1750cm^{-1}; CH_3 and CH_2 stretch at 2880-3010cm^{-1}.

4.3.3 Core-shell Fiber Scaffold Morphology

Both SEM and TEM were employed to investigate the morphological properties of five different core-shell fiber scaffold samples. The morphological analysis elucidated the scaffold fabrication process in relation to the architecture of the electrospun fibers, particularly focusing on the core-shell structures and the distribution of PLGA NP.

Fiber sample 1 comprised a PEO core layer and a PU-PEO shell layer. This sample served as a control to validate the feasibility of the spinning solutions for producing fibrous core-shell scaffolds. Figure 24-1-(A) and 24-2-(B) showed the morphology of fiber sample 1, while Figure 24-1-(C), a TEM image, presented its core-shell structure, with the core layer measuring 0.61μm in diameter and the outer diameter reaching 1.15μm. The absence of NPs in sample 1 resulted in smaller inner and outer diameters, underscoring the critical role of controlling the size distribution of PLGA NPs in core-shell fiber scaffolds fabrication. Fiber diameters for different samples are summarized in Table 7 for further clarification. For fiber sample 2, gentamicin was directly introduced into the core of the fiber without the protection of PLGA NPs. The fibers were uniform and did not show big droplets or chunks on the fiber surfaces. The TEM image shown in Figure 24-2-(B) confirmed a core-shell structure, with inner and outer diameters of 1.43μm and 1.93μm, respectively. Previous literature has suggested that core-shell fiber scaffolds could regulate drug release [14][28][29]. In this study, sample 2 served as a controlled sample for release profiles compared to gentamicin-loaded PLGA NPs CSNSs, as detailed in the subsequent section.

Table 7. Core-Shell fiber scaffolds dimensions: **#1**, PEO (C) + PEO-PU (S); **#2**, Gentamicin-PEO (C) + PEO-PU (S); **#3**, PLGA NPs-PEO (C) + PEO-PU (S); **#4**, Gentamicin-PLGA NPs-PEO (C) + PU (S); **#5**, gentamicin-PLGA NPs-PEO (C)+ PEO-PU (S).

Fiber sample	Fiber diameter (μm)	Core fiber diameter (μm)	Diameter ratio (D_{inner}/D_{fiber})
#1	1.15	0.61	0.530
#2	1.93	1.43	0.741
#3	1.89	1.21	0.640
#4	1.85	1.09	0.589
#5	2.22	1.38	0.622

In fiber sample 3, PLGA NPs loaded into the core of the fibers did not encapsulate gentamicin, making it in a control sample. SEM images (Figure 24-3-(A)) demonstrated smooth and uniform fiber morphology, while the TEM image (Figure 24-3-(B)) illustrated a core-shell structure with core and shell diameters of 1.21μm and 1.89μm, respectively. Sample 4 closely resembled sample 3, except for the absence of PEO in the shell layer, which was made solely of PU). A comparison with other fiber samples revealed noticeable inconsistencies, including large droplets and agglomerates in fiber morphology, suggesting a phase separation during electrospinning due to the lack of PEO as a stabilizer agent. The TEM image in Figure 24-4-(B) showed a core-shell structure with inner and outer diameters of 1.09μm and 1.85μm, respectively. The limited incorporation of NPs into the core fiber layer may be attributed to the absence of PEO in the shell layer, leading to a significant energy barrier for NP diffusion and resulting in NP aggregation in droplets throughout the fiber scaffolds.

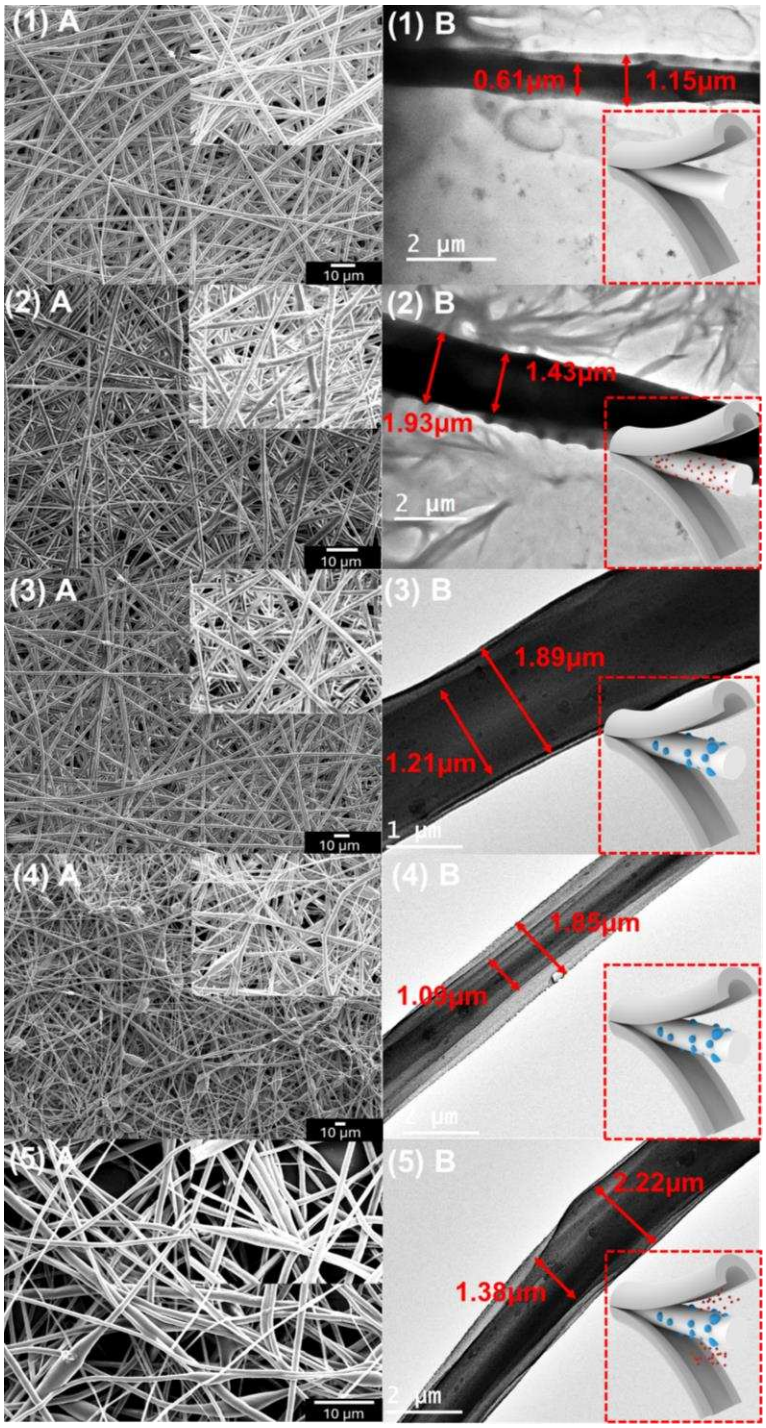

Figure 24. SEM (A) and TEM (B) images showing fiber sample morphologies. **(1)** PEO (C) + PEO-PU (S) fiber scaffolds; **(2)** Gen-PEO (C) + PEO-PU (S) fiber scaffolds; **(3)** PLGA NPs-PEO (C) + PEO-PU (S) fiber scaffolds; **(4)** Gen-PLGA NPs-PEO (C) + PU (S) fiber scaffolds; **(5)** Gen-PLGA NPs-PEO (C)+ PEO-PU (S) fiber scaffolds.

Sample 5 comprised core-shell nanofibers with a PU/PEO shell and a PEO core containing Gen/PLGA NPs. The SEM images (Figure 24-5-(A)) illustrated the morphology of

sample 5, suggesting uniform and smooth fibers in the longitudinal direction. Figure 24-5-(B) showed a TEM image revealing a core and shell structure of the fiber, with approximate core and shell layer diameters of 1.38μm and 2.22μm, respectively. Additionally, PLGA NPs were primarily loaded in the core of the fiber. These images confirmed the successful development of Gen/PLGA NPs loaded PU/PEO core-shell fiber scaffolds, with NPs primarily concentrated within the core layer, as illustrated in the inserted schematic picture in Figure 24-5-(B).

4.3.4 Gentamicin Release Profile

The release of gentamicin from fibrous scaffolds was quantified by measuring the concentration of released gentamicin at different time intervals. Figure 25 shows release profiles for scaffold samples 2, 4 and 5. Samples 1 and 3 did not exhibit release profiles as gentamicin was not loaded in these samples. Sample 5 demonstrated a linear release profile, indicating effective control of gentamicin release in a slow and sustained manner. This linear relationship suggested that gentamicin, encapsulated in PLGA NPs and further loaded into the core of the fibers, exhibited controlled and prolonged release. In contrast, sample 2 exhibited a burst release within the first hour. Since gentamicin in sample 2 was not encapsulated in PLGA nanoparticles but directly incorporated into the fibers, it was released rapidly. This release profile indicated that only 30% of gentamicin was released from sample 5, while 45% was released from fiber sample 2, highlighting the efficiency of utilizing NPs as drug carrier systems for controlled release. In sample 4, the release of gentamicin was minimal, particularly in the initial hours. This minimal release can be attributed to the fact that the fiber's shell consisted of 100 % PU without any PEO. The hydrophobic nature of PU hindered gentamicin release in an aqueous environment. The slight release observed may be attributed to gentamicin diffusion rather than fiber degradation. A comparison with our previous study on gentamicin release from monolithic fibers [34] suggested

that the core-shell structure has enhanced the controlled release of gentamicin from fiber scaffolds by 8% in the first 12 hours. This improvement underscored the effectiveness of core-shell nanofiber scaffolds as a strategy for long-term drug delivery systems.

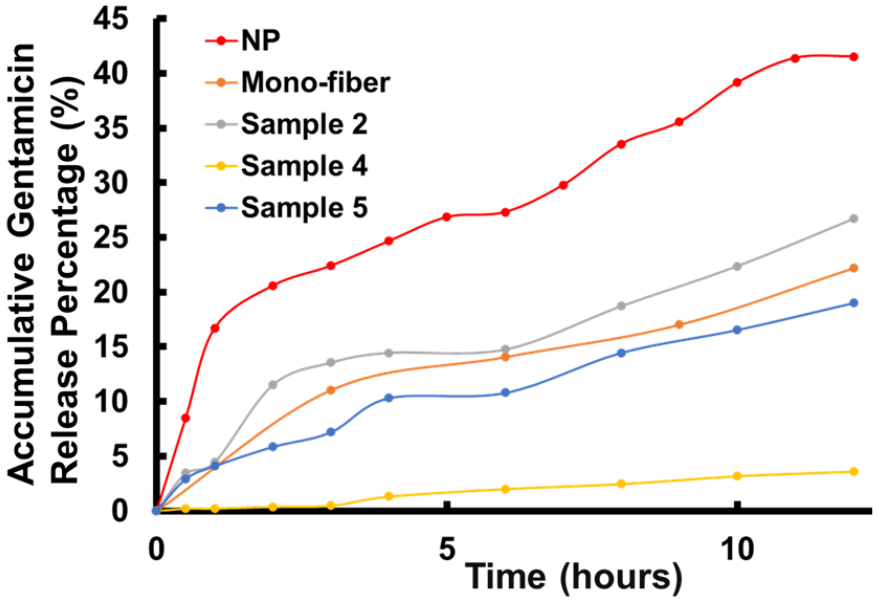

Figure 25. Release profiles of core shell fiber samples. Accumulative gentamicin amount percentage released from scaffolds were presented at different times. **Sample 2**: Gentamicin-PEO (C) + PEO-PU; **Sample 4**: Gentamicin-PLGA NPs-PEO (C) + PU (S) fiber scaffolds. **Sample 5**: gentamicin-PLGA NPs-PEO (C)+ PEO-PU (S) fiber scaffolds.

4.3.5 Antimicrobial Activity

The antimicrobial activities of fiber scaffold samples were assessed by measuring the bacterial inhibition zone using an agar diffusion method adapted from the standard testing method of AATCC 100 for antimicrobial testing of textile materials. The bacterial inhibition zones after 24 hours were captured by photographs shown in Figure 26 (A), with corresponding quantified clear inhalation zone radii presented in Figure 26 (B). Sample 1, serving as a control, exhibited no antimicrobial activity, indicating that core-shell fibers lacking gentamicin were unable to combat bacterial infections. Similarly, fiber sample 3 showed no visible effects in controlling bacterial growth, confirming the absence of antimicrobial activities in PLGA, PEO and PU. Despite the incorporation of Gen/PLGA NPs in sample 4, no bacterial inhibition was

observed. This lack of inhibition could be attributed to the hydrophobic nature of the fiber shell composed solely of PU, which did not dissolve in water, thereby impeding gentamicin release from the fiber core. Sample 2, where gentamicin was directly incorporated into core-shell nanofibers, demonstrated significant antimicrobial activities within 24 hours. The comparison of sample 2 and sample 4, highlighted the critical role of PEO in the shell layer for enhancing drug release due to its water solubility, facilitating diffusion [46][47]. In fiber sample 5, gentamicin was first encapsulated in PLGA NPs which were further loaded in the fiber core. The fiber shell was made of PU/PEO, so the PEO is water soluble, leaving the path for gentamicin to release slowly in 24 hours, demonstrating controlled bacterial infection management. The inhibition zone for sample 5 was 55mm, in contrast to 110.4mm for sample 2, suggesting that using NPs as drug carries protected in core-shell nanofibers can significantly moderate drug release through a prolonged diffusion process.

These results indicate that gentamicin-loaded PLGA NPs within a PEO-PU CSNS effectively control the release rates of gentamicin, aiding in the control of bacterial infections. Future studies should include a quantitative analysis for bacterial infection control, particularly focusing on determining the minimum inhibitory concentration (MIC) and minimum bactericidal concentration (MBC) to further optimize this approach. Additionally, further studies should investigate the release mechanisms of gentamicin that are doubly protected by both the PLGA NPs and the PU/PEO nanofibers.

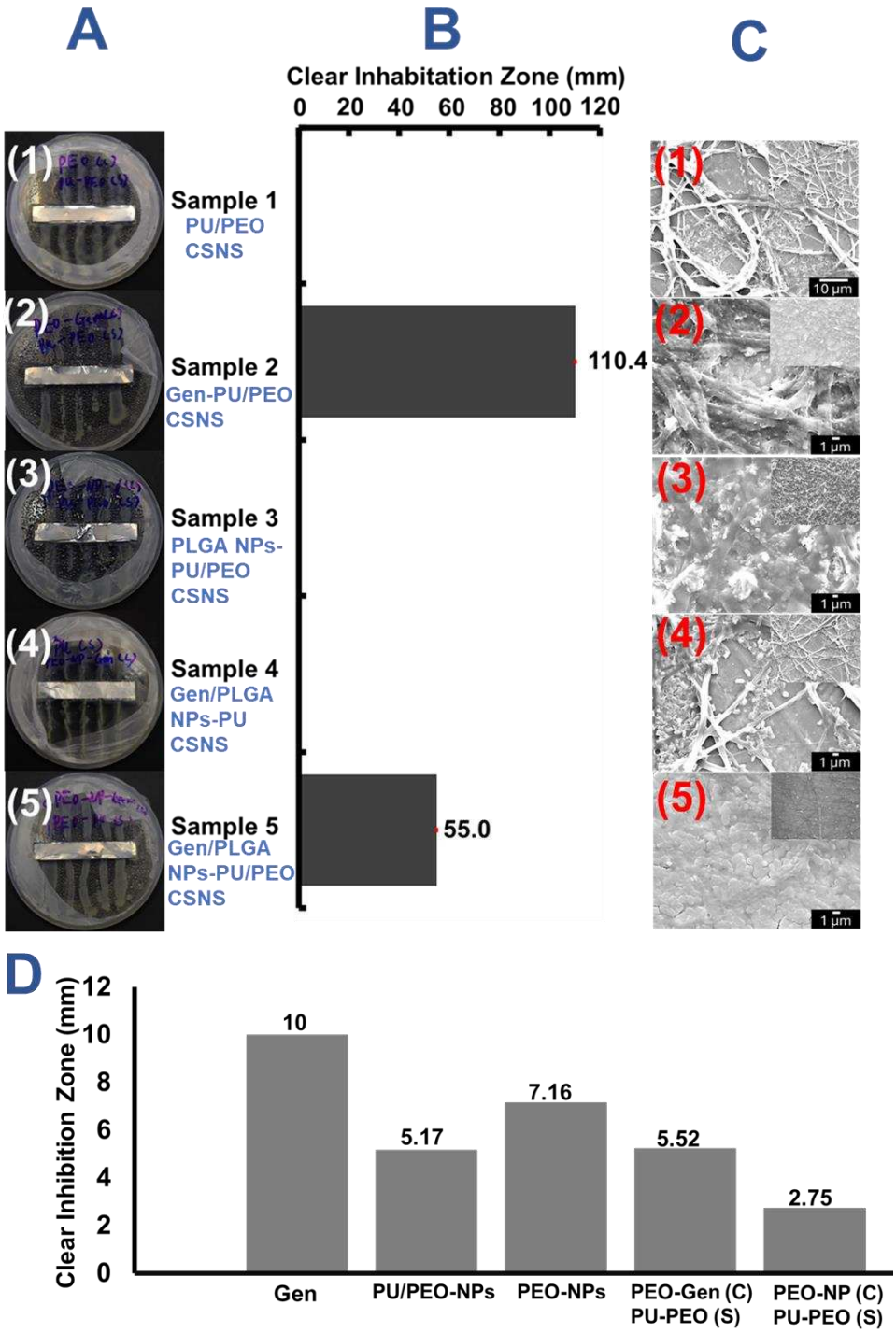

Figure 26. (A) Antimicrobial activity tests. **Sample 1:** PEO (C) + PEO-PU (S) fiber scaffolds; **Sample 2:** Gentamicin-PEO (C) + PEO-PU (S) fiber scaffolds; **Sample 3:** PLGA NPs-PEO (C) + PEO-PU (S) fiber scaffolds; **Sample 4:** Gentamicin-PLGA NPs-PEO (C) + PU (S) fiber scaffolds; **Sample 5:** gentamicin-PLGA NPs-PEO (C)+ PEO-PU (S) fiber scaffolds. **(B)** The average inhabitation diameter of each fiber sample. **(C)** SEM images of CSNS after antimicrobial tests. **1**: sample 1 fibers remain fiber structures covered with *E.coli*. **2**: degraded Sample 2 fibers controlled *E.coli* growth well. **3**: degraded Sample 3 fibers cannot control bacterial growth. **4**: sample 4 fibers remain fiber structure and *E.coli* grew naturally. **5**: degraded Sample 5 fibers covered with *E.coli*. (D) Antimicrobial activity comparison with published

data. Gen: gentamicin coated petri dish. No bacterial inhibition zone; PU/PEO-NPs: PLGA NPs incorporated PU/PEO monolithic fibers; PEO-NPs: PLGA NPs incorporated PEO monolithic fibers; PEO-Gen(C) PU-PEO(S): sample 2; PEO-NP(C) PU-PEO (S): sample 5.

The SEM images presented in Figure 26 showed the condition of the CSNS samples following the antimicrobial tests. As shown in Figure 26-1-(A) and 26-1-(B), fiber sample 1, which lacked gentamicin, showed unimpeded growth of *E.coli*, indicating no bacterial inhibition. In contrast, Figure 26-2-(A) and 26-2-(B) displayed a minimal presence of *E.coli* on the surface of sample 2, suggesting that the rapid release of gentamicin partially inhibited bacterial proliferation. Figure 26-3-(A) and 26-3-(B) reveal extensive growth of *E.coli* on sample 3, which lacked gentamicin-loaded PLGA NPs, allowing for unrestricted bacterial growth. Sample 4, as presented in Figure 26-4-(A) and 26-4-(B), maintained its structural integrity as PU, which did not dissolve in water, preventing the release of gentamicin from the fibers. Figure 26-5-(A) and 26-5-(B) showed the degraded state of sample 5, where *E.coli* were visible across the fiber surface. The rapid degradation observed in sample 5 was due to the high solubility of PEO in water after application to the LB agar petri dish. Sample 5, along with samples 2 and 3, exhibited a similar pattern where the presence of PU contributed to maintaining the fiber structure because of its lower solubility in water. This configuration allowed for the controlled release of gentamicin from the PLGA NPs, effectively managing bacterial infection. The results shown in these images aligned closely with the data presented in Figure 25, illustrating the impact of material composition on the antimicrobial efficacy of the CSNS. The antimicrobial efficiency of these scaffolds is also influenced by other factors, including MIC, MBC, gentamicin loading efficiency, and fiber morphological properties such as fiber aspect ratio. Quantification of these factors will further optimize CSNS development and should be explored in future research.

4.4 Conclusion

In this paper, we discussed an effective fabrication process for novel transdermal materials for wound treatment. The process incorporated gentamicin-loaded PLGA NPs into PU/PEO CSNS through coaxial electrospinning. The Gen/PLGA NPs, synthesized using a double emulsion solvent evaporation method and refined through a-four step purification process, averaged 130 nm in diameter. The purification enhanced their compatibility with the fiber matrix. The core spinning solution combined a PLGA NP solution with PEO dissolved in DCM. This mixture leveraged the complex properties of PEO to ensure high compatibility with the PLGA NP water solution. The shell solution, composed of PU/PEO dissolved in chloroform, used PU to maintain the structural integrity of the fiber scaffold due to its lower water solubility. PEO, serving as the continuous phase, facilitated the integration of core layers and created diffusion paths for drug release, owing to its hydrophilic and hydrophobic functional groups. The fiber morphology confirmed that the advanced system - gentamicin-encapsulated PLGA NPs loaded into PU/PEO CSNSs - can be effectively developed using coaxial electrospinning. Furthermore, the release profiles and antimicrobial tests demonstrated that gentamicin could be released from these CSNS in a controlled manner to inhibit E. coli growth effectively and sustainably.

The work discussed in this paper demonstrated that polymeric NPs hold significant promise for the development of transdermal materials, surpassing previous methodologies that predominantly focused on metal, metal/semi-metal oxide, or natural extracts. Furthermore, the ability to load PLGA NPs with a variety of drugs substantially expands the potential applications of these novel transdermal materials in biomedical fields. The methods and procedures detailed herein effectively demonstrated the successful incorporation of Gen/PLGA NPs into PU/PEO

CSNS. Our findings pave the way for innovative transdermal material development, contributing to further advancements in nanotechnology.

4.5 References

[1] Elahi, M. F., & Lu, W. (2013). Core-shell fibers for biomedical applications-A Review. *J. Bioeng. Biomed. Sci.*, *03*(01). https://doi.org/10.4172/2155-9538.1000121

[2] Liu, T., Burger, C., & Chu, B. (2003). Nanofabrication in polymer matrices. *Prog. Polym. Sci.*, *28*(1), 5–26. https://doi.org/10.1016/s0079-6700(02)00077-1

[3] Zhang, S. (2003). Fabrication of novel biomaterials through molecular self-assembly. *Nat. Biotechnol.*, *21*(10), 1171–1178. https://doi.org/10.1038/nbt874

[4] Smith, L. A., Liu, X., & Ma, P. X. (2008). Tissue engineering with nano-fibrous scaffolds. *Soft Matter*, *4*(11), 2144. https://doi.org/10.1039/b807088c

[5] Xie, X. N., Chung, H. J., Sow, C. H., & Wee, A. T. S. (2006). Nanoscale materials patterning and engineering by Atomic Force Microscopy nanolithography. *Mater. Sci. Eng. R*, *54*(1-2), 1–48. https://doi.org/10.1016/j.mser.2006.10.001

[6] Sperling, L., Reis, K., Pranke, P., & Wendorff, J. (2016). Advantages and challenges offered by bio-functional core–shell fiber systems for tissue engineering and drug delivery. *Drug Discov. Today*, *21*(8), 1243–1256. https://doi.org/10.1016/j.drudis.2016.04.024

[7] Hu, S., Chen, H., Zhou, F., Liu, J., Qian, Y., Hu, K., Yan, J., Gu, Z., Guo, Z., Zhang, F., & Gu, N. (2021). Superparamagnetic core–shell electrospun scaffolds with sustained release of ions facilitating *in vitro* and *in vivo* bone regeneration. *J. Mater. Chem. B*, *9*(43), 8980–8993. https://doi.org/10.1039/d1tb01261d

[8] Loscertales, I. G., Barrero, A., Guerrero, I., Cortijo, R., Marquez, M., & Gañán-Calvo A. M. (2002). Micro/nano encapsulation via electrified coaxial Liquid Jets. *Science*, *295*(5560), 1695–1698. https://doi.org/10.1126/science.1067595

[9] Zhang, Y., Huang, Z.-M., Xu, X., Lim, C. T., & Ramakrishna, S. (2004). Preparation of core−shell structured PCL-r-gelatin bi-component nanofibers by coaxial electrospinning. *Chem. Mater.*, *16*(18), 3406–3409. https://doi.org/10.1021/cm049580f

[10] King, M. W., & Chung, S. (2013). Medical fibers and biotextiles. *Biomater. Sci.*, 301–320. https://doi.org/10.1016/b978-0-08-087780-8.00029-2

[11] Zhang, Y. Z., Venugopal, J., Huang, Z.-M., Lim, C. T., & Ramakrishna, S. (2005). Characterization of the surface biocompatibility of the electrospun PCL-collagen nanofibers using fibroblasts. *Biomacromolecules*, *6*(5), 2583–2589. https://doi.org/10.1021/bm050314k

[12] Perez, R. A., & Kim, H.-W. (2015). Core–shell designed scaffolds for drug delivery and Tissue Engineering. *Acta Biomater.*, *21*, 2–19. https://doi.org/10.1016/j.actbio.2015.03.013

[13] Naeimirad, M., Zadhoush, A., Kotek, R., Esmaeely Neisiany, R., Nouri Khorasani, S., & Ramakrishna, S. (2018). Recent advances in core/shell bicomponent fibers and nanofibers: A Review. *J. Appl. Polym. Sci.*, *135*(21). https://doi.org/10.1002/app.46265

[14] Tiwari, S. K., Tzezana, R., Zussman, E., & Venkatraman, S. S. (2010). Optimizing partition-controlled drug release from Electrospun Core–shell fibers. *Int. J. Pharm.*, *392*(1-2), 209–217. https://doi.org/10.1016/j.ijpharm.2010.03.021

[15] Zheng, X., Tang, J., Wang, P., Wang, Z., Zou, L., & Li, C. (2022). Interfused core-shell heterogeneous graphene/mxene fiber aerogel for high-performance and durable electromagnetic interference shielding. *J. Colloid Interface Sci.*, *628*, 994–1003. https://doi.org/10.1016/j.jcis.2022.08.019

[16] Chen, H., Wang, N., Di, J., Zhao, Y., Song, Y., & Jiang, L. (2010). Nanowire-in-microtube structured core/shell fibers via multifluidic coaxial electrospinning. *Langmuir*, *26*(13), 11291–11296. https://doi.org/10.1021/la100611f

[17] Sun, Z., Zussman, E., Yarin, A. L., Wendorff, J. H., & Greiner, A. (2003). Compound core–Shell polymer nanofibers by CO-electrospinning. *Adv. Mater.*, *15*(22), 1929–1932. https://doi.org/10.1002/adma.200305136

[18] Li, Y., Zhu, J., Cheng, H., Li, G., Cho, H., Jiang, M., Gao, Q., & Zhang, X. (2021). Developments of advanced electrospinning techniques: A critical review. *Adv. Mater. Technol.*, *6*(11). https://doi.org/10.1002/admt.202100410

[19] Pakravan, M., Heuzey, M.-C., & Ajji, A. (2012). Core–shell structured PEO-chitosan nanofibers by coaxial electrospinning. *Biomacromolecules*, *13*(2), 412–421. https://doi.org/10.1021/bm201444v

[20] Doğan, Y. K., Demirural, A., & Baykara, T. (2019). Single-needle electrospinning of PVA hollow nanofibers for core–shell structures. *SN Appl. Sci.*, *1*(5). https://doi.org/10.1007/s42452-019-0446-z

[21] Babapoor, A., Karimi, G., Golestaneh, S. I., & Mezjin, M. A. (2017). Coaxial electro-spun PEG/PA6 composite fibers: Fabrication and characterization. *Appl. Therm. Eng.*, *118*, 398–407. https://doi.org/10.1016/j.applthermaleng.2017.02.119

[22] You, Z.-R., Hu, M.-H., Tuan-Mu, H.-Y., & Hu, J.-J. (2016). Fabrication of poly (glycerol sebacate) fibrous membranes by coaxial electrospinning: Influence of Shell and core solutions. *J. Mech. Behav. Biomed. Mater.*, *63*, 220–231. https://doi.org/10.1016/j.jmbbm.2016.06.022

[23] Liu, F., Jiang, Y., Peng, F., Feng, J., Li, L., & Feng, J. (2023). Fiber-reinforced alumina-carbon core-shell aerogel composite with heat-induced gradient structure for thermal protection up to 1800 °C. *Chem. Eng. J.*, *461*, 141721. https://doi.org/10.1016/j.cej.2023.141721

[24] Alharbi, H. F., Luqman, M., Fouad, H., Khalil, K. A., & Alharthi, N. H. (2018). Viscoelastic behavior of core-shell structured nanofibers of PLA and PVA produced by coaxial electrospinning. *Polym. Test.*, *67*, 136–143. https://doi.org/10.1016/j.polymertesting.2018.02.026

[25] Song, B., Wu, C., & Chang, J. (2012). Dual drug release from Electrospun Poly (lactic-co-glycolic acid)/mesoporous silica nanoparticles composite mats with distinct release profiles. *Acta Biomater.*, *8*(5), 1901–1907. https://doi.org/10.1016/j.actbio.2012.01.020

[26] Mohamady Hussein, M. A., Guler, E., Rayaman, E., Cam, M. E., Sahin, A., Grinholc, M., Sezgin Mansuroglu, D., Sahin, Y. M., Gunduz, O., Muhammed, M., El-Sherbiny, I. M., & Megahed, M. (2021). Dual-drug delivery of ag-chitosan nanoparticles and phenytoin via core-shell PVA/PCL Electrospun nanofibers. *Carbohydr. Polym.*, *270*, 118373. https://doi.org/10.1016/j.carbpol.2021.118373

[27] Awada, H., Al Samad, A., Laurencin, D., Gilbert, R., Dumail, X., El Jundi, A., Bethry, A., Pomrenke, R., Johnson, C., Lemaire, L., Franconi, F., Félix, G., Larionova, J., Guari, Y., & Nottelet, B. (2019). Controlled anchoring of iron oxide nanoparticles on polymeric nanofibers: Easy access to core-shell organic–inorganic nanocomposites for magneto-scaffolds. *ACS Appl. Mater. Interfaces*, *11*(9), 9519–9529. https://doi.org/10.1021/acsami.8b19099

[28] Mahdieh, Z., Mitra, S., & Holian, A. (2020). Core–shell electrospun fibers with an improved open pore structure for size-controlled delivery of nanoparticles. *ACS Appl. Polym. Mater.*, *2*(9), 4004–4015. https://doi.org/10.1021/acsapm.0c00643

[29] Huang, H., He, C., Wang, H., & Mo, X. (2009). Preparation of core-shell biodegradable microfibers for long-term drug delivery. *J. Biomed. Mater. Res. A*, *90A* (4), 1243–1251. https://doi.org/10.1002/jbm.a.32543

[30] Pang, H., Huang, X., Xu, Z. P., Chen, C., & Han, F. Y. (2023). Progress in oral insulin delivery by PLGA nanoparticles for the management of diabetes. *Drug Discov. Today*, *28*(1), 103393. https://doi.org/10.1016/j.drudis.2022.103393

[31] Fleten, K. G., Hyldbakk, A., Einen, C., Benjakul, S., Strand, B. L., Davies, C. de, Mørch, Ý., & Flatmark, K. (2022). Alginate microsphere encapsulation of drug-loaded nanoparticles: A novel strategy for Intraperitoneal Drug Delivery. *Mar. Drugs*, *20*(12), 744. https://doi.org/10.3390/md20120744

[32] Li, H., Palamoor, M., & Jablonski, M. M. (2016). Poly (ortho ester) nanoparticles targeted for chronic intraocular diseases: Ocular Safety and localization after Intravitreal Injection. *Nanotoxicology*, *10*(8), 1152–1159. https://doi.org/10.1080/17435390.2016.1181808

[33] Danafar, H. (2016). MPEG–PCL copolymeric nanoparticles in Drug Delivery Systems. *Cogent Med.*, *3*(1), 1142411. https://doi.org/10.1080/2331205x.2016.1142411

[34] Sun, Y., Heacock, J., Chen, C., Qiu, K., Zou, L., Liu, J., & Li, Y. V. (2023). Incorporation of gentamicin-encapsulated poly (lactic-*co*-glycolic acid) nanoparticles into polyurethane/poly (ethylene oxide) nanofiber scaffolds for biomedical applications. *ACS Appl. Nano Mater.*, *6*(17), 16096–16105. https://doi.org/10.1021/acsanm.3c03549

[35] Sun, Y., Bhattacharjee, A., Reynolds, M., & Li, Y. V. (2021). Synthesis and characterizations of gentamicin-loaded poly-lactic-co-glycolic (PLGA) nanoparticles. *J. Nanoparticle Res.*, *23*(8). https://doi.org/10.1007/s11051-021-05293-3

[36] Hwang, T. H., Lee, Y. M., Kong, B.-S., Seo, J.-S., & Choi, J. W. (2012). Electrospun core–shell fibers for robust silicon nanoparticle-based lithium-ion battery anodes. *Nano Lett.*, *12*(2), 802–807. https://doi.org/10.1021/nl203817r

[37] Anaya Mancipe, J. M., Boldrini Pereira, L. C., de Miranda Borchio, P. G., Dias, M. L., & da Silva Moreira Thiré, R. M. (2022). Novel polycaprolactone (PCL)-type I collagen core-shell electrospun nanofibers for wound healing applications. *J. Biomed. Mater. Res. B Appl. Biomater.*, *111*(2), 366–381. https://doi.org/10.1002/jbm.b.35156

[38] Wang, Ying, Liu, L., Zhu, Y., Wang, L., Yu, D.-G., & Liu, L. (2023). Tri-layer core–shell fibers from coaxial electrospinning for a modified release of Metronidazole. *Pharmaceutics*, *15*(11), 2561. https://doi.org/10.3390/pharmaceutics15112561

[39] Farkas, N.-I., Marincaș, L., Barbu-Tudoran, L., Barabás, R., & Turdean, G. L. (2023). Investigation of the real-time release of doxycycline from PLA-based nanofibers. *J. Funct. Biomater.*, *14*(6), 331. https://doi.org/10.3390/jfb14060331

[40] Esmaeili, A., & Asgari, A. (2015). In vitro release and biological activities of Carum Copticum Essential Oil (CEO) loaded chitosan nanoparticles. *Int. J. Biol Macromol.*, *81*, 283–290. https://doi.org/10.1016/j.ijbiomac.2015.08.010

[41] Kenawy, E.-R., Bowlin, G. L., Mansfield, K., Layman, J., Simpson, D. G., Sanders, E. H., & Wnek, G. E. (2002). Release of tetracycline hydrochloride from Electrospun Poly (ethylene-co-vinyl acetate), poly (lactic acid), and a blend. *JCR*, *81*(1–2), 57–64. https://doi.org/10.1016/s0168-3659(02)00041-x

[42] Tan, H. Y., Widjaja, E., Boey, F., & Loo, S. C. (2009). Spectroscopy techniques for analyzing the hydrolysis of PLGA and PLLA. *Journal of Biomedical Materials Research Part B: Applied Biomaterials*, *91B* (1), 433–440. https://doi.org/10.1002/jbm.b.31419

[43] Wang, Y., Li, P., & Kong, L. (2013). Chitosan-modified PLGA nanoparticles with versatile surface for improved drug delivery. *AAPS PharmSciTech*, *14*(2), 585–592. https://doi.org/10.1208/s12249-013-9943-3

[44] Silva, A. T., Cardoso, B. C., Silva, M. E., Freitas, R. F., & Sousa, R. G. (2015). Synthesis, characterization, and study of PLGA Copolymer in vitro Degradation. *J. Biomater. Nanobiotechnol. 06*(01), 8–19. https://doi.org/10.4236/jbnb.2015.61002

[45] Paragkumar N, T., Edith, D., & Six, J.-L. (2006). Surface characteristics of PLA and PLGA films. *Appl. Surf. Sci.*, *253*(5), 2758–2764. https://doi.org/10.1016/j.apsusc.2006.05.047

[46] Pauelsen, F., Huppertsberg, S., Knepper, T. P., & Zahn, D. (2023). Narrowing the analytical gap for water-soluble polymers: A novel trace-analytical method and first quantitative occurrence data for polyethylene oxide in surface and wastewater. *Sci. Total Environ.*, *882*, 163563. https://doi.org/10.1016/j.scitotenv.2023.163563

[47] Chen, T., Li, Y., Wan, H., Xu, L., Yang, Y., Liu, Z., Gao, K., Huang, J., Zhou, S., & Gao, Z. (2023). Modified PU sponge for water purification. *J. Environ. Chem. Eng.*, *11*(3), 109980. https://doi.org/10.1016/j.jece.2023.109980

Chapter 5

Manuscript: Machine Learning Integrated with In Vitro Experiments for Study of Drug Release from Poly (Lactic-co-Glycolic Acid) Particles

Overview

This paper investigates delivery of encapsulated drug from poly lactic-co-glycolic (PLGA) micro-/nano-particles (MPs/NPs). Experimental data collected from about 50 papers are analyzed by machine learning (ML) algorithms including linear regression, principal component analysis (PCA), Gaussian process regression (GPR), and artificial neural networks (ANNs). The focus is to understand the effect of drug solubility, drug molecular weight, particle size, and pH-value of the release matrix/environment on drug release profiles. The results obtained from machine learning are then used as guidelines for designing new *in vitro* experiments to examine dependence of drug release profiles on those four factors. It is interesting to see that indeed the results of the new *in vitro* experiments are in basic agreement with the results obtained from machine learning

5.1 Introduction

Antibiotics are the most widely used drugs of antibacterial agents, so developing and improving corresponding drug delivery has always been a great concern for the pharmaceutical industry. With the development of nanotechnology, the application of nano-techniques has revolutionized drug delivery methods for the past decades.

Nano-structures, such as nanoparticles (NPs), nano-micelles, dendrimers, liposomes, and nanotubes, have emerged as powerful drug carriers for biomedical applications. Literature

research suggests that NPs were among the most effective drug carriers for drug delivery. Integrating drugs into NPs shows great advantages compared to other nano-structures [1].

NPs usually have a core-shell structure where the drugs are encapsulated inside. The loaded drug bioactivity can be preserved for weeks, leading to scalable production [2]. Previous research has shown that NP size distributions can be controlled around 100nm, which make it capable for delivering drugs through blood capillaries and allow for access into cells. In addition, NPs can deliver drugs to targeted sites precisely by modifying NPs to synthesize polymers with specific ligands [3]. Due to NPs' outstanding properties, NP-base drug delivery systems are effective and versatile.

Due to the widely adoption of NP-based drug delivery systems, study of its properties has aroused great research interests. Release profiles of encapsulated drugs are an important aspect of drug delivery systems Modeling the release processes mathematically has been being an active interdisciplinary research area.

Various factors affect release profiles of drug from NPs. Among those factors, pH value of the release matrix or environments, and solubility of the encapsulated drug are the most important [4].

pH plays an important role in human body. Various diseases can alternate local lesion matrix of pH, in which PLGA NP release profiles change accordingly [5]. Results in literature reveal that pH-values of human organs are quite different. For example, the pH-value of a health lung is maintained at 7. But cystic fibrosis causes its pH to decrease to become acidic [6]. Normally, the pH-value of skin surfaces is in the range of 4.1-5.8 with small variations among different parts of the human body. However, inflammatory diseases with an involvement of the

epidermis can break the skin antimicrobial barriers, leading to an increase in pH-value [7]. The pH-value of blood and interstitial fluid is in the range of 7.35-7.45. On the other hand, a highly acidic pH value 1-1.5 can be measured in an empty stomach [7].

Modelling the processes of drug release from micro-/nanoparticles has been attracting researchers from various disciplines. In 2012, Siepmann summarized empirical/semi-empirical governing equations for various NP-based drug delivery systems [8]. But these mathematical models described release profiles under idealized circumstances and postulations, which limited their predictability.

Recently, machine learning (ML) has become a power research tool for a wide range of scientific and engineering problems [9-10] ML algorithms can handle and analyze complicated datasets and identify linear and nonlinear relationships among variables accurately and effectively [10]. These include classical algorithms like linear regression and principal component analysis (PCA) and recent more advanced algorithms such as Gaussian regression process (GPR), and artificial neural networks (ANNs) [9, 11, 12].

As a new research paradigm, machine learning provides an inexpensive and environment-friendly approach for conducting certain types of research, e.g., drug release, which previously relies on tedious and error-prone experiments [13]. Once a machine learning model is established, it can be readily used with various parameter values.

Mechanisms for drug release from PLGA micro-/nanoparticles have been widely studied. The following four release mechanisms have been well recognized when drugs are encapsulated within PLGA nanoparticles [14–16].

(1) Diffusion through polymeric shells, which usually governs the early stage of release;

(2) Convection through pores on the shells;

(3) Osmotic Pumping: Caused by the drug concentration gradient;

(4) Degradation: As the particles degrade in the late stage.

As for medical applications of drugs encapsulated in PLGA particles, minimum bactericidal concentration (MBC) is one of our major concerns, when applying antibiotics for bacterial infection control. MBC is the minimum concentrations of antibiotics that is bactericidal [17]. In addition, existing research works have shown that most MPs/NPs experienced a burst at the early stage. Therefore, quantification of the burst release profiles, and determination of effects of pH-value and drug solubility becomes critical for MP/NP-based drug delivery systems because neither underdose nor overdose can control bacterial infections, without mentioning local side effects.

The goals of this paper lied on applying ML algorithms integrating with in vitro experimental results to study effects of pH and drug solubility on NP-based drug delivery system release profiles. While a variety of approaches have been conducted to study release profiles from different perspectives, this paper applied ML algorithms to reveal the relationships among pH, drug solubility, and release rates. Our objectives were establishing cognitive mathematical models and aided by the powerful ML algorithms to generalize computational results for various circumstances. In summary, the paper focuses lies on:

(1) Study factors like pH-value of release environment/matrix, particle size, drug molecular weight, and drug solubility that affect drug release profiles;
(2) Apply machine learning algorithms to the release data collected from literature; These data are known results from in vitro experiments by various authors conducted on a

variety of drugs; These include data on the release amount percentage, pH-values of the environment/matrix, particle size, drug solubility, and drug molecular weight;

(3) Conduct our in vitro experiments with various drugs and conditions with the results of machine learning as guidelines for experiment design; Characterize release profiles;

(4) Compare results of our new in vitro experiments with that from machine learning algorithms to check potential agreement. The novelty of our approach lies in a synergistic combination of two research paradigms: in vitro experiments and machine learning, both are utilized for study of drug release from PLGA particles.

5.2 Machine Learning Algorithms

In this section, we briefly review four main algorithms for machine learning: linear regression, principal component analysis (PCA), Gaussian process regression (GPR), and artificial neural networks (ANNs). and a corresponding ML algorithm flow chart summarizes our methodology in Figure 27.

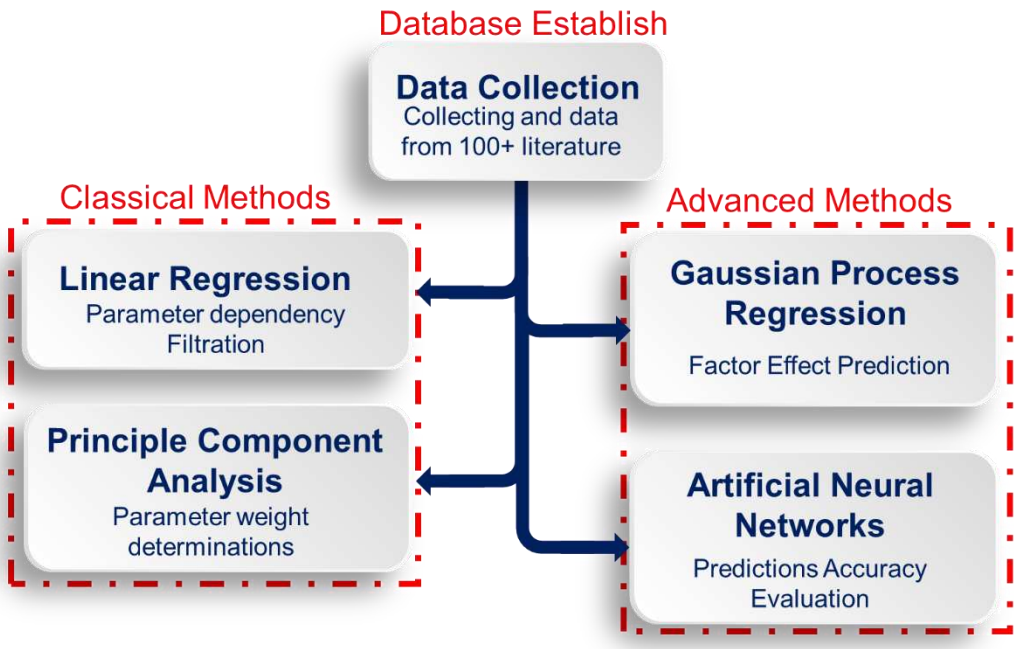

Figure 27. Task modules of machine learning for study of drug release from PLGA particles. Data was collected from over 50 literature, and linear regression, principal component analysis, Gaussian process regression, and artificial neural networks were adopted to analysis data.

5.2.1 Linear Regression

Linear regression is a simple but widely used supervised machine learning model that provides a linear model for correlation among a dependent variable and one or more explanatory variables.

Mathematically, linear regression can be expressed as:

$$y = X\beta + \varepsilon \qquad (28)$$

where β (as a vector) represents the coefficients that quantify the influence of each independent variable (a component of X), and ε is the error term. In practical use, β can be approximated by $\hat{\beta} = (X^T X)^{-1}(X^T y)$using the ordinary least squares (OLS).

For linear regression, Python provides has an OLS class in statsmodels.api

5.2.2 Principal Component Analysis (PCA)

Principal component analysis (PCA) is a classical unsupervised learning method that uses patterns present in a data set to reduce the complexity of the data while retaining the most important information.

Mathematically, PCA utilizes the eigenvalues and eigenvectors of the covariance matrix of a given set of data. Let X be a data matrix with m rows (observations) and n columns (features or variables). Assume matrix X is already standardized. Then the covariance matrix C is given by

$$C = \frac{1}{n-1} X^T X \qquad (29)$$

It is known that C is a symmetric positive semi-definite (SPD) matrix. Let$(\lambda_i, n_i), 1 \leq i \leq n$ be the eigenvalues and eigenvectors of C with all eigenvalues arranged in descending order.

If V is the matrix whose columns are the eigenvectors of C, then xV are the Principal Components (PCs), where $x = [x_1, \dots x_n]$.

$S = XV$ is the score matrix. The entries of loading matrix V represents the contribution of each original variable to the principal components, i.e., v_{ij} stands for how much i-th feature contributes to j-th principal component.

In Python, principal component analysis is implemented using 'sklearn.decomposition,PCA'. One way to visualize PCA result is using biplot. Biplot can be seen as a combination of PC score plot and loading plot. To be seen in a 2d graph, we keep only PC1 and PC2 for example. These two PCs will be the two axes of the plot, and the vectors of features from loading matrix V are projected onto these two axes. The projected values on each PC show the influence of the original variables, and the angles between vectors show how much they correlate with each other

5.2.3 Gaussian Process Regression (GPR)

GPR is a supervised learning technique and a non-parametric method. It is employed to handle smaller datasets, providing a probabilistic output, while capturing complexities, e.g., highly nonlinearity in the data. A Gaussian-type kernel is used in the model. Radial basis function (RBF) is a common choice of kernel.

$$k(x, x') = \exp\left(-\frac{(x-x')^2}{2l^2}\right) \quad (30)$$

where ‘l is the length scale parameter that determines the smoothness of the function. The predictive mean function is then given by

$$\mu(x^*) = k(x^*, X)[K(X, X) + \delta_n^2 I]^{-1} y \quad (31)$$

Among widely used Python packages, scikit-learn has an implementation of GPR as Gaussian Process Regressor, with common kernels like RBF, Matern, White-Kernel, and RQ (Rational Quadratic). Matern is more flexible when smoothness of the function can vary. White-Kernel is used to model noise in the data. RQ can be seen as a scale mixture of RBF.

5.2.4 Artificial Neural Networks (ANNs)

ANNs is another tool applied for dataset further advanced analysis [18]. Artificial neural network was employed to predict the drug loaded PLGA MP/NP release profiles under effects of release matrix pH, drug solubility, particle size distributions, and drug molecular weight resulting in a 4-dimension error curve. In Figure 28, an ANN flow chart summarizes all inputs and aimed outputs.

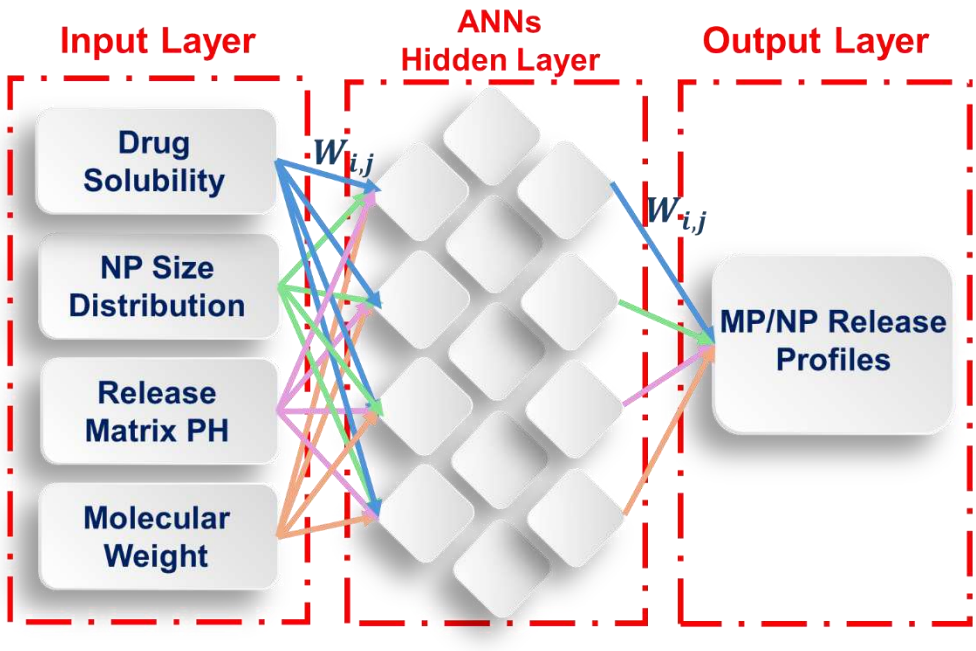

Figure 28. An artificial neural network (ANN) designed for study of drug release from PLGA micor-/nanoparticles.

5.3 *In Vitro* Experiments (Protocols & Procedures)

5.3.1 Materials Used in *In Vitro* Experiments

Poly (D, L-lactide-co-glycolic acid) (PLGA, lactide: glycolic 75:25, Mw 4000 15000, Sigma-Aldrich) and polyvinyl alcohol (PVA, 99+%, Mw 89000 98000, Sigma-Aldrich) were used for PLGA NP/MP synthesis. Gentamicin (99+%, SigmaAldrich) and Penicillin (99+%, Sigma-Aldrich) were used as the encapsulated drugs. Deionized water (Fisher Scientific) and Dichloromethane (DCM. Mw 84.93, 99.8%, Sigma-Aldrich) were used to dissolve PLGA for NP synthesis. Buffer solutions with pH at 4, 7 10 (Reagecon, #1040525CTT, #1070525CTT, and #1100525CTT) were used for study of release profiles.

5.3.2 Methods for Synthesis of PLGA MPs/NPs

PLGA NPs/MPs were synthesized via a double emulsion solvent evaporation method derived from [2] 100mg PLGA powder dissolved in 4ml dichloromethane (DCM) was mixed

with 45mg gentamicin in 0.5ml water to yield a primary solution that was mixed with 75m L, 750mL, 7.5ml of 9% PVA, respectively, to get three different droplet dispersed solutions. Those solutions were sonicated at 35% amplitude for 20 minutes via a sonic dismembrator (Fisherbrand^{TM}) Model 505 and the obtained dispersion solutions were titrated into 50ml 3% PVA solution resulting in opaque solutions. PLGA NPs/MPs precipitated after 8-hour solvent evaporation. Penicillin encapsulated PLGA NPs were synthesis with the same procedure

5.3.3 Characterization for PLGA Particles

PLGA MPs/NPs size distributions were measured via the dynamic light scattering (DLS, Malvern Zetasizer Nano ZS). A comprehensive size distribution profile was derived from the collective data obtained from the DLS measurements for each PLGA MP/NP solution. PLGA MP/NP morphology exploration utilized scanning electron microscopy (SEM, JEOL JSM-6500F field emission scanning electron microscope). Drug release profiles were determined with an ultraviolet-visible spectroscopy (UV-Vis, Agilent Cary 4000). Gentamicin loaded PLGA NP release profiles were representative by the accumulative release percentage at 5 discretized time points. A batch of PLGA NPs was well distributed into 5 test tubes at pH of 4, 7 and 10 respectively with 3ml particle-solution for each tube. Time intervals for the release measurements were 0 hours, 0.5 hours, 1 hour, 1.5 hours, and 2 hours. Release profiles of penicillin were determined via the same procedure.

5.4 Machine Learning Results and Discussion

Our data is collected from literature with 97 observations as shown in Table 8. We focus on five features: the accumulative released amount percentage of the drug, drug solubility, drug molecular weight, PLGA particle size, and pH-value of the environment or matrix.

Table 8. Summary of literature for data collection (More details can be found in the Appendix)

pH-Value	Drug	Polymeric MPs/NPs	Reference
7.0-9.0	Piperine, Rifampicin, miRNA, Ovalbumin, Heparin, Rhein, Risperidone, Griffithsin, Resveratrol, Gentamicin, Caffeine, Curcumin, Platensimycin, Doxorubicin, Hydroxyl, Insulin, Rapamycin, Platelte Lysate, Tamoxifen, Zoledronic Acid, Salidroside, Entecavir, Cannabidiol, Prednisolone	PLGA, PLH, Lactel, PEG, Polyscitech, PEM	[19-21]
7.0	Rhein, Rifampicin, Paeonol	PLGA	[22-24]
5.0-7.0	Piperine, miRNA, Rhein, Insulin, Doxorubicin, Hydroxyl, Resveratrol Cranberry-extract, Rivaroxaban, Atorvastatin Calcium	PLGA, PEG	[5], [25-26]
1.0-5.0	Rifampicin, Gentamicin, Insulin, Paeonol, Thymol, Prednisolone	PLGA, PLH	[27-29]

5.4.1 Linear Regression

The first step for our study of drug release from PLGA particles is to filter out parameters that can affect the release profiles. Linear regression was employed to establish roughly the correlation among release rates, release matrix pH-value, temperature, particle size distribution, drug solubility, and molecular weight. As shown in Figure 29.

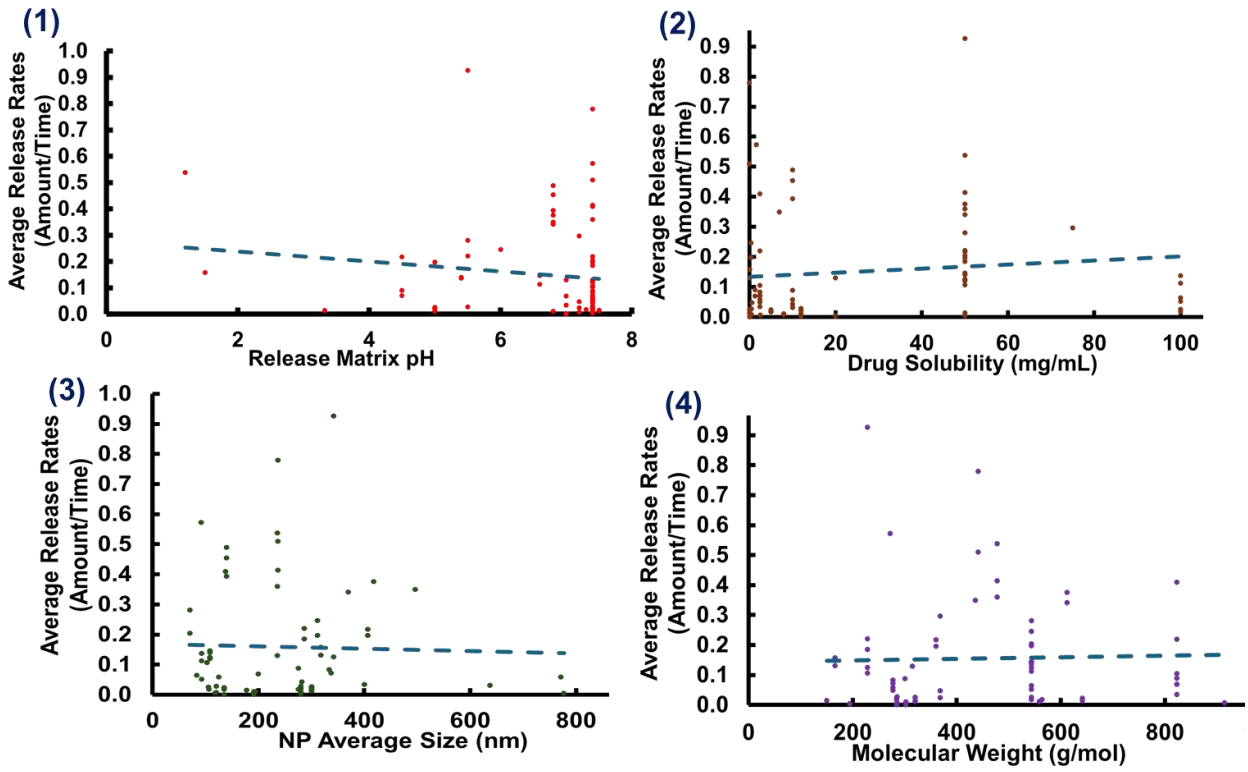

Figure 29. Results by linear regression. Linear correlation cannot be established between the released amount (percentage) and other factors.

However, the results in Figure 3 showed that most data items were highly condensed in partial areas and the correlation could be nonlinear. Therefore, more advanced machine learning models need to be explored.

5.4.2 Principal Component Analysis (PCA)

Among several factors relevant to drug release from PLGA particles, the released amount percentage, pH-value, drug solubility(mg/ml), drug molecule weight (g/mol), and particle size are important. These are treated as five features in the data we collected from literature. PCA is used to this data set (97 by 5) to identify the most important component (PC1, PC2).

As shown in Figure 30, PCA results imply that pH-value is likely to have negative correlation with release, since it has the strongest positive loading on PC1 whereas the released amount percentage has a strong negative loading. Similarly, particle size and the released amount

percentage might be negatively correlated also. Moreover, the strong influence of pH-value on PC1 suggests that it significantly affects the properties being studied.

In summary, PCA reveals correlation among the five features, but is insufficient to reveal all important patterns in the dataset. Among these features, PC1 and PC2 could explain only about 48% of the variance. Other machine learning methods need to be explored for this topic on drug release.

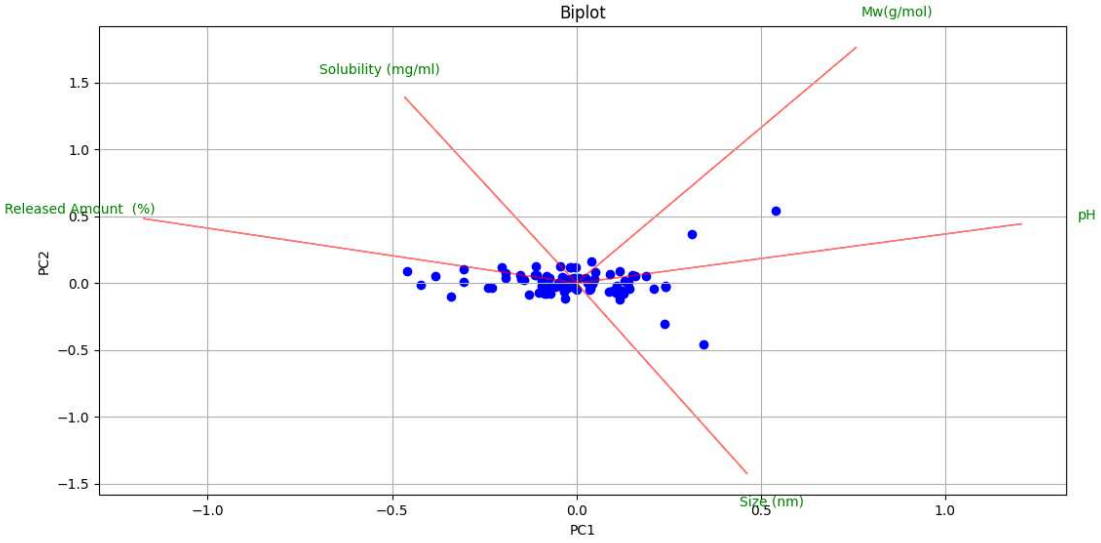

Figure 30. Results of PCA (biplot): Five original features (release amount %, solubility, molecular weight (Mw), pH value, NP size) are projected onto the plane spanned by (PC1, PC2); PC scores are plotted as blue points.

5.4.3 Gaussian Process Regression (GPR)

For our study of drug release from PLGA particles, release matrix pH-value, drug solubility, and MP/NP size distribution were the three most important factors to be investigated. GPR was adopted to explore those three parameters in detail. In the regression process, all the data were regrouped using the clustering method known as K-Nearest Neighbors (KNN). The processed data were sent to GPR resulting in 1-dim and 2-dim Gaussian distributions.

A dual-kernel, i.e., a linear combination of RBF and RQ, was adopted to predict effects of pH-values on release profiles. One kernel with a small length scale ‘enhancing the model responsiveness to rapid changes in data was combined with another kernel with a large initial length scale allowing it to capture broad and smooth trends across the dataset, resulting in a more nuanced understanding and predictions of dynamic processes governing drug release from PLGA MPs/NPs [30-31]. Therefore, this approach accommodates both localized variations and overarching trends within the data.

Given that multiple factors affect release profiles, focusing initially only on pH values is essential as shown in Figure 31-(1) and Figure 31-(2). In particular, Figure 31-(3) illustrates the effects of pH values on the release profiles of Doxorubicin-encapsulated PLGA MPs/NPs. It showed a clear parabolic shape under the effects of pH-value when the encapsulated drugs were fixed. Thus, the release profiles were enhanced as the release matrix’s pH became more acidic or alkaline.

As shown in Fig.31-(4), the release was more efficient than those with a larger size. This can also be explained mathematically. For a sphere with radius of r, the volume, surface area, and surface-to-volume ratio are, respectively,

$$Vol = \frac{4}{3}\pi r^3, \quad Surf = 4\pi r^2, \quad R = \frac{Surf}{Vol} = \frac{4\pi r^2}{\frac{4}{3}\pi r^3} = \frac{3}{r} \tag{32}$$

Therefore, the smaller the particle size, the larger the surface-to-volume ratio, the more efficient the release from a porous spherical shell.

Since multiple factors had great impact on release profiles, it is essential to isolate pH from other parameters to have a deep understanding of pH. Therefore, Figure 31-(3) focused on

doxorubicin encapsulated PLGA MP/NP release profiles under effects of pH. Figure 31-(3) showed a clear parabolic shape under the effects of pH when the encapsulated drugs, doxorubicin, were fixed. Therefore, release profiles were increased as the release matrix pH went acidic or alkaline, which proved postulates acquired from Figure 31-(2) not to be correct.

In summary, 4 postulations can be concluded from Gaussian process regression results.

(1) Acidic release environment favored drug release from particles. As the pH decreased, the release profiles were increased.
(2) When the pH value increases from acid to alkaline in the comprehensive region, the release rates decrease.
(3) Acidic and alkaline release environment benefited doxorubicin released from PLGA particles, and the minimum release
(4) rates occurred at neutral pH.
(5) The release profiles were enhanced as the surface-to-volume ratio was increased around region of 0.002 to 0.004, but the
(6) surface-to-volume ratio made less difference when the ratio passed through a critical value of 0.004.

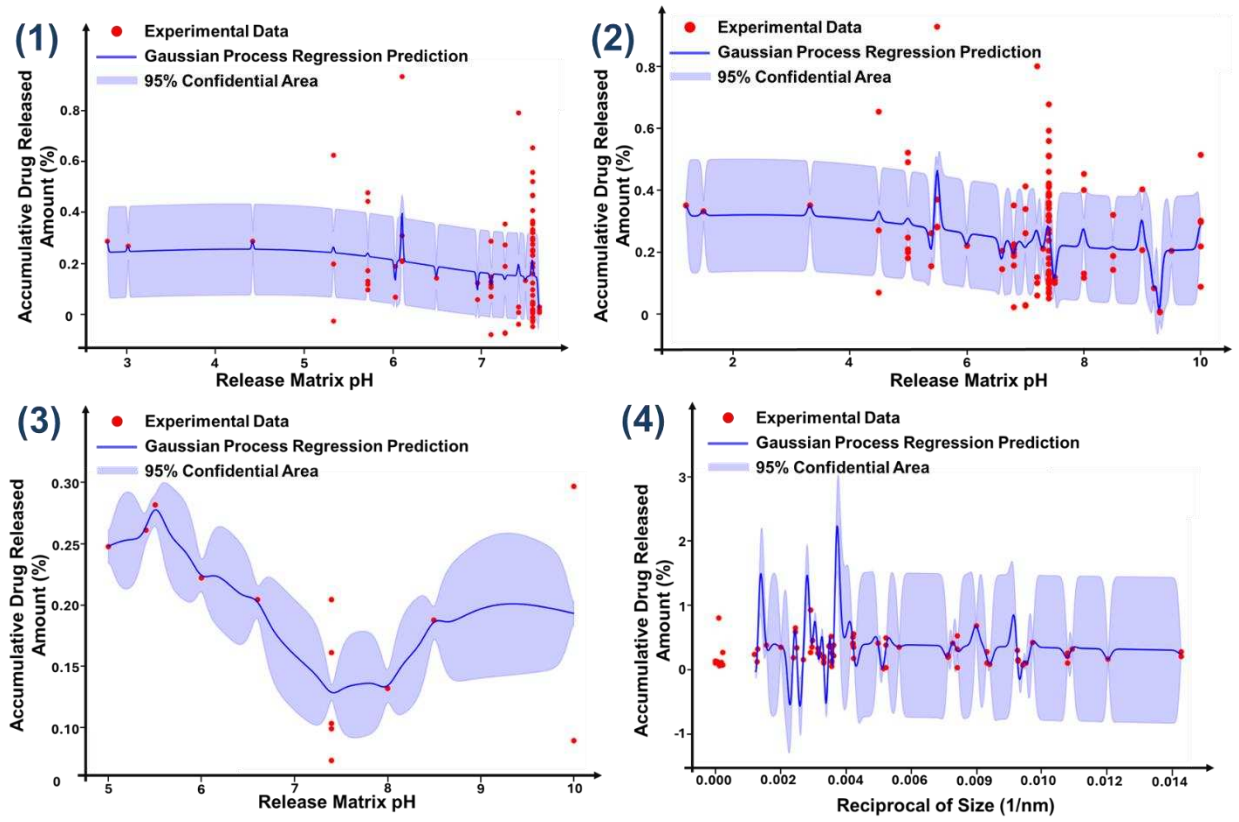

Figure 31. Results by GPR on effect of pH-value and particle size. **(1)** Effect of pH-value 3-7.4, Release enhanced when with decrease of pH-value, Minimum release occurred at the neutral pH; **(2)** For a larger range of pH-values, as pH-value increase, release decreased; **(3)** Effect of pH-value for drug doxycycline: Release enhanced as pH-value goes to extreme (acidic or alkaline), minimum release at around pH=7.2; **(4)** Effect of particle size (actually the reciprocal), Release enhanced as the surface-to-volume ratio increases

5.4.4 Artificial Neural Networks (ANNs)

Figure 32 presented our artificial neural network results, in which factors of release matrix pH, drug solubility, MP/NP average size, and molecular weight against release rates were taken into consideration resulting in a 4-dimension error histogram. According to Figure 32, most data falling into the areas close to the zero errors line indicating the artificial neural network model successfully predicted release rates under the effects of various factors. In addition, the error distribution was well normalized demonstrating the model was convincible and reliable. There were a couple of data points having large errors which were attributed to the

limited database, but the artificial neural network accuracy can be improved once more data becomes accessible.

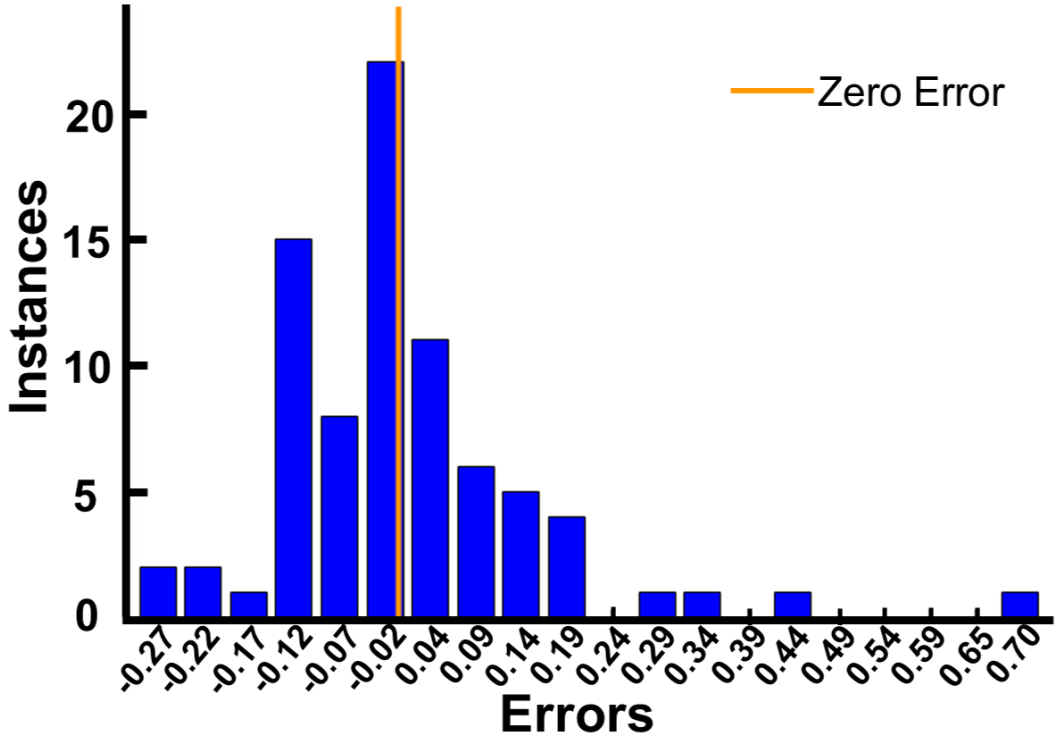

Figure 32. Results by a 4-dim ANN: Histogram of prediction error. Most data fell into the area close to the zero-error vertical line indicating the ANN model able to predict release profiles with high accuracy.

5.5 *In Vitro* Experimental Results and Discussion

5.5.1 Morphology and Size Distribution of PLGA MPs/NPs

PLGA MPs/NPs were spherical shapes with pores all over the surface, and particles had a core-shell structure where the drugs were encapsulated within the core as shown in Figure 33. When PLGA MPs/NPs were precipitated from the droplet dispersion solution, the water within the particle diffused through the particle shell causing the formulation of the porous structures, and those pores were benefit for the encapsulated drug release. When the volume of the second aqueous phase was fixed, penicillin loaded PLGA MPs/NPs had a smaller size distribution compared to those of gentamicin loaded PLGA MPs/NPs, which may be caused by the variant in

the molecular weight. According to the literature penicillin has a molecular weight of 334.39g/mol while gentamicin has a molecular weight of 1390.71g/mol. The results indicated that the encapsulated drug could affect antibiotics loaded PLGA MP/NP size distributions in which a higher molecular weight of drug lead to an increase in the resulting particle size distributions.

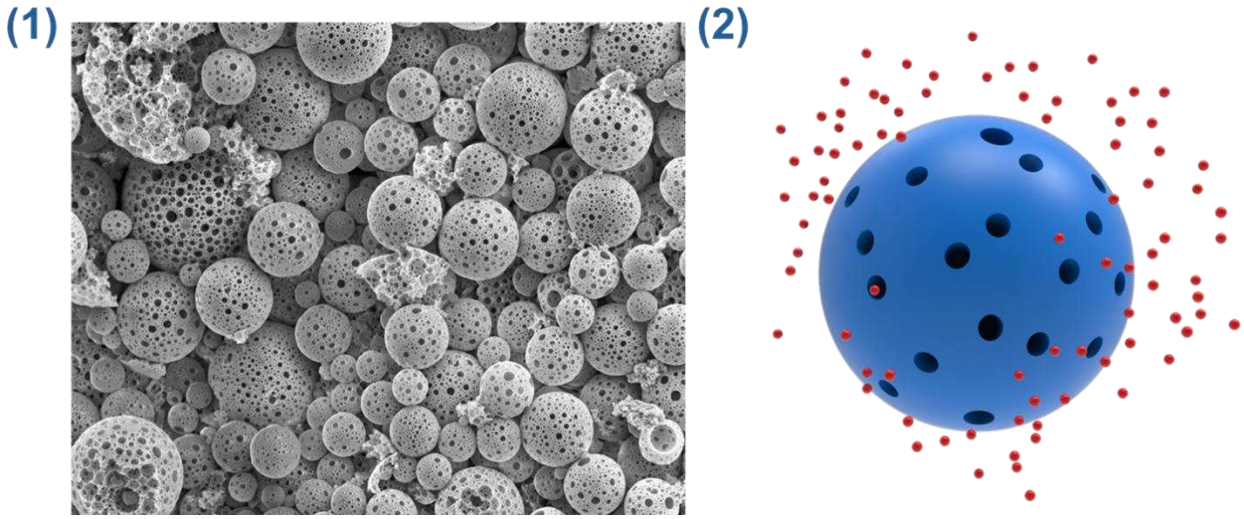

Figure 33. Morphology of PLGA particles. **(1)** An SEM image of particles with pores on surfaces. **(2)** Illustration of a spherical particle.

5.5.2 Release Profiles of Drug from PLGA MPs/NPs

According to the literature, there are four widely accepted release mechanisms which are diffusion, convection, osmotic pumping, and degradation. One or multiple release mechanisms occur from time to time, but the release rates are determined by the denominated mechanisms. Commonly, a burst release occurs when particle start to delivery encapsulated drugs, which is mainly caused by the diffusion of drugs on the surface of particles.

Gentamicin/Penicillin loaded PLGA MPs/NPs were synthesized via a double emulsion solvent evaporation method reported by Sun et, al. The resulting MP/NP release profiles at pH of 4, 7, and 10 were measured via UV-Vis. The acquired accumulative release percentages at

different times were plotted against time, and the resulting diagrams represented the antibiotics loaded PLGA MP/NP release profiles shown in Figure 34 and Figure 35.

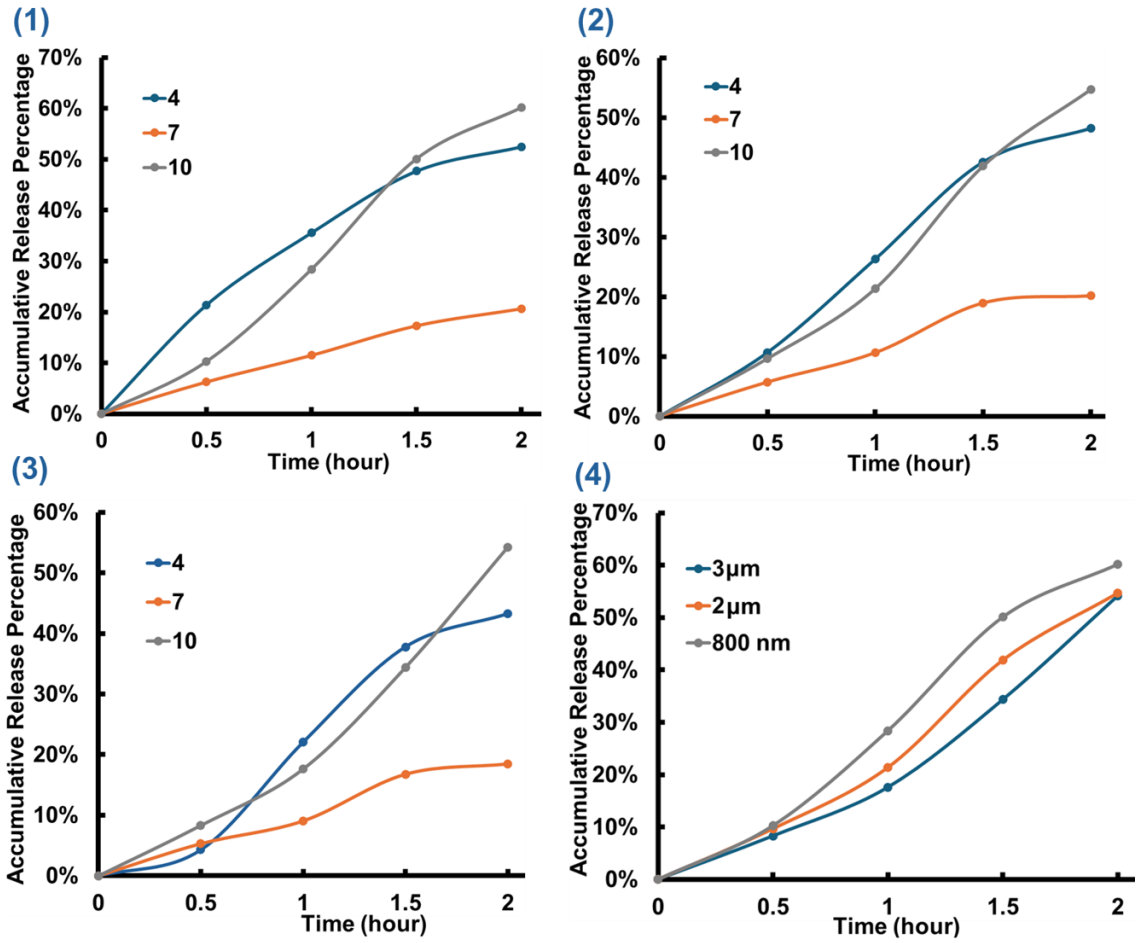

Figure 34. In-vitro experiments: Release of gentamicin (GEN) from PLGA particles. **(1)** 800nm release profile at pH-value 4,7,10; **(2)** 2μm release profile at pH-value 4,7,10; **(3)** 3μm release profile at pH-value 4,7,10; **(4)** Three different MP/NP release profile at pH-value 10.

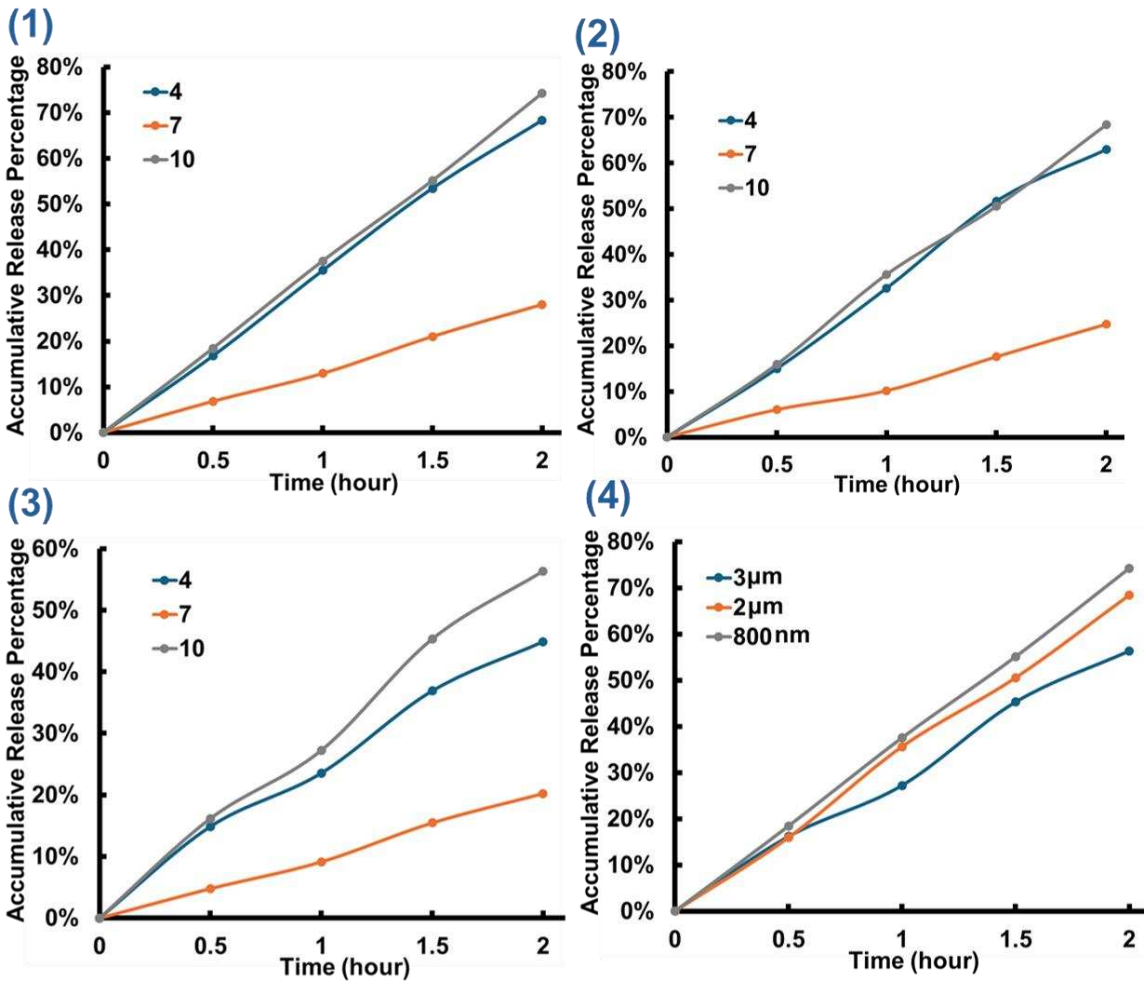

Figure 35. In-vitro experiments: Release of penicillin (PCN) from PLGA particles. **(1)** 800nm release profile at pH-value 4,7,10; **(2)** 2μmrelease profile at pH-value 4,7,10; **(3)** 3μm release profile at pH-value 4,7,10; **(4)** Three different MP/NP release profile at pH-value 10.

In Figure 34 and Figure 35, the release profiles presented a linear relation at the first 1.5 hours and 2 hours, which indicated a burst release caused by the diffusion. Commonly, the burst effect caused by the diffusion of gentamicin and penicillin on the MP/NP surface. Once the MPs//NPs were embedded in the buffer solution to release, the antibiotics on the surface can be released immediately into the outer matrix. Each batch of MP/NP had a higher average release rate under an alkaline release environment because the alkaline release environment can accelerate the hydrolysis of ester bonds in PLGA. Since antibiotics can be easily released from

degraded MPs/NPs, the higher degree of degradation of MPs/NPs leads to an increasing release rate. At pH of 7, no more than 30% of antibiotics can be released at every batch. Compared to those acidic or alkaline release surroundings, neutral release matrix has the least impact on release profile, which may be attributed to the tiny solubility of PLGA in water. Because PLGA can barely be dissolved in water, PLGA MP/NP degradation processes were slowed down leading to an extent in drug release profiles.

In addition, Figure 34-(4) and Figure 35-(4) showed that MP/NP size distributions can affect release profiles. Those NPs with an average size of 800nm can release more antibiotics during the first 2 hours. With an increase in MP/NP dimension, a decrease in release rates can be observed. According to literature, size distributions can affect MP/NP release profiles due to the surface-to-volume ratios. The surface-to-volume ratios reveal the factor of relative surface areas, and a large relative surface enables a wide diffusion panel for drug diffusion resulting in an increase in diffusion flux. Besides, penicillin loaded PLGA MP/NPs had higher average release rates than those of gentamicin loaded PLGA MP/NPs, which was attributed to the smaller molecular weight of penicillin resulting into a smaller particle compared to the gentamicin loaded PLGA MPs/NPs.

In summary, four main findings can be concluded as follows.

(1) An acidic or alkaline release matrix/environment can accelerate release rates;

(2) High solubility resulted in a high release rate;

(3) An increase in the surface-volume ratio leads to an increase in the release rate;

(4) Particles synthesized with a smaller molecular weight tend to have a smaller size, leading to an increase in release efficiency

5.6 Conclusion

This paper presents a novel approach for the study of drug release from PLGA particles that combines the traditional paradigm in vitro experiments and the recent new paradigm machine learning.

First, in vitro experimental data about drug release from PLGA particles reported in around 50 research papers are collected. Data collection focuses on released amount percentage, pH-value of release matrix or environment, drug solubility, drug molecular weight, and PLGA particle. Such a data set is analyzed by linear regression, PCA, GPR, and ANNs, respectively.

Then the learnt results obtained from machine learning algorithms were used as guidelines for designing our own in vitro experiments. And it is interesting to note that the results of release profiles from these experiments agree well with that by machine learning algorithms.

5.7 References

[1] Thananukul, K., Kaewsaneha, C., Opaprakasit, P., Zine, N., & Elaissari, A. (2022). Biodegradable porous micro/nanoparticles with thermos responsive gatekeepers for effective loading and precise delivery of active compounds at the body temperature. *Scientific Reports*, *12*(1). https://doi.org/10.1038/s41598-022-15069-x

[2] Sun, Y., Bhattacharjee, A., Reynolds, M., & Li, Y. V. (2021). Synthesis and characterizations of gentamicin-loaded poly-lactic-co-glycolic (PLGA) nanoparticles. *Journal of Nanoparticle Research*, *23*(8). https://doi.org/10.1007/s11051-021-05293-3

[3] Sun, Y., Heacock, J., Chen, C., Qiu, K., Zou, L., Liu, J., & Li, Y. V. (2023). Incorporation of gentamicin-encapsulated poly (lactic-*co*-glycolic acid) nanoparticles into polyurethane/poly (ethylene oxide) nanofiber scaffolds for biomedical applications. *ACS Applied Nano Materials*, *6*(17), 16096–16105. https://doi.org/10.1021/acsanm.3c03549

[4] Ulbrich, K., Holá, K., Šubr, V., Bakandritsos, A., Tuček, J., & Zbořil, R. (2016). Targeted drug delivery with polymers and magnetic nanoparticles: Covalent and noncovalent approaches, release control, and clinical studies. *Chemical Reviews*, *116*(9), 5338–5431. https://doi.org/10.1021/acs.chemrev.5b00589

[5] Huang, S.-J., Wang, T.-H., Chou, Y.-H., Wang, H.-M. D., Hsu, T.-C., Yow, J.-L., Tzang, B.-S., & Chiang, W.-H. (2022). Hybrid pegylated chitosan/PLGA nanoparticles designed as ph-responsive vehicles to promote intracellular drug delivery and cancer chemotherapy. *International Journal of Biological Macromolecules*, *210*, 565–578. https://doi.org/10.1016/j.ijbiomac.2022.04.209

[6] Lange, T. J., Baron, M., Seiler, I., Arzt, M., & Pfeifer, M. (2014). Outcome of patients with severe ph due to lung disease with and without targeted therapy. *Cardiovascular Therapeutics*, *32*(5), 202–208. https://doi.org/10.1111/1755-5922.12084

[7] Proksch, E. (2018). ph in nature, humans and skin. *The Journal of Dermatology*, *45*(9), 1044–1052. https://doi.org/10.1111/1346-8138.14489

[8] Siepmann, Juergen, & Siepmann, F. (2012). Modeling of Diffusion Controlled Drug Delivery. *Journal of Controlled Release*, *161*(2), 351–362. https://doi.org/10.1016/j.jconrel.2011.10.006

[9] Zawbaa, H. M., Szlęk, J., Grosan, C., Jachowicz, R., & Mendyk, A. (2016). Computational intelligence modeling of the macromolecules release from PLGA microspheres—focus on feature selection. *PLOS ONE*, *11*(6). https://doi.org/10.1371/journal.pone.0157610

[10] Noorain, L., Nguyen, V., Kim, H.-W., & Nguyen, L. T. (2023). A machine learning approach for PLGA nanoparticles in Antiviral Drug Delivery. *Pharmaceutics*, *15*(2), 495. https://doi.org/10.3390/pharmaceutics15020495

[11] Rasmussen, C. E., & Williams, C. K. (2005). *Gaussian Processes for Machine Learning*. https://doi.org/10.7551/mitpress/3206.001.0001

[12] Damiati, S. A., Rossi, D., Joensson, H. N., & Damiati, S. (2020). Artificial intelligence application for rapid fabrication of size-tunable PLGA microparticles in Microfluidics. *Scientific Reports*, *10*(1). https://doi.org/10.1038/s41598-020-76477-5

[13] Bannigan, P., Bao, Z., Hickman, R. J., Aldeghi, M., Häse, F., Aspuru-Guzik, A., & Allen, C. (2023). Machine learning models to accelerate the design of polymeric long-acting injectables. *Nature Communications*, *14*(1). https://doi.org/10.1038/s41467-022-35343-w

[14] Siepmann, J., & Siepmann, F. (2008). Mathematical Modeling of Drug Delivery. *International Journal of Pharmaceutics*, *364*(2), 328–343. https://doi.org/10.1016/j.ijpharm.2008.09.004

[15] Klose, D., Siepmann, F., Elkharraz, K., Krenzlin, S., & Siepmann, J. (2006). How porosity and size affect the drug release mechanisms from PLGA-based microparticles. *International Journal of Pharmaceutics*, *314*(2), 198–206. https://doi.org/10.1016/j.ijpharm.2005.07.031

[16] Siepmann, J., Siepmann, F., & Florence, A. T. (2006). Local controlled drug delivery to the Brain: Mathematical Modeling of the underlying mass transport mechanisms. *International Journal of Pharmaceutics*, *314*(2), 101–119. https://doi.org/10.1016/j.ijpharm.2005.07.027

[17] Shehabeldine, A., & Hasanin, M. (2019). Green synthesis of hydrolyzed starch–chitosan nanocomposite as drug delivery system to gram negative bacteria. *Environmental Nanotechnology, Monitoring & Management*, *12*, 100252. https://doi.org/10.1016/j.enmm.2019.100252

[18] Habeeb, M., Woon You, H., Balasaheb Aher, K., Balasaheb Bhavar, G., Suryabhan Pawar, S., & Dnyaneshwar Gaikwad, S. (2023). Artificial Neural Networks for the prediction of mechanical properties of CGNP/PLGA nanocomposites. *Materials Today: Proceedings*. https://doi.org/10.1016/j.matpr.2023.08.354

[19] Kaur, J., Singh, R. R., Khan, E., Kumar, A., & Joshi, A. (2021). Piperine-loaded plga nanoparticles as cancer drug carriers. *ACS Applied Nano Materials*, *4*(12), 14197–14207. https://doi.org/10.1021/acsanm.1c03664

[20] Maghrebi, S., Joyce, P., Jambhrunkar, M., Thomas, N., & Prestidge, C. A. (2020). Poly(lactic-*CO*-glycolic) acid–lipid hybrid microparticles enhance the intracellular uptake and antibacterial activity of rifampicin. *ACS Applied Materials & Interfaces*, *12*(7), 8030–8039. https://doi.org/10.1021/acsami.9b22991

[21] Muniyandi, P., Palaninathan, V., Mizuki, T., Maekawa, T., Hanajiri, T., & Mohamed, M. S. (2020). Poly (lactic-*co*-glycolic acid)/polyethylenimine nanocarriers for direct genetic

reprogramming of MicroRNA targeting cardiac fibroblasts. *ACS Applied Nano Materials*, *3*(3), 2491–2505. https://doi.org/10.1021/acsanm.9b02586

[22] Hu, B., Gao, F., Li, C., Zhang, B., An, M., Lu, M., Liu, Y., & Liu, Y. (2020). Rhein laden ph-responsive polymeric nanoparticles for treatment of osteoarthritis. *AMB Express*, *10*(1). https://doi.org/10.1186/s13568-020-01095-3

[23] Park, K., Otte, A., Sharifi, F., Garner, J., Skidmore, S., Park, H., Jhon, Y. K., Qin, B., & Wang, Y. (2020). Potential roles of the glass transition temperature of PLGA microparticles in drug release kinetics. *Molecular Pharmaceutics*, *18*(1), 18–32. https://doi.org/10.1021/acs.molpharmaceut.0c01089

[24] Wang, F., Shan, Q., Chang, X., Li, Z., & Gui, S. (2021). Paeonol-loaded plga nanoparticles as an oral drug delivery system: Design, optimization and evaluation. *International Journal of Pharmaceutics*, *602*, 120617. https://doi.org/10.1016/j.ijpharm.2021.120617

[25] Scheeren, L. E., Nogueira-Librelotto, D. R., Macedo, L. B., de Vargas, J. M., Mitjans, M., Vinardell, M. P., & Rolim, C. M. (2020). Transferrin-conjugated doxorubicin-loaded plga nanoparticles with ph-responsive behavior: A synergistic approach for cancer therapy. *Journal of Nanoparticle Research*, *22*(3). https://doi.org/10.1007/s11051-020-04798-7

[26] Li, J., Qiang, H., Yang, W., Xu, Y., Feng, T., Cai, H., Wang, S., Liu, Z., Zhang, Z., & Zhang, J. (2022). Oral insulin delivery by epithelium microenvironment-adaptive nanoparticles. *Journal of Controlled Release*, *341*, 31–43. https://doi.org/10.1016/j.jconrel.2021.11.020

[27] Akhtar, B., Muhammad, F., Aslam, B., Saleemi, M. K., & Sharif, A. (2020). Pharmacokinetic profile of chitosan modified poly lactic co-glycolic acid biodegradable nanoparticles following oral delivery of gentamicin in rabbits. *International Journal of Biological Macromolecules*, *164*, 1493–1500. https://doi.org/10.1016/j.ijbiomac.2020.07.206

[28] Akhavan Farid, E., Davachi, S. M., Pezeshki-Modaress, M., Taranejoo, S., Seyfi, J., Hejazi, I., Tabatabaei Hakim, M., Najafi, F., D'Amico, C., & Abbaspourrad, A. (2020). Preparation and characterization of polylactic-co-glycolic acid/insulin nanoparticles encapsulated in methacrylate coated gelatin with sustained release for specific medical applications. *Journal of Biomaterials Science, Polymer Edition*, *31*(7), 910–937. https://doi.org/10.1080/09205063.2020.1725863

[29] Acharya, S., & Guru, B. R. (2020). Prednisolone encapsulated plga nanoparticles: Characterization, cytotoxicity, and anti-inflammatory activity on c6 glial cells. *Journal of Applied Pharmaceutical Science*, *10*(4), 14–21. https://doi.org/10.7324/japs.2020.104003

[30] Deringer, V. L., Bartók, A. P., Bernstein, N., Wilkins, D. M., Ceriotti, M., & Csányi, G. (2021). Gaussian process regression for materials and molecules. *Chemical Reviews*, *121*(16), 10073–10141. https://doi.org/10.1021/acs.chemrev.1c00022

[31] Tighineanu, P. et al., (2022). Transfer learning with Gaussian process for Bayesian optimization. *International Conference on Artificial Intelligence and Statistics*, 6152-6181. https://proceedings.mlr.press/v151/tighineanu22a.html

Chapter 6 Conclusion & Future Work

6.1 Introduction

This dissertation summarizes most of my work throughout my academic research life. In this dissertation, a facile but effective research procedure showed a novel transdermal material development process in which computational approaches were integrated with experimental research to improve the transdermal material properties in terms of release profiles, dimensions, and antibacterial activities. In chapter **2 Incorporation of Gentamicin-Encapsulated Poly (lactic-co-glycolic acid) Nanoparticles into Polyurethane/Poly (ethylene oxide) Nanofiber Scaffolds for Biomedical Applications,** size of gentamicin encapsulated PLGA nanoparticles were controlled to 132nm for well incorporation with nanofiber scaffolds. Then, the gentamicin loaded PLGA nanoparticles were incorporated into PU/PEO monolithic nanofiber scaffolds. The monolithic scaffolds were characterized to study their morphologies, dimensions, release profiles, and antibacterial activities. The results showed that gentamicin loaded PLGA nanoparticles were successfully incorporated into PU/PEO monolithic nanofiber scaffolds which can release gentamicin to control bacterial infections at a controlled release rate. Chapter 3 **Mathematical Modeling and Numerical Simulations for Drug Release from PLGA Particles** presented a numerical methodology that was adopted to fit the drug release profiles from PLGA nanoparticles. The computational results acquired from finite element analysis well fitted with experimental data. In chapter 4 **Enhanced Transdermal Medication Delivery: Core-Shell Nanofiber Scaffolds with Antibiotic-encapsulated Poly (lactic acid-co-glycolic acid) Nanoparticles Applications**, gentamicin encapsulated PLGA nanoparticles incorporated monolithic nanofiber scaffolds were developed into core-shell fibrous scaffolds as transdermal materials. Gentamicin loaded PLGA nanoparticles were introduced into the core-shell fibrous

scaffolds core layers with a diameter of 1.38μm, and core layers was shielded with the shell made of PU/PEO. The core-shell fibrous scaffolds were characterized to study their morphologies, dimensions, release profiles, and antibacterial activities. According to our results, the gentamicin loaded PLGA nanoparticles incorporated PU/PEO core-shell fibrous scaffolds can control *E.coli* infections with a long term release. The core-shell fibrous scaffolds have a diameter of 2.22μm, and nanoparticles were mostly concentrated within the core layers. Chapter 5 **Machine Learning Integrated with In Vitro Experiments for Study of Drug Release from Poly (Lactic-co-Glycolic Acid) Particles** demonstrated machine learning as a powerful academic research tools were applied to study release profiles of drug released from PLGA nanoparticles. Factors of release matrix pH, particle size distributions, drug solubilities, and molecular weights were explored in this study. All the factors did not have linear relationships with release rates, and the principal component analysis cannot provide useful information about the critical components. However, advanced approaches including Gaussian process regression and artificial neural networks revealed the insights correlations between parameters. According to the results, extreme pH value likely strong acidic or alkaline pH benefited release rates, and particles with small diameter can release drug quickly. In addition, the encapsulated drugs with high water solubility enhanced the release profiles.

Although this dissertation well illustrated the procedure to develop novel transdermal materials, more research should be conducted to improve the current transdermal materials. Experimentally, a couple of potential research interests can further develop novel transdermal materials to extend and strength its medication properties. Chitosan and cellulose nanocrystal are nature extractions can be applied as fiber and particle reinforcement materials to improve their mechanical and antimicrobial properties [1][2][3][4]. According to literature, chitosan shows

potential antimicrobial activity in controlling bacterial infections. Incorporating chitosan into fibrous scaffolds will not only enhance fiber antibacterial activity, but also it can strengthen fiber mechanical properties. Cellulose nanocrystals will be introduced into PLGA nanoparticle synthesis procedure as reinforcement materials to keep particles from degradation for the benefits of a sustainable drug release. In addition to improve transdermal material physical or chemical properties, endowing transdermal materials with the function of bacterial infection recognition will be promising research to leverage our novel transdermal material outstanding compared to conventional wound dressing materials. PCDA, a complex polymer, can react with *E.coli* turning fiber matrix color from blue to red once it is incorporated into scaffolds[5][6][7]. Therefore, PCDA can be incorporated into the shell layer open-sites, and it will cause color change of the shell layers when the fibrous scaffolds encounter *E.coli*. As a result, the core-shell fibrous scaffolds can be turned into a biosensor for therapeutic treatments.

From the perspective of computational modeling, our database used for machine learning model development is not considerable and comprehensive. In our research, burst effect was explored but all the other associated release mechanisms should be studied. According to literature, release mechanisms including osmotic pumping, convection, and degradation are involved in a process of drug release from particles [8][9][10]. Thus, establishing mathematical models to quantify release profiles is critical for particle-based drug delivery system optimization. The following work will be applying computational methods for polymeric particle exploration. In our experimental research, drug encapsulated nanoparticles were applied to fibrous scaffolds as drug carrier. Consequently, studying the relative release mechanisms of drug release from fibrous scaffolds plays an important role in quantifying drug loading efficiency. Therefore, the

second potential research goal will be utilization of computational methods for nanoparticles incorporated core-shell fiber release profile study.

6.2 References

[1] Knaul, J. Z., Hudson, S. M., & Creber, K. A. (1999). Crosslinking of chitosan fibers with dialdehydes: Proposal of a new reaction mechanism. *Journal of Polymer Science Part B: Polymer Physics*, *37*(11), 1079–1094. https://doi.org/10.1002/(sici)1099-0488(19990601)37:11<1079::aid-polb4>3.0.co;2-o

[2] Albanna, M. Z., Bou-Akl, T. H., Walters, H. L., & Matthew, H. W. T. (2012). Improving the mechanical properties of chitosan-based heart valve scaffolds using chitosan fibers. *Journal of the Mechanical Behavior of Biomedical Materials*, *5*(1), 171–180. https://doi.org/10.1016/j.jmbbm.2011.08.021

[3] Li, Jianhui, Fu, J., Tian, X., Hua, T., Poon, T., Koo, M., & Chan, W. (2022). Characteristics of chitosan fiber and their effects towards improvement of antibacterial activity. *Carbohydrate Polymers*, *280*, 119031. https://doi.org/10.1016/j.carbpol.2021.119031

[4] Yusefi, M., Soon, M. L.-K., Teow, S.-Y., Monchouguy, E. I., Neerooa, B. N., Izadiyan, Z., Jahangirian, H., Rafiee-Moghaddam, R., Webster, T. J., & Shameli, K. (2022). Fabrication of cellulose nanocrystals as potential anticancer drug delivery systems for colorectal cancer treatment. *International Journal of Biological Macromolecules*, *199*, 372–385. https://doi.org/10.1016/j.ijbiomac.2021.12.189

[5] Bhattacharjee, A., Clark, R., Gentry-Weeks, C., & Li, Y. V. (2020). A novel receptor-free polydiacetylene nanofiber biosensor for detecting *E. coli via* colorimetric changes. *Materials Advances*, *1*(9), 3387–3397. https://doi.org/10.1039/d0ma00619j

[6] Bhattacharjee, A., Sabino, R. M., Gangwish, J., Manivasagam, V. K., James, S., Popat, K. C., Reynolds, M., & Li, Y. V. (2022). A novel colorimetric biosensor for detecting SARS-COV-2 by utilizing the interaction between nucleocapsid antibody and Spike proteins. *In Vitro Models*, *1*(3), 241–247. https://doi.org/10.1007/s44164-022-00022-z

[7] Bhattacharjee, A., Goodall, E., Popat, K. C., Zou, L., & Li, Y. V. (2023). Selective detection of gram-negative bacteria and antibacterial properties of colorimetric polydiacetylene nanofibers. *Journal of Materials Science*, *58*(19), 8261–8273. https://doi.org/10.1007/s10853-023-08550-z

[8] zur Mühlen, A., Schwarz, C., & Mehnert, W. (1998). Solid lipid nanoparticles (SLN) for Controlled Drug Delivery – drug release and release mechanism. *European Journal of Pharmaceutics and Biopharmaceutics*, *45*(2), 149–155. https://doi.org/10.1016/s0939-6411(97)00150-1

[9] Kamaly, N., Yameen, B., Wu, J., & Farokhzad, O. C. (2016). Degradable controlled-release polymers and polymeric nanoparticles: Mechanisms of controlling drug release. *Chemical Reviews*, *116*(4), 2602–2663. https://doi.org/10.1021/acs.chemrev.5b00346

[10] Barzegar-Jalali, M. (2008). Kinetic analysis of drug release from nanoparticles. *Journal of Pharmacy & Pharmaceutical Sciences*, *11*(1), 167. https://doi.org/10.18433/j3d59t

Appendix

PLGA Nanoparticles Synthesis

PLGA nanoparticles were synthesized via a double emulsion solvent evaporation method shown in Figure 11. First, 200mg PLGA powder was dissolved in 4ml dichloromethane, resulting in an oil phase, while 45mg gentamicin was dissolved in 0.5ml DI water, resulting in an aqueous phase 1. An 8ml of 3% PVA solution was an aqueous phase 1 where 3% PVA solution was made of 3g PVA dissolved in 100ml DI water. The oil phase solution was mixed with the aqueous phase 1 solution. Then, the mixture was combined with an aqueous phase 2. Thus, a water-oil-water solution was formed that contained three phases where nanodroplets were floating. The nanodroplet dispersion was sonicated for 10min at 40% amplitude and 10s pause after each round of 30s, resulting in a uniform emulsion solution. The emulsion solution was titrated into a beaker that contained a second 25ml 0.1% PVA solution. The solution mixture was placed on a hot plate and stirring shear force was applied, which allowed the solution to evaporate for 8 hours. An opaque solution containing PLGA nanoparticles was obtained after the evaporation. The obtained PLGA nanoparticles were examined using a scanning electron microscope (SEM, JEOL JSM-6500).

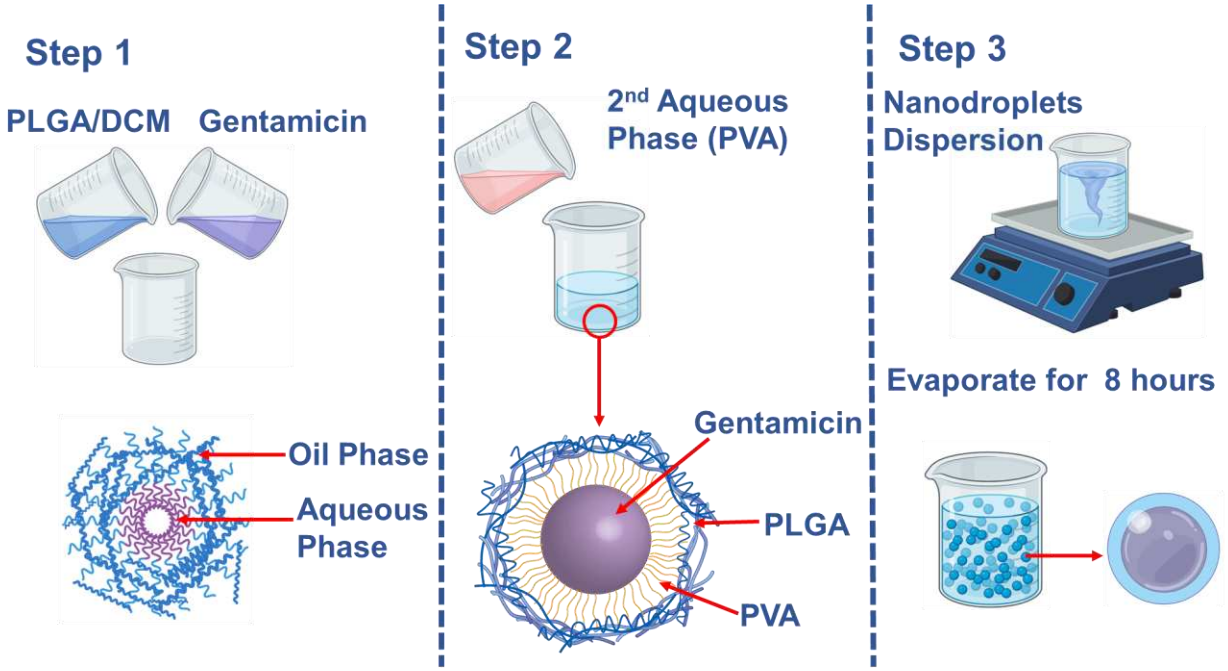

Figure 11. PLGA nanoparticles were synthesized via a double emulsion solvent evaporation method. Step 1: An oil phase of PLGA and DCM was mixed with an aqueous phase 1 of a gentamicin solution; Step 2: An aqueous phase 2 of a PVA solution was added, resulting in a double emulsion with PLGA nanodroplets; Step 3: The double emulsion was kept allowing water to evaporate. Gentamicin was encapsulated inside the PLGA nanoparticles.

PLGA Nanoparticle Purification

The four steps for PLGA Nanoparticles purification were explained as shown in Figure 12.

1. Solution condensation: the resulting solution after the double emulsion evaporation method was kept in fume hood where the temperature was controlled around 2~3^{o}C to allow evaporation and hence to consolidate the solution.
2. Dialysis: the condensed PLGA solution was poured into a dialysis tube to further condense the solution at 2~3^{o}C. The tube was fully immersed in a beaker that contained a 25% NaCl solution and kept in refrigerator.

3. Purification: 10ml DCM was added into the condensed PLGA nanoparticle solution before the combined solution was well mixed using appropriate agitation, resulting in an opaque solution.
4. Centrifugation: the mixed solution was centrifuged at 6000rpm/min for 15 minutes resulting in a phase separated solution. After that, nanoparticles in water solution can be transferred by using pipettes.

In addition, several comparison experiments were conducted, which were DCM mixed with water, 3% PVA solution mixed with water. 3% PVA solution mixed with DCM. The comparison experiments were designed to prove the PLGA nanoparticles can be purified via this procedure. And the gel in the solution was caused by the combination of PVA and DCM.

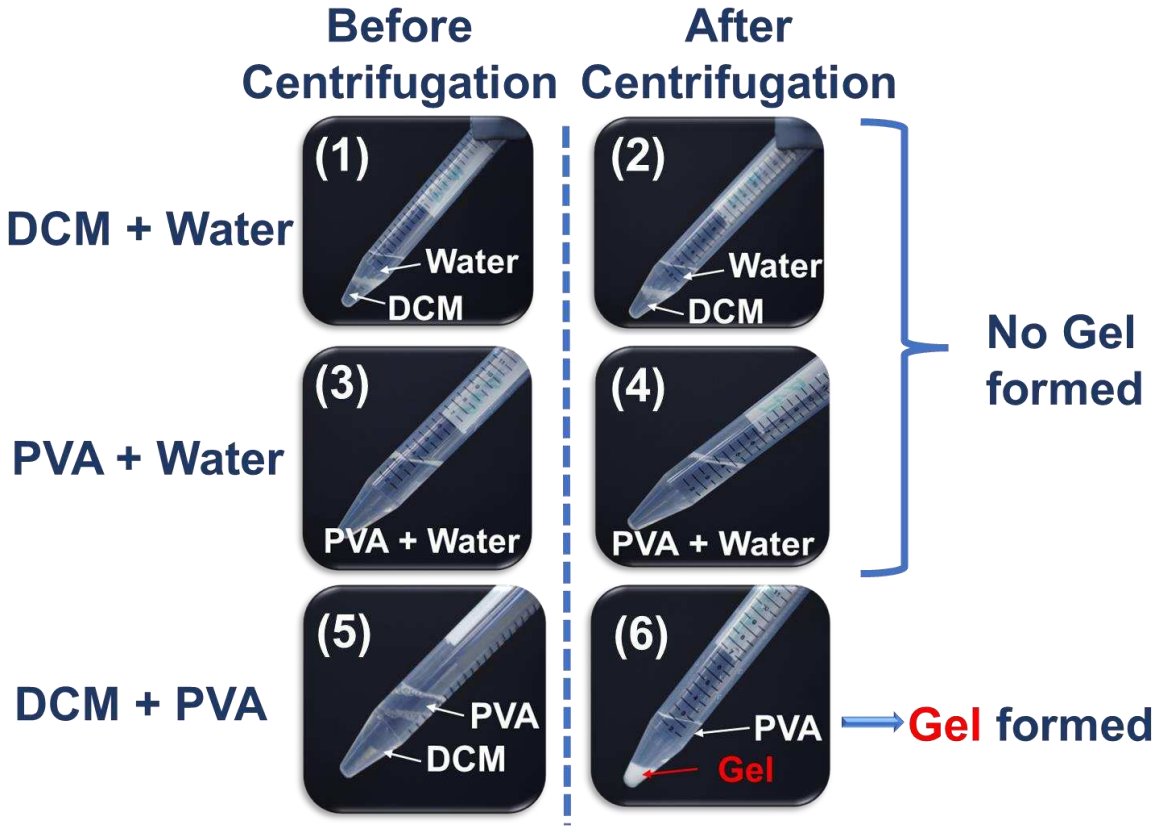

Figure 12. Purification controlled experiments. (1)-(2): DCM was mixed with water, and no gel was formed after centrifugation; (3)-(4): 3% PVA was mixed with water, and no gel was formed after centrifugation; (5)-(6): DCM mixed with 3% PVA, and gel was formed at the bottom of the test tube.

In order to further confirm the conclusion, comparison experiments were conducted to determine if the PLGA nanoparticles were purified. As illustrated by Fig S2, several sample solutions were prepared first, which were DCM mixed with water (Fig S2 (1)), 3% PVA solution mixed with water (Fig S2 (3)), and 3% PVA solution mixed with DCM (Fig S2 (5)). Before centrifugation, all three solutions were clear and phase layers were easy to see. After centrifugation, there was no change in water DCM mixed with water (Fig S2 (2)) or 3% PVA solution mixed with (Fig S2 (4)). The separated phase layer was still in the solution of DCM mixed with water and no gel was formed. PVA solution mixed with water can only dilute the solution due to PVA solubility in water. Neither "PVA and water" nor "DCM and water" could form into gel. However, there was gel precipitation at the bottom of the tube after centrifuging PVA and DCM mixture (Fig S2 (6)). Therefore, the gel was derived from PVA and DCM, or rather DCM could drag PVA from the solution. In conclusion, adding DCM to the condensed PLGA nanoparticles can surely purify PLGA nanoparticles. The corresponding experiments can be found in the Supporting Information Figure S2.

Electrospinning

In each recipe, the total mass of PLGA nanoparticles was fixed at 200mg with an average diameter of 120 nm. Then, every solution was sonicated for 10 minutes to let the nanoparticles fully disperse in the mixture. The emulsion solutions were spined under parameters of an injection rate of 0.45ml/hour, a voltage of 20kV, and a spinning distance of 20cm. Fig 2 (A) showed PLGA nanoparticles incorporated fibers that were synthesized via electrospinning. And the diagram presented emulsion spinning solution in syringe was gradually squeezed out of a

needle, and polymers in the solution were stretched into fibers with PLGA nanoparticles incorporated.

E.coli Growth

An *E.coli* ATCC25922 pellet (7.1×10^3 CFU/pellet) was mixed with 50ml LB Broth medium. The solution was incubated at 37° C for 24 hours. An inoculation loop was used to transfer the bacteria to an LB-Agar streak plates, and the bacteria culture was placed in an incubator for 24 hours at 37° C to allow bacteria to grow. BBL Muller Hinton (MH) II Agar was used to prepare MH agar plates. 12.5 g LB powder and 7.5 g Agar powder were dissolved in 500ml distilled water. The MH agar solution was autoclaved at 131 °C for 20 minutes at 15psi. The solution was distributed to a number of petri dishes with 25ml solution for each dish. The plates were left to set in the laminar flow hood for 10-30 minutes before they were stored in the fridge for the following antibacterial textile testing.

Database

Ref						**Burst Release Stage**		
	NP Materials	Drug	NP Size (nm)	pH	Solubility (mg/ml)	Time (hr)	Released Amount (%)	Average Release Rates
1	PLGA	piperine	120	5.5	0.5	10	28%	0.028
	PLGA	piperine	120	7.2	0.5	12	10%	0.00833
	PLGA	rifampicin	5390	4.5	1.3	1	7%	0.07
	PLGA	rifampicin	5390	7.4	2.5	0.5	11%	0.22
2	PLH	rifampicin	4560	4.5	1.3	3	27%	0.09
	PLH	rifampicin	4560	7.4	2.5	0.65	6.80%	0.10461
3	PLGA	miRNA-1	300	5	0.1	8	20%	0.025
	PLGA	miRNA-1	300	7.5	0.1	8	11%	0.01375
	PLGA	miRNA-133	300	5	0.1	8	21%	0.02625
	PLGA	miRNA-133	300	7.5	0.1	8	10%	0.0125

	PLGA	miRNA-dual	300	5	0.1	8	18%	0.0225
	PLGA	miRNA-dual	300	7.5	0.1	8	12%	0.015
4	PLGA	ovalbumin	777	7.4	50	24	12.8%	0.00533
5	PLGA	heparin	108	7.4	50	2.5	30.0%	0.12
6	PLGA	risperidone	67600	7.4	0.001	0	0.0%	0
	PLGA	risperidone	64100	7.4	0.001	0	0.0%	0
	Lactel	risperidone	73400	7.4	0.001	0	0.0%	0
	Polyscitech	risperidone	65600	7.4	0.001	0	0.0%	0
7	mPEG-PLGA	griffithsin	280	7.4	12	12	34.0%	0.02833
	mPEG-PLGA	griffithsin	280	7.4	12	12	26.0%	0.02166
	mPEG-PLGA	griffithsin	280	7.4	12	12	5.0%	0.00416
	PLGA	griffithsin	280	7.4	12	12	11.1%	0.00925
	PLGA	griffithsin	280	7.4	12	12	12.90%	0.01075
	PLGA	griffithsin	280	7.4	12	0	0%	0
8	PLGA	gentamicin	236	1.2	50	0.65	35.0%	0.53846
	PLGA	gentamicin	236	7.4	50	0.5	18%	0.36
9	PLGA	caffeine	62000	7.4	20	29	13.2%	0.00455
	PLGA	caffeine	94000	7.4	20	27	10.60%	0.00392
10	PLGA	curumin	13400	7.2	0.6	2.5	12.0%	0.048
	PLGA	curumin	9400	7.2	75	2.7	80.00%	0.29629
	PLGA	curumin	7900	7.2	12	2.4	6.00%	0.025
11	PLGA	gentamicin	236.7	7.4	50	1	41.4%	0.414
12	PLGA	platensimycin	236.7	7.4	0.015	1	51.0%	0.51
	PAM	platensimycin	236.7	7.4	0.015	0.5	39.0%	0.78
13	PLGA	rifampicin	137.5	7.4	2.5	1	41.0%	0.41
14	PLGA	doxorubicin	92.5	5.4	100	1.9	26.1%	0.13736
	PLGA	doxorubicin	92.5	6.6	100	1.8	20.4%	0.11333
	PLGA	doxorubicin	92.5	7.4	100	1.9	9.9%	0.05210
	PLGA	TF-doxorubicin	107.8	5.4	50	1.1	15.5%	0.14090
	PLGA	TF-doxorubicin	107.8	6.6	50	1	14.6%	0.146
	PLGA	TF-	107.8	7.4	50	1.1	13.7%	0.12454

		doxorubicin						
15	PLGA	rhein	134.6	5	5	29	52.1%	0.01796
	PLGA	rhein	134.6	7	0.1	24	3%	0.00125
	PLGA	rhein	134.6	7.4	5	13.4	32.0%	0.02388
	PLGA	rhein-NH4	191	5	8	45.6	49.10%	0.01076
	PLGA	rhein-NH4	191	7	0.1	25	2.80%	0.00112
	PLGA	rhein-NH4	191	7.4	8	50.4	38.20%	0.00757
16	PLGA	hydroxyl-FK866	132.00	6.4	0.01	0	0.0%	0
	PLGA	hydroxyl-FK866	130	7.4	0.01	0	0.0%	0
	PLGA	hydroxyl-FK866	134	8.4	0.01	0	0.0%	0
17	PLGA-hyd-PEG	insulin	140	6.8	10	0.46	20.9%	0.45434
	PLGA-PEG	insulin	140	6.8	10	0.5	19.7%	0.394
	PLGA	insulin	140	6.8	10	0.46	22.5%	0.48913
18	PLGA	insulin	125	7.4	10	11.5	67.7%	0.05886
	PLGA	insulin	125	3	10	0	0.0%	0
	PLGA	insulin	282	7.4	10	11.8	51.1%	0.04330
	PLGA	insulin	282	3	10	0	0.0%	0
	PLGA	insulin	637	7.4	10	12.3	38.6%	0.03138
	PLGA	insulin	637	3	10	0	0.0%	0
19	PLGA	rifampicin	200	7	2.5	5.9	41.1%	0.06966
	PLGA	rifampicin	400	7	2.5	9.7	33.80%	0.03484
20	PLGA	cranberry extract	417.7	6.8	50	0.5	18.8%	0.376
	OP-PLGA	cranberry extract	370	6.8	50	0.46	15.70%	0.34130
21	PLGA	atorvastatin calcium	194.3	6.8	0.1	2	2.3%	0.0115
22	PLGA	platelet lysate	318	7.2	0.01	0	0.0%	0
23	PLGA	paeonol	318	1.5	0.12	2.1	33.2%	0.15809
	PLGA	paeonol	318	7	0.12	2	26.20%	0.131
24	PLGA	doxorubicin	106	7.4	100	4	7.3%	0.01825

	PLGA	doxorubicin	83	7.4	100	2.5	16.10%	0.0644
	PLGA	doxorubicin	105	7.4	100	4	10.30%	0.02575
25	PLGA	Zoledronic Acid	91.36	7.4	1.6	0.55	31.50%	0.57272
26	PLGA	rapamycin	118.8	7.4	2.6	11.5	8.29%	0.00720
27	PLGA	rivaroxaban	496	6.8	7	1	34.99%	0.3499
28	PLGA	Sal-Tam: Salidroside	275.3	7.4	10	4.3	38.08%	0.08855
	PLGA	Sal-Tam: Tamoxifen	275.3	7.3	5	12	21.22%	0.01768
29	PLGA	entecavir	334	7.4	2.5	5.5	45.87%	0.0834
	PLGA	entecavir	337.4	7.4	2.5	4.9	35.34%	0.07212
	PLGA	entecavir	771.4	7.4	2.5	5.38	31.58%	0.05869
	PLGA	entecavir	828.6	7.4	2.5	4.84	23.70%	0.04896
30	PLGA	Cannabidiol	236	7.4	20	4.3	55.87%	0.12993
31	PLGA	Thymol	177.4	3.32	50	24	35.10%	0.01462
32	PLGA	resveratrol	286.13	7.4	50	1.95	36.05%	0.18487
	PLGA	resveratrol	341.56	7.4	50	2.17	27.21%	0.12539
	PLGA	resveratrol	286.13	5.5	50	1.67	36.91%	0.22101
	PLGA	resveratrol	341.56	5.5	50	1	92.69%	0.9269
33	PLGA	doxorubicin	70	5.5	50	1	28.12%	0.2812
	PLGA	doxorubicin	70	7.4	50	1	20.42%	0.2042
34	PLGA	Resveratrol	102.7	7.4	50	3.94	42.20%	0.10710
35	PLGA	doxorubicin	311	5	0.45	1.25	24.72%	0.19776
	PLGA	doxorubicin	311	6	0.45	0.9	22.18%	0.24644
36	PLGA	Prednisolone	406.85	7.4	50	3	59.06%	0.19686
	PLGA	Prednisolone	406.85	4.5	50	3	65.24%	0.21746

References

[1] Kaur, J., Singh, R. R., Khan, E., Kumar, A., & Joshi, A. (2021). Piperine-loaded PLGA nanoparticles as cancer drug carriers. *ACS Applied Nano Materials*, *4*(12), 14197–14207. https://doi.org/10.1021/acsanm.1c03664

[2] Maghrebi, S., Joyce, P., Jambhrunkar, M., Thomas, N., & Prestidge, C. A. (2020). Poly(lactic-*CO*-glycolic) acid–lipid hybrid microparticles enhance the intracellular uptake and antibacterial activity of rifampicin. *ACS Applied Materials & Interfaces*, *12*(7), 8030–8039. https://doi.org/10.1021/acsami.9b22991

[3] Muniyandi, P., Palaninathan, V., Mizuki, T., Maekawa, T., Hanajiri, T., & Mohamed, M. S. (2020). Poly(lactic-*co*-glycolic acid)/polyethylenimine nanocarriers for direct genetic reprogramming of MicroRNA targeting cardiac fibroblasts. *ACS Applied Nano Materials*, *3*(3), 2491–2505. https://doi.org/10.1021/acsanm.9b02586

[4] Angkawinitwong, U., Courtenay, A. J., Rodgers, A. M., Larrañeta, E., McCarthy, H. O., Brocchini, S., Donnelly, R. F., & Williams, G. R. (2020). A novel transdermal protein delivery strategy via electrohydrodynamic coating of PLGA microparticles onto microneedles. *ACS Applied Materials & Interfaces*, *12*(11), 12478–12488. https://doi.org/10.1021/acsami.9b22425

[5] Akolpoğlu Başaran, D. D., Gündüz, U., Tezcaner, A., & Keskin, D. (2021). Topical delivery of heparin from PLGA nanoparticles entrapped in nanofibers of sericin/gelatin scaffolds for wound healing. *International Journal of Pharmaceutics*, *597*, 120207. https://doi.org/10.1016/j.ijpharm.2021.120207

[6] Kohno, M., Andhariya, J. V., Wan, B., Bao, Q., Rothstein, S., Hezel, M., Wang, Y., & Burgess, D. J. (2020). The effect of PLGA molecular weight differences on risperidone release from Microspheres. *International Journal of Pharmaceutics*, *582*, 119339. https://doi.org/10.1016/j.ijpharm.2020.119339

[7] Tyo, K. M., Lasnik, A. B., Zhang, L., Mahmoud, M., Jenson, A. B., Fuqua, J. L., Palmer, K. E., & Steinbach-Rankins, J. M. (2020). Sustained-release Griffithsin nanoparticle-fiber composites against HIV-1 and HSV-2 infections. *Journal of Controlled Release*, *321*, 84–99. https://doi.org/10.1016/j.jconrel.2020.02.006

[8] Akhtar, B., Muhammad, F., Aslam, B., Saleemi, M. K., & Sharif, A. (2020). Pharmacokinetic profile of chitosan modified poly lactic co-glycolic acid biodegradable nanoparticles following oral delivery of gentamicin in rabbits. *International Journal of Biological Macromolecules*, *164*, 1493–1500. https://doi.org/10.1016/j.ijbiomac.2020.07.206

[9] Tamani, F., Hamoudi, M. C., Danede, F., Willart, J., Siepmann, F., & Siepmann, J. (2019). Towards a better understanding of the release mechanisms of caffeine from PLGA microparticles. *Journal of Applied Polymer Science*, *137*(25). https://doi.org/10.1002/app.48710

[10] Di Natale, C., Onesto, V., Lagreca, E., Vecchione, R., & Netti, P. A. (2020). Tunable release of curcumin with an in silico-supported approach from mixtures of highly porous PLGA microparticles. *Materials*, *13*(8), 1807. https://doi.org/10.3390/ma13081807

[11] Pudełko, I., Moskwik, A., Kwiecień, K., Kriegseis, S., Krok-Borkowicz, M., Schickle, K., Ochońska, D., Dobrzyński, P., Brzychczy-Włoch, M., Gonzalez-Julian, J., & Pamuła, E. (2023). Porous zirconia scaffolds functionalized with calcium phosphate layers and PLGA nanoparticles loaded with hydrophobic gentamicin. *International Journal of Molecular Sciences*, *24*(9), 8400. https://doi.org/10.3390/ijms24098400

[12] Liu, X., Wang, Z., Feng, X., Bai, E., Xiong, Y., Zhu, X., Shen, B., Duan, Y., & Huang, Y. (2020). Platensimycin-encapsulated poly (lactic-*co*-glycolic acid) and poly(amidoamine) dendrimers nanoparticles with enhanced anti-staphylococcal activity *in vivo*. *Bioconjugate Chemistry*, *31*(5), 1425–1437. https://doi.org/10.1021/acs.bioconjchem.0c00121

[13] Hernández-Giottonini, K. Y., Arellano-Reynoso, B., Rodríguez-Córdova, R. J., de la Vega-Olivas, J., Díaz-Aparicio, E., & Lucero-Acuña, A. (2023). Enhancing therapeutic efficacy against *brucella canis* infection in a murine model using rifampicin-loaded PLGA nanoparticles. *ACS Omega*, *8*(51), 49362–49371. https://doi.org/10.1021/acsomega.3c07892

[14] Scheeren, L. E., Nogueira-Librelotto, D. R., Macedo, L. B., de Vargas, J. M., Mitjans, M., Vinardell, M. P., & Rolim, C. M. (2020). Transferring-conjugated doxorubicin-loaded PLGA nanoparticles with pH-responsive behavior: A synergistic approach for cancer therapy. *Journal of Nanoparticle Research*, *22*(3). https://doi.org/10.1007/s11051-020-04798-7

[15] Hu, B., Gao, F., Li, C., Zhang, B., An, M., Lu, M., Liu, Y., & Liu, Y. (2020). Rhein laden ph-responsive polymeric nanoparticles for treatment of osteoarthritis. *AMB Express*, *10*(1). https://doi.org/10.1186/s13568-020-01095-3

[16] Bai, X., Tang, S., Butterworth, S., & Tirella, A. (2023). Design of PLGA nanoparticles for sustained release of hydroxyl-FK866 by microfluidics. *Biomaterials Advances*, *154*, 213649. https://doi.org/10.1016/j.bioadv.2023.213649

[17] Li, J., Qiang, H., Yang, W., Xu, Y., Feng, T., Cai, H., Wang, S., Liu, Z., Zhang, Z., & Zhang, J. (2022). Oral insulin delivery by epithelium microenvironment-adaptive nanoparticles. *Journal of Controlled Release*, *341*, 31–43. https://doi.org/10.1016/j.jconrel.2021.11.020

[18] Akhavan Farid, E., Davachi, S. M., Pezeshki-Modaress, M., Taranejoo, S., Seyfi, J., Hejazi, I., Tabatabaei Hakim, M., Najafi, F., D'Amico, C., & Abbaspourrad, A. (2020). Preparation and characterization of polylactic-co-glycolic acid/insulin nanoparticles encapsulated in methacrylate coated gelatin with sustained release for specific medical applications. *Journal of Biomaterials Science, Polymer Edition*, *31*(7), 910–937. https://doi.org/10.1080/09205063.2020.1725863

[19] Park, K., Otte, A., Sharifi, F., Garner, J., Skidmore, S., Park, H., Jhon, Y. K., Qin, B., & Wang, Y. (2020). Potential roles of the glass transition temperature of PLGA microparticles in drug release kinetics. *Molecular Pharmaceutics*, *18*(1), 18–32. https://doi.org/10.1021/acs.molpharmaceut.0c01089

[20] Mostafa, M. M., Amin, M. M., Zakaria, M. Y., Hussein, M. A., Shamaa, M. M., & Abd El-Halim, S. M. (2023). Chitosan surface-modified plga nanoparticles loaded with cranberry powder extract as a potential oral delivery platform for targeting colon cancer cells. *Pharmaceutics*, *15*(2), 606. https://doi.org/10.3390/pharmaceutics15020606

[21] Arafa, M. G., Girgis, G. N., & El-Dahan, M. S. (2020). chitosan-coated PLGA nanoparticles for enhanced ocular anti-inflammatory efficacy of atorvastatin calcium . *International Journal of Nanomedicine*, *Volume 15*, 1335–1347. https://doi.org/10.2147/ijn.s237314

[22] Bernal-Chávez, S. A., Alcalá-Alcalá, S., Cerecedo, D., & Ganem-Rondero, A. (2020). Platelet lysate-loaded plga nanoparticles in a thermo-responsive hydrogel intended for the treatment of wounds. *European Journal of Pharmaceutical Sciences*, *146*, 105231. https://doi.org/10.1016/j.ejps.2020.105231

[23] Wang, F., Shan, Q., Chang, X., Li, Z., & Gui, S. (2021). Paeonol-loaded PLGA nanoparticles as an oral drug delivery system: Design, optimization and evaluation. *International Journal of Pharmaceutics*, *602*, 120617. https://doi.org/10.1016/j.ijpharm.2021.120617

[24] Kumskova, N., Ermolenko, Y., Osipova, N., Semyonkin, A., Kildeeva, N., Gorshkova, M., Kovalskii, A., Kovshova, T., Tarasov, V., Kreuter, J., Maksimenko, O., & Gelperina, S. (2020). How subtle differences in polymer molecular weight affect doxorubicin-loaded PLGA nanoparticles degradation and drug release. *Journal of Microencapsulation*, *37*(3), 283–295. https://doi.org/10.1080/02652048.2020.1729885

[25] Saka, O. M., Öz, U. C., Küçüktürkmen, B., Devrim, B., & Bozkır, A. (2018). Central Composite design for optimization of zoledronic acid loaded PLGA nanoparticles. *Journal of Pharmaceutical Innovation*, *15*(1), 3–14. https://doi.org/10.1007/s12247-018-9365-6

[26] Cheraga, N., Sun, N.-C., Huang, X.-X., Ye, Z., Xiao, Q.-R., & Huang, N.-P. (2021). Optimized rapamycin-loaded pegylated PLGA nanoparticles: Preparation, characterization and pharmacokinetics study. *Journal of Drug Delivery Science and Technology*, *61*, 102144. https://doi.org/10.1016/j.jddst.2020.102144

[27] Anwer, Md. K., Mohammad, M., Iqbal, M., Ansari, M. N., Ezzeldin, E., Fatima, F., Alshahrani, S. M., Aldawsari, M. F., Alalaiwe, A., Alzahrani, A. A., & Aldayel, A. M. (2020). Sustained release and enhanced oral bioavailability of rivaroxaban by PLGA nanoparticles with no food effect. *Journal of Thrombosis and Thrombolysis*, *49*(3), 404–412. https://doi.org/10.1007/s11239-019-02022-5

[28] Yu, X., Sun, L., Tan, L., Wang, M., Ren, X., Pi, J., Jiang, M., & Li, N. (2020). Preparation and characterization of PLGA–PEG–PLGA nanoparticles containing salidroside and tamoxifen for breast cancer therapy. *AAPS PharmSciTech*, *21*(3). https://doi.org/10.1208/s12249-019-1523-8

[29] Ayoub, M. M., Jasti, B., Elantouny, N. G., Elnahas, H., & Ghazy, F. (2020). Comparative study of PLGA in-situ implant and nanoparticle formulations of entecavir; in-vitro and in-vivo evaluation. *Journal of Drug Delivery Science and Technology*, *56*, 101585. https://doi.org/10.1016/j.jddst.2020.101585

[30] Fraguas-Sánchez, A. I., Torres-Suárez, A. I., Cohen, M., Delie, F., Bastida-Ruiz, D., Yart, L., Martin-Sabroso, C., & Fernández-Carballido, A. (2020). PLGA nanoparticles for the intraperitoneal administration of CBD in the treatment of ovarian cancer: In vitro and in OVO Assessment. *Pharmaceutics*, *12*(5), 439. https://doi.org/10.3390/pharmaceutics12050439

[31] Folle, C., Marqués, A. M., Díaz-Garrido, N., Espina, M., Sánchez-López, E., Badia, J., Baldoma, L., Calpena, A. C., & García, M. L. (2021). Thymol-loaded PLGA nanoparticles: An efficient approach for acne treatment. *Journal of Nanobiotechnology*, *19*(1). https://doi.org/10.1186/s12951-021-01092-z

[32] Aldawsari, H. M., Alhakamy, N. A., Padder, R., Husain, M., & Md, S. (2020). Preparation and characterization of chitosan coated PLGA nanoparticles of resveratrol: Improved stability, antioxidant and apoptotic activities in H1299 lung cancer cells. *Coatings*, *10*(5), 439. https://doi.org/10.3390/coatings10050439

[33] Huang, S.-J., Wang, T.-H., Chou, Y.-H., Wang, H.-M. D., Hsu, T.-C., Yow, J.-L., Tzang, B.-S., & Chiang, W.-H. (2022). Hybrid pegylated chitosan/PLGA nanoparticles designed as ph-responsive vehicles to promote intracellular drug delivery and cancer chemotherapy. *International Journal of Biological Macromolecules*, *210*, 565–578. https://doi.org/10.1016/j.ijbiomac.2022.04.209

[34] Bhatt, P., Fnu, G., Bhatia, D., Shahid, A., & Sutariya, V. (2020). Nano delivery of resveratrol-loaded PLGA nanoparticles for age-related macular degeneration. *AAPS PharmSciTech*, *21*(8). https://doi.org/10.1208/s12249-020-01836-4

[35] Raposo, C. D., Costa, R., Petrova, K. T., Brito, C., Scotti, M. T., & Cardoso, M. M. (2020). Development of novel galactosylated PLGA nanoparticles for hepatocyte targeting using molecular modelling. *Polymers*, *12*(1), 94. https://doi.org/10.3390/polym12010094

[36] Prednisolone encapsulated PLGA nanoparticles: Characterization, cytotoxicity, and anti-inflammatory activity on c6 glial cells. (2020). *Journal of Applied Pharmaceutical Science*, *10*(4), 14–21. https://doi.org/10.7324/japs.2020.104003